ROYAUME DU MAROC
Université Mohammed V - RABAT -
جامعة محمد الخامس – الرباط –
Faculté des sciences
كلية العلوم
CENTRE D'ETUDES DOCTORALES - SCIENCES ET TECHNOLOGIES

THESE

En vue de l'obtention du :

DOCTORAT

Structure de recherche: Materials, Nanomaterials for Photovoltaic conversion and Electrochemical Storage (MANAPSE)
Discipline : Physique
Spécialité : Energie et matériaux

Présentée et soutenue le 26/03/2022 par :

Houssain ZITOUNI

Experimental investigation and modeling of photovoltaic soiling loss as a function of environmental variables

JURY

Mohammed ABD-LEFDIL	PES, Université Mohammed V, Faculté des sciences-Rabat	Président
M'Hamed TAIBI	PES, Université Mohammed V, Ecole normale supérieur-Rabat	Rapporteur/Examinateur
Rachid TADILI	PES, Université Mohammed V, Faculté des sciences-Rabat	Rapporteur/Examinateur
Abdelkader OUTZOURHIT	PES, Université Cadi Ayyad, Faculté des sciences-Marrakech	Rapporteur/Examinateur
Zakaria NAIMI	Directeur du Green Energy Park-Benguerir	Invité
Lahoucine ATOURKI	PA, Université Mohammed V, Faculté des sciences-Rabat	Invité
Mohammed REGRAGUI	PES, Université Mohammed V, Faculté des sciences-Rabat	Directeur de Thèse

Année Universitaire : 2021-2022

✉ Faculté des Sciences, avenue Ibn Battouta, BP. 1014 RP, Rabat –Maroc
☎ 00212 (05) 37 77 18 76 🖷 00212(05) 37 77 42 61; http://www. fsr.um5.ac.ma

DEDICACE

Je souhaiterais souligner ici le rôle important de mon entourage professionnel et personnel ; je n'aurai pas pu effectuer le travail décrit dans cette thèse sans eux.

Un grand merci aussi spécial qu'il puisse l'être, à l'attention de mes chers **Parents**. Merci d'être mes parents, de m'avoir donné des racines et des ailes, de m'avoir supportée et appuyée durant toutes ces années, de me faire confiance. Grace à vous j'ai pu m'épanouir et m'ouvrir à la vie et surtout surmonter toute sorte d'épreuves que je rencontre.

A ma chère **Femme**, Pour tout l'encouragement, le respect et l'amour que tu m'as présentés tout au long de cette période, pour toutes les nuits blanches que tu as passé à mes côtés pour réussir ce travail, je te dédie ce travail, qui n'aurait pas pu être achevé sans ton éternel soutien et optimisme. Aucun remerciement ne saurait exprimer mon sincère attachement et ma gratitude pour l'amour, la douceur et la galanterie dont tu m'as entouré, je t'aime énormément.

Je dédie également ce travail à mes **Frères** qui ont été toujours à mes côtés. Je vous remercie pour tout ce que vous avez fait pour moi… je vous remercie tous du fond du cœur.

Mes derniers remerciements sont adressés à la famille de ma femme et à toutes les personnes qui, de près ou de loin, ont contribué à l'accomplissement de ce cheminement.

REMERCIEMENTS

Je tiens à remercier tout d'abord mon laboratoire de recherche **MANAPSE** au nom de son directeur, Monsieur **Mohammed ABD-LEFDIL** pour m'avoir accueilli dans son laboratoire et de m'avoir offrir tous les moyens nécessaires pour réussir mon travail de thèse.

Je remercie vivement Monsieur **Mohammed REGRAGUI**, mon directeur de thèse pour sa grande disponibilité, ses conseils et pour m'avoir fait partager sa passion pour la physique, je voudrai lui exprimer mes meilleurs remerciements pour avoir dirigé ce travail avec beaucoup d'intérêt et de patience. Je suis particulièrement honoré d'avoir été le thésard de **Mr le Doyen**.

Je tiens a remercié infiniment Monsieur **Mohammed ABD-LEFDIL** d'avoir accepté de presidé ma thèse de doctorat.

Je remercie profondément Monsieur **M'hamed TAIBI** pour avoir accepté d'être un rapporteur et examinateur de mon travail de thèse.

Je remercie profondément Monsieur **Rachid TADILI** pour avoir accepté d'être un rapporteur et examinateur de mon travail de thèse.

Je remercie profondément Monsieur **Abdelkader OUTZOURHIT** pour avoir accepté d'être un rapporteur et examinateur de mon travail de thèse.

Je remercie également Messieurs **Lahoucine ATOURKI et Zakaria NAIMI** pour leur relecture et commentaires de mon manuscrit de thèse.

Je suis particulièrement redevable au Messieurs **Mohammed REGRAGUI et Jesus POLO** et au programme **MEDSOL** pour leur aide précieuse, pour l'accueil qu'ils m'ont réservé en Espagne et chez qui j'ai pu trouver beaucoup de soutien et conseils.

Résumé

La production d'électricité à partir des centrales photovoltaïques a un impact considérable à l'avenir pour assurer la sécurité énergétique dans la région MENA. Néanmoins, l'encrassement reste un problème majeur provoquant des pertes indésirables de réflectance, de transmission et d'absorbance. Dans cette thèse, le taux de salissure est modélisé en fonction des données environnementales avec plusieurs méthodes de modélisation telles que le modèle de régression linéaire multiple (MLR), la régression linéaire multiple avec modèle d'interaction (MLRWI), le modèle mathématique généré par la méthodologie de surface de réponse (RSM) et des réseaux de neurones artificiels (ANN), en utilisant une année de mesures au sol à partir d'un système amorphe d'une capacité de 2,16 kWc. Nous avons également développé un dispositif électronique intelligent afin de calculer automatiquement le taux de salissure en utilisant deux panneaux photovoltaïques
Dans le dernier chapitre, nous avons développé un système de nettoyage robotisé pour l'optimisation des performances.

Mots-clefs (5) : Prédiction des salissures PV, analyse des poussières, taux de salissures, système robotique, réseaux de neurones artificiels

Abstract

Electricity production from the photovoltaic plants has a considerable impact in the future to ensure energy security in the MENA region. Nevertheless, soiling remains a major problem causing undesirable reflectance, transmittance, and absorbance losses. In this thesis, the soiling rate is modeled as a function of environmental data with several modeling methods such as the multiple linear regression model (MLR), multiple linear regression with interaction model (MLRWI), the mathematical model generated by the response surface methodology (RSM) and Artificial Neural Networks (ANNs), by using a one-year of ground measurements from an amorphous array with a capacity of 2.16 kWc. We also developed a smart electronic device in order to calculate the soiling ratio automatically by using two photovoltaic panels

In the last chapter we developed a robotic cleaning system for the optimization of the performance.

Key Words (5): PV soiling prediction, Dust analysis, soiling ratio, robotic system, Artificial Neural Networks

Table of content

INTRODUCTION

Global energy demand increases proportionally with population and economic growth. Developed countries, developing countries and emerging countries have systematically shown a great interest in renewable energies which offer great flexibility and satisfactory reliability to alleviate the energy deficit due to the increase in demand and also to the environmental problems. Morocco, which imports more than 89.4% of its energy needs from abroad, is one of those countries that focus in an accentuated way on renewable energies to preserve its energy security and adhere to the sustainable development currently imposed.

With this in mind, the Moroccan authorities planned to increase the share of renewable energies to 42% of the installed electrical capacity in 2020 and to 52% in 2030, mainly based on renewable solar, hydraulic and wind energy. Energy policy is primarily the responsibility of the Ministry of Energy, Mines and Sustainable Development and is supported by the following institutions:

- IRESEN (Institute for Research in Solar Energy and New Energies);
- MASEN (Moroccan Agency for Sustainable Energy);
- ONEE (National Office for Electricity and Drinking Water / Electricity branch);
- AMEE (Moroccan Energy Efficiency Agency);
- SIE (Energy Investment Company).

The development of solar stations based on different technologies (CSP and PV) comes down to the geographical location of Morocco having a solar field in the different regions (Arid and Semi-arid) of the Kingdom which ensures its energy independence and achieves its route drawn by the high authorities of the state. Various programs have been launched by the government planning to put in place an additional capacity of 6,000 MW in terms of renewable energies by 2020. In 2019, the installed solar capacity was 711 MW. The performance and sustainability of these technologies, the theme of our research work, represents an essential aspect for investors and stakeholders.

PV technology, which is the objective of this thesis, has undergone continuous development from a performance point of view since the PV effect was discovered in 1839 by the French physicist Edmond Becquerel. Subsequently, the first practical solar generator (cell) was developed by the Bell Laboratory in the United States in 1954 when a long-term energy supply was needed for the space project program. In 1958, with improved technology, the efficiency of silicon PV cells under real sunlight and temperature was 14%. As research and development for improving the efficiency of PV cells continues continuously, the performance of PV cells has been improved and costs have been reduced considerably. Currently, the yield of crystalline silicon-based cells in the laboratory is around 26.7%.

The PV electricity produced depends on the reliability, durability, performance and service life of PV modules in the form of an assembly of several cells. The PV module is designed to operate with a power greater than 80% of its initial power for a period of ≥ 25 years. However, the operation of PV modules over time leads to aging related to the severity of climatic conditions. In this sense, the appearance of different problems such as the soiling take place, and can consequently lead to a decrease in the performance of the PV module before the manufacturer's warranty is satisfied.

Today, there is a lack of information on the different modes of degradation of photovoltaic modules in terms of frequency, rate of evolution and degree of impact on the life and reliability of PV modules. In

recent years, research on photovoltaic modules has rather focused on the race to develop new technologies without having enough feedback on those that are already operational.

The meteorological parameters and the characteristics of the installation site remain one of the drastically most influencing parameters on the performance of photovoltaic solar panels. They can significantly reduce both the efficiency of electrical performance and the capacity of the panels, knowing that most panels are designed for proper operation for more than two decades, but this time is reduced due to the hard-environmental conditions. However, the accumulation of dust on the photovoltaic panels remains one of the most influencing parameters on the performance of the panels as well as their lifespan.

The main objective of this thesis is to make a deep study of the effect of soiling on the photovoltaic solar panels and the use of these results to develop an optimal cleaning strategy. This objective can be achieved by a precise evaluation of the impact of soiling on the performance of the photovoltaic system in function of the climatic and environmental factors (temperature, humidity, wind speed and precipitation). For this reason, our work was divided into four chapters:

First chapter: we give a general overview of the different components of a photovoltaic system (ranging from the cell to the photovoltaic field), the different form of degradation that can affect the photovoltaic panels and provide a state of the art of the dust life cycle and the influence of dust accumulation on the performance of the panels.

Second chapter: we modeled the soiling rate as a function of environmental data with several modeling methods such as the multiple linear regression model (MLR), multiple linear regression with interaction model (MLRWI), the mathematical model generated by the response surface methodology (RSM) and Artificial Neural Networks (ANNs), by using one-year of ground measurements from an amorphous array with a capacity of 2.16 kWc. The experiment is carried under a semi-arid climate at Green Energy Park research facility (Benguerir, Morocco). The dust analysis was carried out by Scanning Electron Microscope (SEM), Energy Dispersive X-Ray Spectroscopy (EDS), and X-ray fluorescence (XRF) in two periods (December 2017 and June 2018) in order to define the mineralogy and morphology of our dust samples.

Third chapter: we were studying, designing and implementing a system that allow the solar panels to self-control and to collect various data of the production, and send them to a central computer which, in turn, stores and analyzes this data in order to place orders with the actuators, which in turn initiate or end the cleaning process. This work is based on the creation of an automatic, embedded system able to monitor the evolution of soiling ratio of photovoltaic modules, and display them in a graphical interface in order to save the results in a text file.

Fourth chapter: we have designed a stand-alone photovoltaic module cleaning system, which uses the cleaning mechanism with water, using a rotating cylindrical brush and water injected by a pump. This cleaning system contains obstacle sensors so that it can operate on photovoltaic chains of different sizes, and it is also equipped with Wifi to allow the user to remotely control and monitor the operation of the robot.

Chapter 1

General Introduction

I.1. Introduction

In recent decades, the world has experienced relentless exponential growth in energy demand due to continued economic and industrial development. This demand is mainly satisfied by means of fossil resources, which are in the process of rarefaction and present harmful environmental effects because of the ejections of greenhouse gases.

In order to minimize this dependence on fossil resources, the world has turned to the use of renewable energies, which are inexhaustible sources of energy on a human scale, which will undoubtedly be the energies of tomorrow. The development of these energies is a solution that will both meet global energy demand in a sustainable manner and limit harmful impacts on the environment.

Renewable energies have grown rapidly in the electricity sector, while progress has been much less in the heating and transportation sectors. According to the International Energy Agency (IEA), they also experienced a new record in the year 2019, with an increase in installed capacity of more than 200 GW, (Fig.1.1) “this is the largest increase ever registered”.

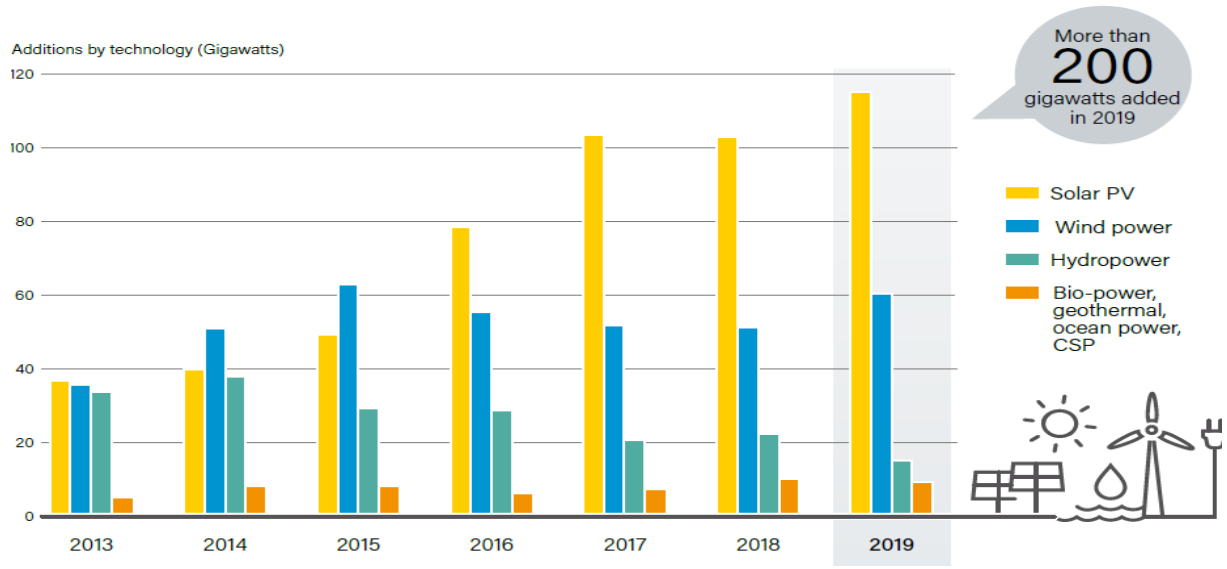

Fig 1.1. Annual increase in renewable energy capacity (by technology and total)

In 2019, around 115 GW of photovoltaic solar energy was added worldwide, thus consolidating the status of this technology as a leader in new power generation capacities. During the year, 57% of the renewable energy capacity additions were achieved through solar photovoltaic energy (direct current), followed by wind energy (around 60 GW for 30%) and hydropower (around 16 GW for 8%). The remaining 5% of the additions were made using bioelectricity, geothermal energy and concentrated solar thermal energy.

At the end of 2019, at least 32 countries had more than 10 GW of renewable energy capacity (including hydropower) in operation, compared to 19 countries in 2009. The change is even more impressive if hydropower is excluded, because the solar photovoltaic and wind energy markets have experienced spectacular growth in recent years. Overall, the installed capacity of renewable energy was sufficient to provide an estimated 27.3% of global electricity production at the end of 2019.

Hydropower still accounted for the majority of this production share. estimated, followed by wind power, solar PV, and bioelectricity (Fig.1.2).

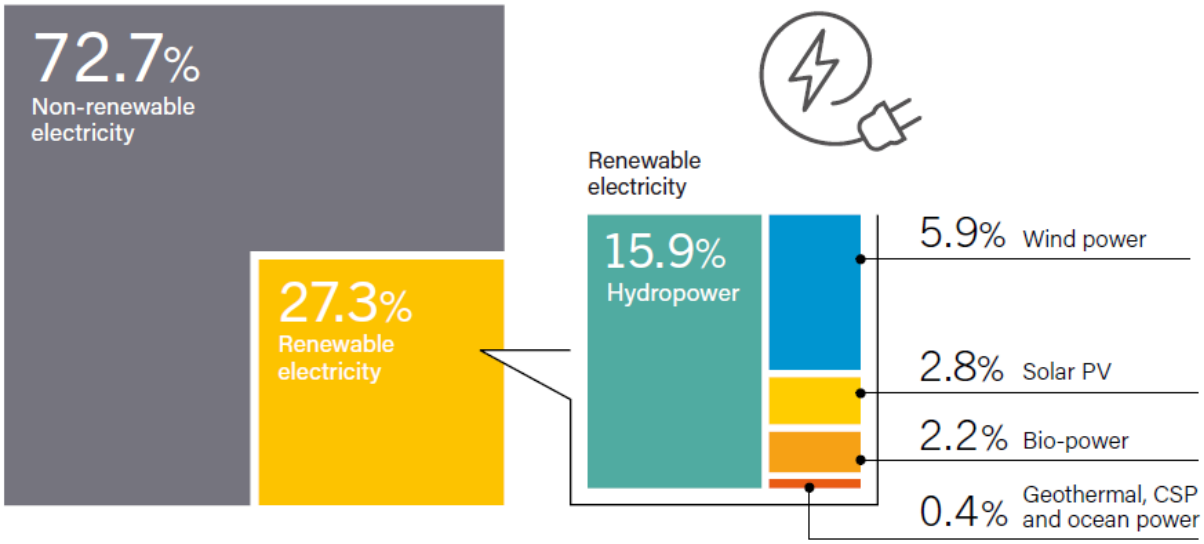

Fig.1.2. Estimated share of renewable energy in global final energy consumption

Among all the renewable energy sources, Africa pays particular attention to solar photovoltaic (PV) because it has a solar deposit suitable for the development of this form of energy. In the context of large-scale photovoltaic power generation, solar photovoltaic power plants are crucial. Photovoltaic installations are mainly divided into two categories:

- Autonomous installations called “off-grid”, in which, if it is not used immediately, the energy produced by the sun must generally be stored in batteries.
- Installations connected to the network, capable of debiting the energy produced and which consists of a centralized system (direct injection into the electricity network) and decentralized (injection into the network of the user's surplus energy).

I.2. PV system:

Photovoltaic (PV) panels capture light energy and convert it into electrical energy to generate direct current. Photovoltaic panels are modular, which means that several panels can be easily combined to achieve the required production capacity. It will then be easy to add new panels to increase the capacity of the energy production system. The panels can be installed on the roof, posts or any other structure. Some of them are installed on a pivot system, which can turn them towards the sun at any time to increase electricity production.

The PV system consists of three main parts, a PV generator, a group of converters and the power grid. The role of the "converter" group is to extract the maximum continuous power from the PV generator, then convert it into alternating current, and inject it into the network.

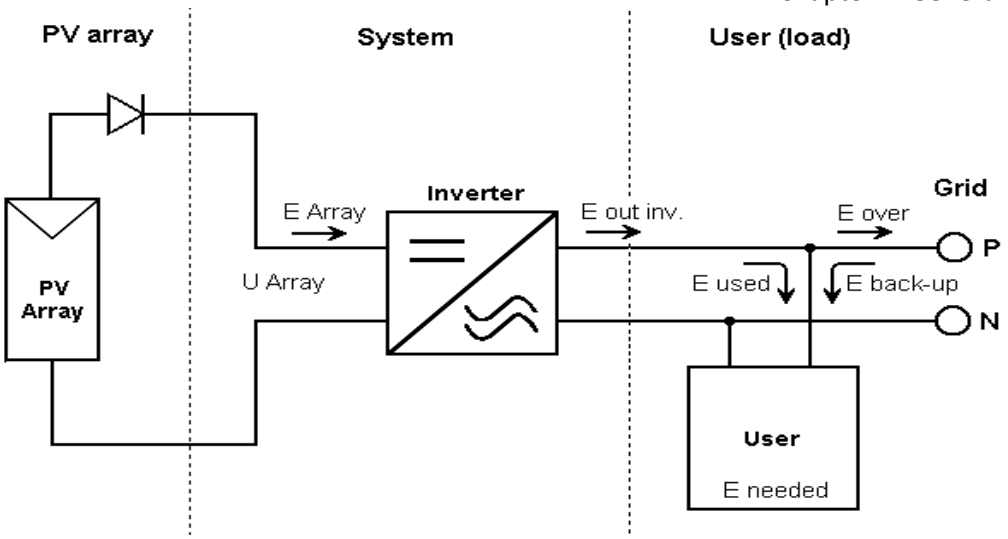

Fig.1.3. Photovoltaic system

I.2.1. Photovoltaic generator:

The PV generator converts solar energy into electrical energy. The key component of this generator is the PV cell.

PV cell:

The PV cell, also called a solar cell, is the basic element of photovoltaic conversion. A semiconductor device absorbs light energy and converts it directly into electric current. Some semiconductor materials like silicon have the property of generating electricity when they receive sunlight.

I.2.2. Principle of operation:

The photovoltaic effect used in solar cells allows the light energy of the sun's rays to be directly converted into electricity through the production and transport in a semiconductor material of positive and negative electric charges under the effect of light. This material has two parts, one with an excess of electrons and the other with an electron deficit, called n-type doped and p-type doped, respectively. When the first is brought into contact with the second, the electrons in excess in the material n diffuse in the material p. The initially n-doped zone becomes positively charged, and the initially p-doped zone negatively charged.

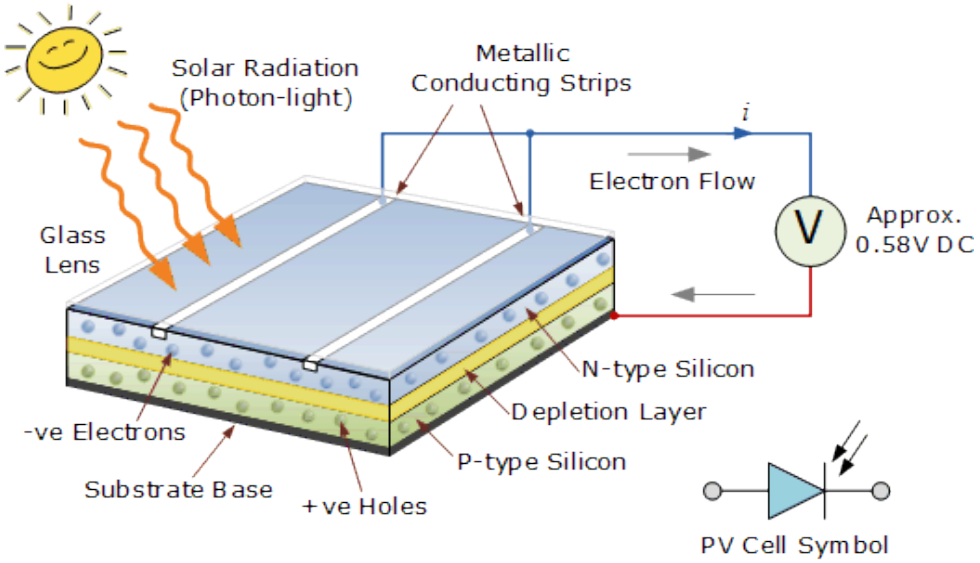

Fig.1.4. Operating diagram of a photovoltaic cell

An electric field is therefore created between them which tends to push the electrons back into zone n and the holes towards zone p. A junction (called p-n) has been formed. By adding metal contacts on the n and p areas, a diode is obtained. When the junction is illuminated, photons with energy equal to or greater than the width of the forbidden band impart their energy to the atoms, each of which passes an electron from the valence band into the conduction band. If a charge is placed at the terminals of the cell, the electrons of the n zone join the holes of the p zone via the external connection, giving rise to a potential difference: the electric current flows [1].

I.2.3. Types of PV cells:

There are many technologies for making photovoltaic cells, but many are still in the research stage. Fig.1.5 represents the chronological evolution of the distribution of the various industrial sectors of photovoltaics [2].

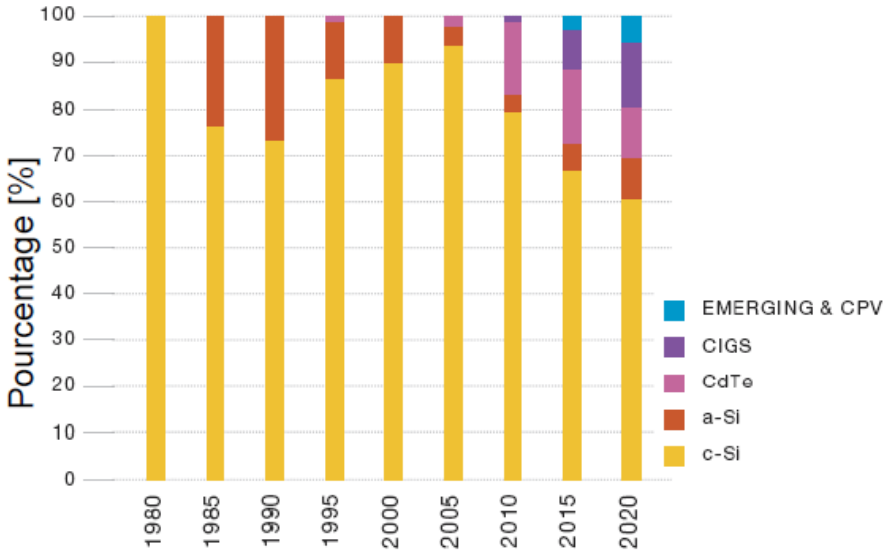

Fig.1.5. Evolution of the distribution of industrialized cell technologies [2]

Silicon is now the essential element in the global production of photovoltaic panels. It is an extremely abundant, stable and non-toxic material. Due to the nature of the silicon used and / or its manufacturing process, the industry itself is subdivided into several different technologies. Silicon PV cells are the first generation, and they fall into three categories: monocrystalline, polycrystalline, and amorphous cells.

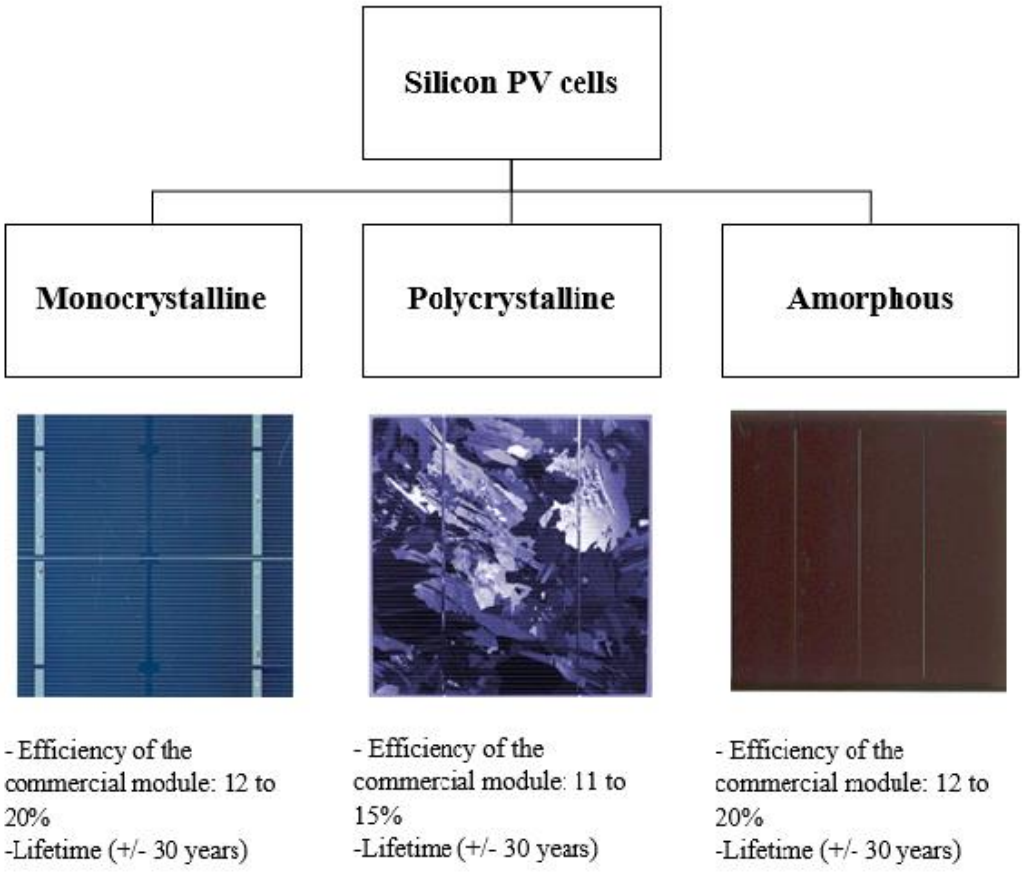

Fig.1.6. Types of silicon PV cells

Various materials are used for the manufacture of the second generation such as:

Cadmium Telluride (CdTe), Copper-Indium-Selenium (CIS), and Copper-Indium-Gallium-Selenium (CIGS). These raw materials are easily obtainable than the silicon used in conventional photovoltaic cells. Although their yield is lower (around 9-10%) than crystalline panels, they have certain advantages:

- The cell can be built on a flexible substrate.
- Low sensitivity to temperature rises (unlike crystalline panels whose performance decreases with increasing temperature). They can therefore be easily integrated into the roof.
- Better production in diffused light. Their use is more suitable in less sunny regions.

Amorphous technology, which has been one of the preferred technologies, has seen a decline in the current market compared to thin film technology. For example, CdTe technology increased from 2% in 2005 to 13% in 2010 (see figure 5).

Other photovoltaic cell technologies are in the research and development phase, such as:

Concentrated PV (CPV) technology:

Concentrating photovoltaic systems are formed by inserting a concentrator device between the sun and the photovoltaic cells. We can then use a much smaller cell surface (but with very high yields of 30-40%). The concentration is obtained by a system of parabolic mirrors or Fresnel lenses. The following figure shows an example of this technology.

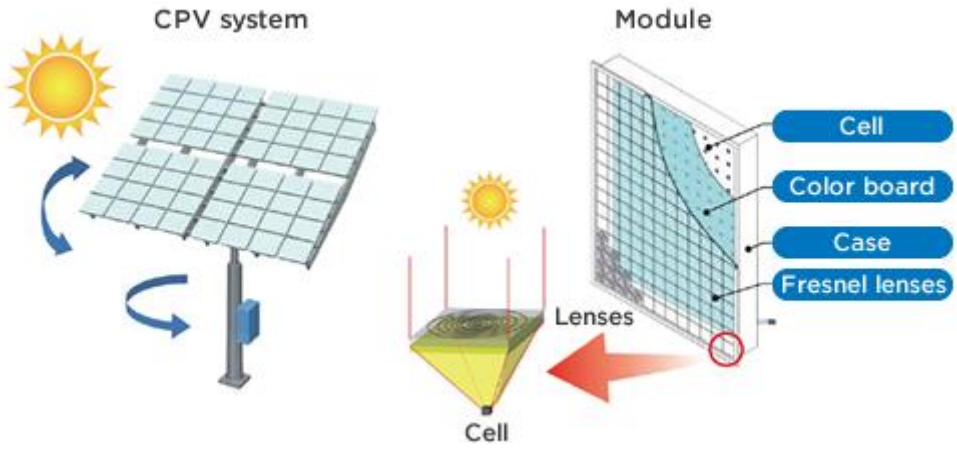

Fig.1.7. Example of a parabolic concentration PV installation

The collector (the first mirror) through a focal point on a second mirror reflects all incoming parallel light. This second mirror, which is much smaller, is also a parabolic mirror with the same focal point. It reflects the beams of light in the middle of the first parabolic mirror where they hit the solar cell.

Organic PV cells:

Organic photovoltaic cells convert solar energy into electrical energy using organic molecules. One of their advantages over "traditional" silicon solar cells is that they can be mounted on lightweight, flexible and easy to replace sheets, which can be spread over roofs and buildings like wallpaper, converting solar energy into electric current. In the future, they could also be used to provide a cost-effective and reliable source of electricity in remote areas. Fig.1.8 shows an example of this kind of PV cell.

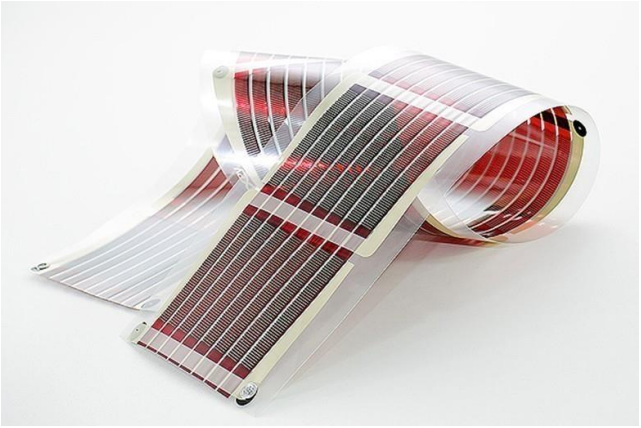

Fig.1.8. Printed strip of organic photovoltaic cells

A single cell produces very little electrical power, typically 1 to 3 W with a voltage of less than one volt. To produce more power, the cells are put together to form a module (or panel). Connecting multiple cells in series increases voltage for the same current, while paralleling increases current while maintaining voltage. The output current, and therefore the power, will be proportional to the area of the module.

I.3. Degradation of PV modules

Degradation modes in a PV module can be classified into threetypes:

i. Degradation of packagingmaterials,
ii. Degradation ofinterconnect,
iii. Semiconductor devicedegradation.

In the following sections PV module performance function of degradation modes will be discussedonly for crystalline silicon technologies.

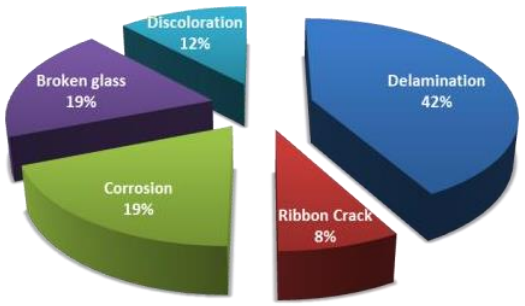

Fig.1.9. Statistical analyses of the most popular degradation modes [3]

The performance of a PV module under outdoor conditions depends on several factors such as the PV technology used as well as the environmental conditions of the site where the module is deployed. For crystalline silicon PV module, each one of various intrinsic or extrinsic named factors may induce one or more types of module degradation [4], [5]. Fig.1.9 gives a review of the representativeness of the main silicon PV modules degradation modes.

Following the history of field failures for C-Si as mentioned in NREL: Broken interconnects, Broken cells, Corrosion, Delamination and/or loss of elastomeric properties of encapsulant,

Encapsulating discoloration, Solder bond failures, broken glass, Hot Spots, Ground faults, Junction box, Bypass Diode failures, Open circuiting leading to arcing. Each one of those filed failures will be discussed and documented in the following sections.

I.3.1. Broken interconnects:

Changes into the structure or geometry of the cells interconnect due to the segregation of metals (SbPb) in the soldering alloy results into interconnect degradation fig.1.10. Such structural changes in the soldering material occur due to thermo-mechanical fatigue resulting into an increased series resistance and reduced performance. Substrates with high thermal expansion coefficients, larger cells, thicker ribbon and kinks in ribbon are the factors could lead to interconnects degradation [6].

For this category of faults, we can distinguish two different cases, which result in three severity stages in terms of power loss rate and safety risk. If only one of the two interconnection ribbons in a cell is disconnected, the corresponding cell part appears as heat source in the IR image and as bright area in the EL one, and vice versa. However, the current still flows through all the strings and the submodules of the defective PV module. According to Buerhop et al.[7], for a specific type of cell with an interrupted grid on the top surface. A typical P_{MAX} loss of about 6W/cell, and significant drop of FF, are expected; but, depending on the resultant temperature differences ΔT (between "healthy" and defective areas), even a single disconnection (one of the two ribbons) of one cell in a module may result in a further power loss of up to 35%. In this case ("severity stage 1"), safety risk is not high as long as the temperature of the evolving hot spot does not exceed 100 °C. On the other hand, if both two ribbons of a cell become electrically disconnected, inevitably the current stops flowing through this "path" and goes through a bypass diode. As a result, the corresponding sub-module stops generating electrical power. The power loss in this case ("severity stage 2") may further increase, up to 50%, and the safety risk depends on the durability of the bypass diode. If the diode further degrades during this permanent operation and fails, there comes the final "severity stage 3" where severe failure and extreme localized heating occur (ΔT4500 °C) at the disconnected part, with high safety risks (fire). The power loss of this kind of failure occurs stepwise [6], [8].

Several others failure may be accompanied with this failure mode, like excessive heating of PV module, hot spot generation, arcing of solder-joint (series and parallel arc) and burning of back sheet.

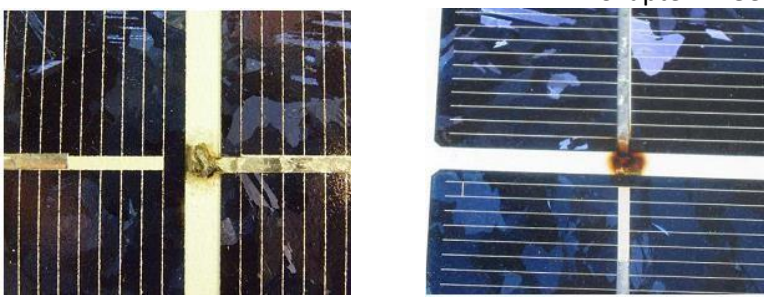

Fig.1.10. Cases of broken interconnecting ribbons "front-to-back" [6]

Broken interconnections can be easily detected by optical methods like electroluminescence (EL), IRT and ultraviolet (UV) imaging, as well as by simple I–V characterization [6]

I.3.2. Broken cells:

Broken cells can be occurring during manufacturing, in manual soldering, for example, when mechanical and thermal stress is applied, or in the field exposure by the mechanical stresses applied on the PV solar cells. Broken cells can be visually identified on the PV module, if they are large enough fig.1.11. Under further stress, after years in the field, those cracks can become larger and more obvious for visual detection. Furthermore, since there was only one attachment point for each polarity, module will be in open circuits [9]. The resultant power loss due to broken cells is strongly dependent on the crack pattern, i.e. the size, the geometry, the topology and the orientation of the crack [6].

Due to the dependence of the power loss on the orientation of the cell crack, the correlation between the absolute number of cell cracks and power loss is often very weak. However, for inactive cracked parts of more than 8% of the total cell area, it can be fairly assumed that the mean power loss rate is linear with the number of cracked cells [6], [10], [11].

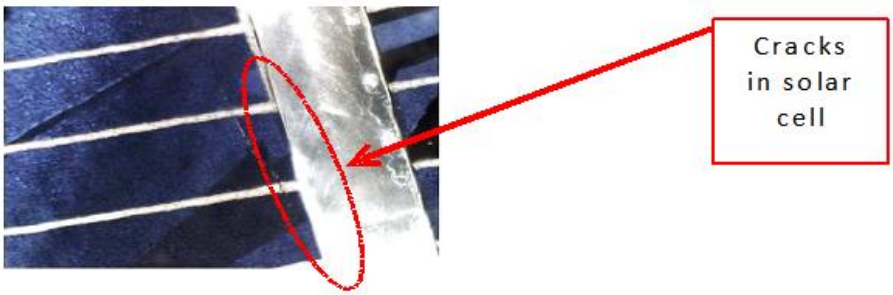

Fig.1.11. Cracks in PV solar cells [10]

A thinner and larger cell in large modules is responsible on this defect in PV solar cells. Broken cells can become visible when they permit delamination along cracks[11]. Broken cells can be easily detected by electroluminescence (EL) fig.1.12.

Fig.1.12. EL of a PV module with occurring Broken cells [9]

In order to save silicon and reduce the manufacturing costs of PV cells, producers have varied the thickness and the surface of cells in recent years [3].

The thickness of silicon PV cells decreased from 300 um to less than 200 um and sometimes to less than 100 um. In addition to the reduction in thickness of PV cells, the cell surface increased to 210 mm [12]. This makes PV cells more fragile and more susceptible to breakage during handling (rolling and storage). It is generally impossible to detect cracks on the already operational PV module to the naked eye. Detection can be done by using optical methods [3].

I.3.3. Corrosion:

For crystalline Si corrosion of front contacts is dependent on both the metallization system and the encapsulation system. Corrosion or oxidation of busbar is a decomposition of contact or absorber layers driven by moisture, heat and/or electric field [12].

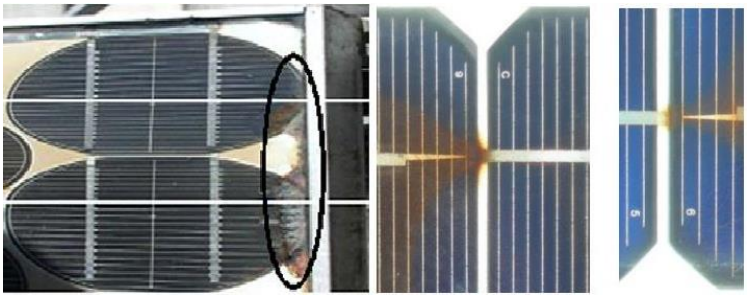

Fig.1.13. PV module affected by corrosion of the edge and near the busbars

The moisture that enters the module through the laminate edges causes corrosion [13]. The moisture retention in the housing of the module increases the electrical conductivity of the material. Indeed, the corrosion attacks the metallic connections of PV cells causing a loss of performance by increasing leakage currents. Corrosion also degrades the adhesion between cells and metallic frame. Fig.1.3 shows a PV module affected by corrosion at the edge [3], [4].

Wohlgemuth and Kurtz[14]studied the impact of humidity and temperature on PV module degradation. They found out that corrosion appeared after 1000 h of exposure of PV module under 85 °C and 85% of relative humidity. Other studies[15] also argue that corrosion is among of the

predominant modes of photovoltaic modules degradation. Carlson et al. [16], in collaboration with NREL, after tests on BP Solar modules, showed that the sodium contained in the glass which is reactive with moisture is a major factor of the corrosion of PV modules edges. Osterwald et al. [17]argues that the first and faster silicon PV module degradations are caused by oxygen which is the main factor of the corrosion of silicon junctions. Kempe [13] showed that the moisture in the PV module is correlated with the rate of degradation, especially in hot and humid geographic zones such as Miami in Florida. Corrosion can be visually observed which is often coincident with delamination.

I.3.4. Delamination and/or loss of elastomeric properties of encapsulant:

Adhesion loss called delamination occurs between the PV module layers (packaging materials and solar cell) driven by moisture, mechanical stress and UV light. It represents a major problem because it causes two effects: the increase of the light reflection and of water penetration inside the module structure [4]. Skoczek et al. [18] studied the PV modules degradation related to delamination module from tests based on IEC 61215 standard.

A common observation argues that delamination is more frequent in hot and humid climate, at certain case occurred less than 5 years of exposure. It causes moisture penetration in the module and therefore causes various chemical and physical degradations such as metal corrosion of the module structure most frequently. Paula, et al. [19] Highlighted that the origin of the defect could lie in a chemical reaction between the cell antireflecting coating (TiOx) and certain additives in the module encapsulant [20]. Also, by using Auger electron spectroscopy, it has been shown that concentrations of phosphorous and sodium migrating from the cell emitter and the glass respectively, have a direct negative impact on the adhesional strength cell-EVA encapsulant[21]. This type of defect is always found at the same location on the solar cells between metallization fingers in the proximity of the cell busbars and at the cell perimeter. There is, however, no additional concentration of phosphorous or sodium in these areas. The particular location of the defect is likely to be related to geometrical factors, as the highest device thickness discontinuities are found at these areas [19]. Jansen and Delahoy[22] claim that delamination may be caused by salt accumulation and moisture penetration into the PV module. Moreover, they argue that interfacial connection may be etched by hydrofluoric acid formed by fluorine and tin oxide contained in the PV module[3].

Delamination defect can be visually observed. Which is often follows ribbons and grid fingers fig.1.14,a,band causing corrosion fig.1.14,c, but some corrosion occurs without delamination also delamination can accompany discoloration

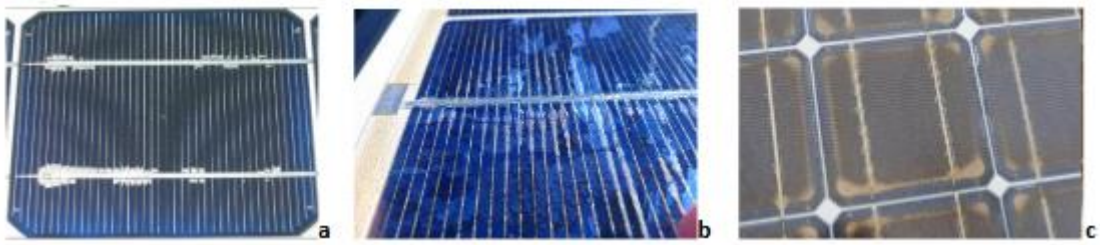

Fig.1.14. Delamination defect on PV module [23].

I.3.5. Encapsulant discoloration:

Discoloration usually results in a degradation of the encapsulant module, EVA (Ethylene Vinyl Acetate (33 % vinyl acetate, 65%-70% gel content (degree of cross-linking)) or adhesive material between the glass and the PV cells [24]. Module discoloration is a change in color of the EVA films, which turns yellow and sometimes brown (Fig.1.15). As it is reported by Djordjevic et al.[13], such faults are caused by internal factors (e.g. low encapsulant quality or poor/incorrect lamination) and/or external ones (high temperature, humidity, UV light) [6]. It modifies transmittance of light reaching PV cells which lead to a decrease in the short circuit current (Isc) and therefore the power generated by the module is reduced fig.1.16 [3].

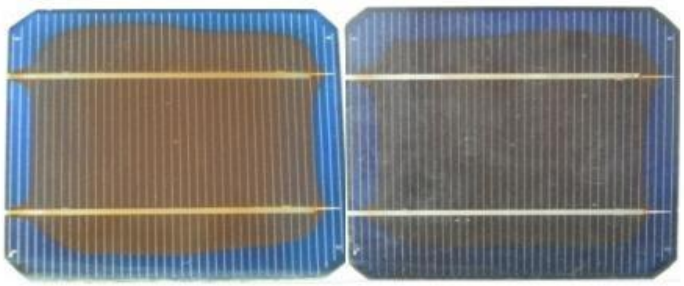

Fig.1.15. Discoloration of a crystalline solar cell

The three levels of EVA discoloration were yellowing (Y), browning (B), and dark browning (DB). The weathering-degraded yellow-brown EVA films have lost the ultraviolet (UV) absorber, Cyasorb UV 531 and the degree of cross-linking (gel content) has increased. The obvious evidence for EVA degradation is a visually discernible discoloration ranging from light yellow to dark brown [25]–[27].

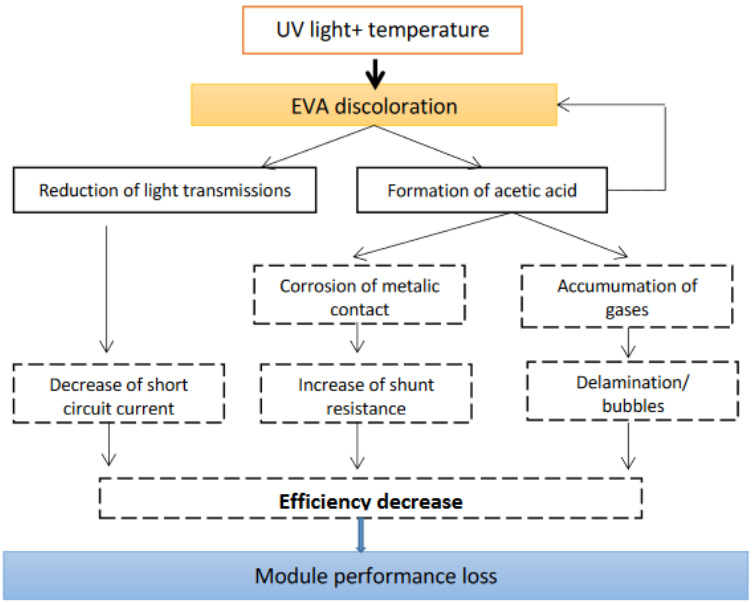

Fig.1.16. Effect of temperature combined with UV light on encapsulating material

While the initial concerns about EVA discoloration were raised about themirror-enhanced power plant at Carrisa Plains. California [28]. The yellowing of EVA has been reported not only without mirror enhancement in numerous hot dry climates (Segment 10 of Carrisa Plains; Sacramento, California; Phoenix, Arizona; Las Cruces and Albuquerque, New Mexico; Morroco; Australia; and Saudi Arabia), but also in a hot humid climate (Namibia, South Africa, Cape Canaveral, Florida). Furthermore, exposure times have ranged from 3 to 12years.

A large number of simulated degradation experiments and various analyses carried out by PERN 1992 [27] have been performed on various EVA films to verify or identify the mechanisms responsible for the EVA degradation and discoloration. The results show that three primary factors are involved:

i. Heating,
ii. Acetic acid-catalyzed reactions,
iii. UVexposure.

The secondary factors contributing to the EVA degradation are:

i. Metal ion-catalyzeddegradation,

ii. The deactivation of antioxidants by the acetic acid (per literature) produced from the primary degradingreaction.

I.3.6. Broken glass:

Glass breakage is an important degradation factor of PV modules. They occur in most of the cases during installation, maintenance, and especially during the transportation of modules on their installation sites [14]. The broken modules or with cracks may keep functioning correctly. In fig.1.17, a cracked polycrystalline PV module was operated for five years without any noticeable power degradation is shown. However, the risk of an electrical shock and of moisture inalterationincreases.

Other degradation types such as corrosion, discoloration and delamination usually follow breakages and cracks.

Fig.1.17. Broken glass of a polycrystalline PV module

I.3.7. Hot spot:

A hot spot is an area of a PV module, which has a very high temperature that could damage a cell or any other element of the module. The hot spot cause could be a variety of cell failures, including partial shadowing, cells mismatch or failures in the interconnection between cells[3], [29]. In a PV module, all the cells are connected in series, thus the same current must flow through each cell.

Shading causes a reduction of irradiation and thus a reduction of the current through the control source Iirr, on the shaded cells. On the other hand, the unshaded cells will force a larger current through the shaded cells. Since the current must be the same through the module, the difference will circulate through the shunt resistor RP of the shaded cells causing (i) heat dissipation leading to "hot spots" on the shaded cells and (ii) a reduction of the module output voltage. The latter translates in an incident operation of the module. In the long term, hot spots will reduce the lifespan of the module and must be avoided. A standard solution for this problem is the use of bypass diode protection [30], [31]. When the current through RP (and thus the voltage, according to Ohm's law V = R*I) increases above a threshold, the bypass diode becomes forward biased and provides a path for the current to circulate, thereby bypassing the shaded cells [32].

Hot spots may cause breakage of the cell and burning of the backsheet, as shown in fig.1.18. [19]. An infrared analysis of the PV installation was conducted in order to investigate further the possible origin of the hot spots fig.1.19. [33].

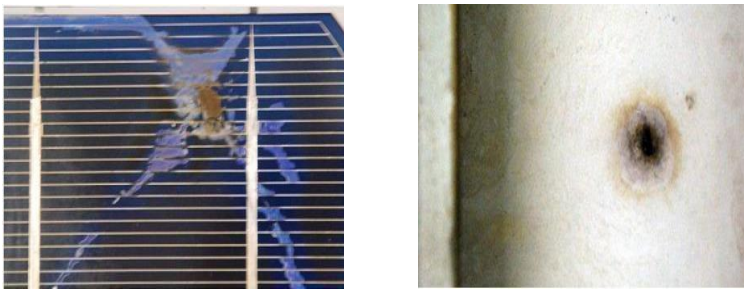

Fig.1.18. Hot spot leading to breakage of the cell and burning of the backsheet

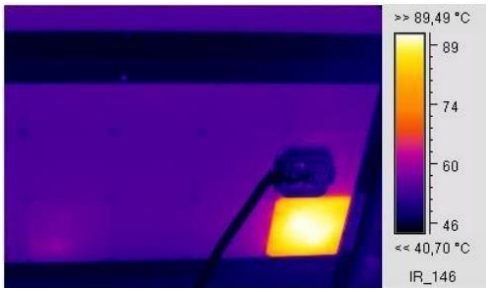

Fig.1.19. Hot spot detected using infrared camera

I.3.8. Junction box (JB)failures:

The JB is the container fixed on the backside of the module which protects the connection of cell strings of the modules to the external terminals. Generally the JB contains the bypass diodes to protect the cells in a string in case of hot spot or shadowing. Observed failures in the field are:

Poor fix of the JB to the back sheet. Some adhesive systems are good for short-term pull but poor for long term adhesion[34].

Opened or badly JBs due to poor manufacturingprocess.

Moisture ingress which causes corrosion of the connections and the string interconnects in theJB.

Bad wiring causes internal arcing in the JB. This failure is particularly dangerous because the arcing can initiatefire.

Not reliable soldering contacts of the string interconnects could cause high a resistance and consequent heating in the JB. In extreme cases the fire danger increases. These bad soldering contacts are caused by low soldering temperature or chemical residuals of the previous production process on the solder joints. [35]

A B C

Fig.1.20. JB failures: a) an open JB in the field, b) a poorly bonded JB on the back sheet, c) a JB with poor wiring. [35]

I.3.9. Bypass diode failures:

The bypass diodes reduce the power loss caused by partial shading on the PV module. Besides the power loss the diode avoids the reverse biasing of single solar cells higher than the allowed cell reverse bias voltage of the solar cells. If a cell is reversed with a higher voltage than it is designed for the cell may evolve hotspots that may cause browning, burn marks or, in the worst case, fire. Typically, Schottky diodes are used as bypass diodes in PV modules. Schottky diodes are very susceptible to static high voltage discharges and mechanical stress. So, they must be handled with care and human contact without grounding must be avoided. Consequently, many bypass diode failures may occur due to overheating [6] (fig.1.21). However, it is difficult to find them because they only attract attention when the PV modules have severe mismatch in the individual I-V characteristic of single cells, e.g. caused by shading or disconnected parts of a cell due to cell cracks.

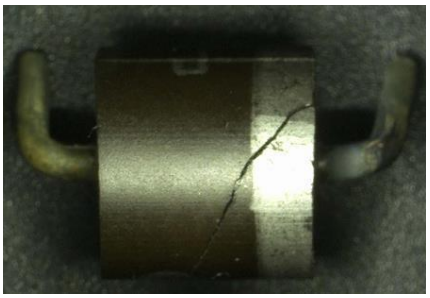

Fig.1.21. Defective (failed) bypass diode of a PV module, evidenced by visual inspection.

A burn marks are found along cell edges on the back sheet such as shown in fig.1.22. All of these PV modules are partially shaded by neighbor trees, streetlights, and PV installation. Edge isolation faults on the solar cell level are under normal condition no problem, but when the bypass diode is in open-circuit the current is driven in reverse through the shunts of the solar cells and burns the encapsulation.

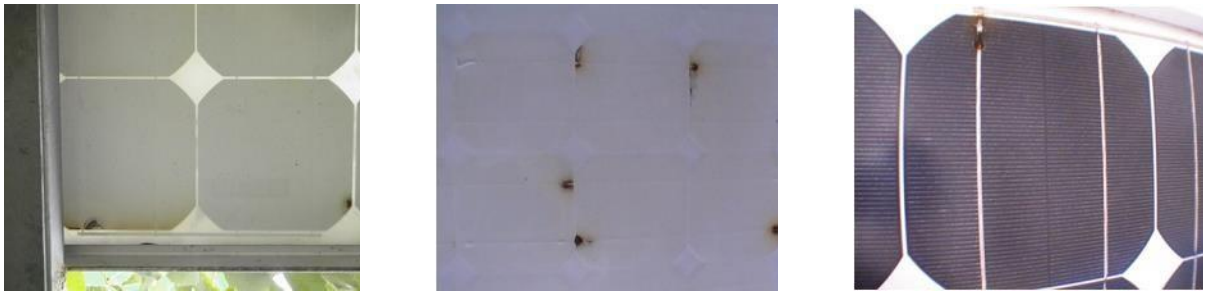

Fig.1.22. Burn marks caused by open-circuit bypass diodes [35].

For a PV module with three BP diode, if 1 is defective, the resultant I–V characteristic gives an approximately 33% drop of the V_{OC} and, thus, P_{MAX}. Similarly to electrical mismatches, the resultant power loss from defective bypass diodes has no limit loss and the PV module may end up unusable (total failure). Moreover, defective bypass diodes have a high probability of causing follow-up failures of the modules in the field, with further power loss or safety issues

I.3.10. Potential Induced Degradation (PID):

PID is a recently "discovered" fault mechanism in operating PV modules and, yet, not extensively studied and understood. It comprises a critical, externally induced factor, which is typically accelerated under hot and humid conditions and leads to excessive degradation and significant loss of power in the affected PV modules [6], [36].

Individual modules in PV systems are often connected in series to increase the voltage of the system. The potential difference of this so formed chain can sometimes reach several hundred [37].Inordertoprotectpeopleagainstelectricalshocks,allmetallicstructuresofmodulesareoften grounded. Because of this electrical voltage between PV modules and their structure, it is possible that electrons in materials used for PV modules escape via the grounded framework when the insulation between structure and active layers is not perfect and creating then leakage currents [37]. The interaction of the different panel materials is resulting in certain leakage current paths, which are illustrated in fig.1.23.

According to Mc Mahon et al [38], the leakage current path Ip2 is dominating the others. Higher leakage currents can be caused by water (vapor) entering the solar panel causing the encapsulation material becoming more conductive.

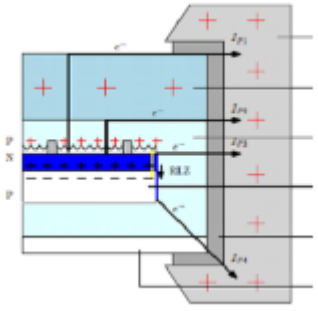

Fig.1.23. Leakage currents paths within a solar panel

From this phenomenon subsists a polarization that may degrade the electrical characteristics of the photovoltaic cells. This phenomenon known as PID is characterized by the progressive performance

deterioration of photovoltaic modules, due to the presence of an electrical current induced in the module [39]. Hacke et al. [40] showed that PID is more favorable in humid climates than in hot and dry ones. Schütze et al. [41] confirm this idea by showing that leakage current increases with humidity [3].

Depending on the technology different types of PID occur. The most prominent case for PID in silicon solar cell technology is Sunpower's polarization effect [42] but also other technologies like a-Si and ribbon silicon have been reported in the past to be prone to different types of PID under certain circumstances – either reversible e.g. polarization or irreversible e.g. electro chemical corrosion [5]. All known PID effects have one common characteristic: The degradation is depending on polarity and level/extent of the potential between cell and ground, which is determined by the actual configuration of the PV system.

Whereas increasing system voltages and the introduction of transformer less inverters certainly have a positive impact on the overall cost efficiency of solar parks, it has to be put into account that on the same time solar panels are exposed to increasing (High Voltage Stress) HVS within solar systems. So, investigating PID for standard silicon cells cannot only avoid significant power degradation in future systems. It also can be considered as a clear track for the reduction of the overall degradation of a panel is therefore a suitable method in order to expand the lifetime of a solar panel even further.

The EL image of a PV module reveals several micro-cracks, shunts, in-active regions and non-uniform EL emission (fig.1.24). According to the image some cells degrade strongly - finally being short circuited - while others appear to be stable. Being the cell the origin for PID this observation can be explained by variation of certain cell properties relevant for PID.

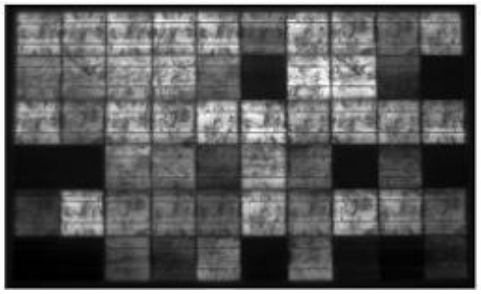

Fig.1.24. EL image of a PV module with several hundred hours of field operation

I.3.11. Bubbles:

This type of degradation is similar to delamination but in this case, the loss of EVA adhesion only affects a small area and is combined with the surface swelling whose adhesion was degraded. The bubbles are generally due to chemical reactions that emit gases trapped in the PV module. When this happens on the back side of module, congestion appears either in the encapsulating polymer or on the back side of the module thus forming the bubbles.

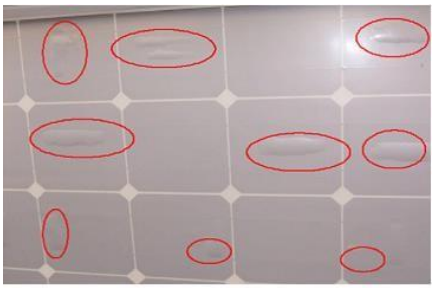

Fig.1.25. Bubbles defects shown on the PV module backside

They make it more difficult for cells heat dissipation, increasing their overheating and reduce then their lifetime [36]. In Fig.1.25, a PV module with a large number of bubbles on the back side is shown, which are usually appear in the center of the cell and may be due to poor adhesion of the cell caused by the high temperature[3], [4].

Fig.1.26 presents the IR image a PV module containing bubbles and demonstrates how a lower temperature in the back cover is detected where a bubble is situated. The bubble forms an air chamber, and although the air temperature in the chamber appears lower than in the adjacent cells, the cell temperature is actually higher because the heat of the cell is less dissipated [4].

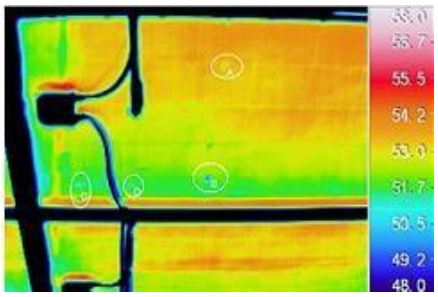

Fig.1.26. IR image a PV module containing bubbles

In fig.1.27, it can be observed how bubbles can also appear on the front side of a PV module between the glass and the cells. In this case, the bubbles are caused by a detachment between part of the cell and the glass. This kind of defect is not very common on the front side of the module [4].

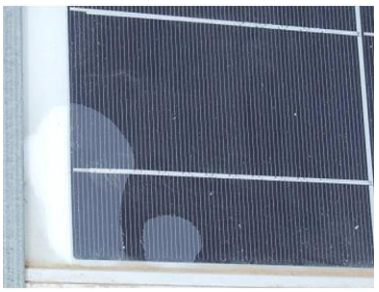

Fig.1.27. Bubbles on the front side of a PV module

Bubbles usually do not appear because cells are more rigid than polymeric encapsulant. Air or gas is accumulated in the bubbles probably due to some chemical reaction as in the case of bubbles on the backside. In the case of bubbles on the front side, apart from an excess of heating effect, a reduction in the light that can reach the solar cell may occur, as there is a decoupling of the light, and the reflection is increased[4].

I.4. Soiling phenomena

Solar radiation is one of the most abundant clean resource existing in the planet especially in region with desert land. MENA region and other countries in the Sunbelt enjoy high potential of incoming solar irradiation and the availability of area for the development and deployment of solar power plants [43]–[45]. However, those regions are known with their harsh weather conditions; hot and dry in the summer season, and wet climate with rainy days in winter. Soiling is the main challenge that impact directly the efficiency of a solar power plant (concentrated solar power or photovoltaic systems) [46]–[51]. Soiling on the front glass of PV modules results in optical losses due to the area shaded by dust particle [52]–[55]. On the other hand, the deposition of contaminants such as mineral dust deposit, biofilms of bacteria, algae, lichen, mosses or fungi, plant debris or pollen, bird droppings, engine exhausts or agricultural emissions, and industry emissions [56]–[60] onto the PV modules surface leads to an excessive reduction of power generation. This can be quantified by more than 1% power loss per day [52], [56], [61], [62]. It often makes the installation economically unreliable. To this end, the MENA region was reported to be the worst region that exhibit dust accumulation regarding the other regions [63], [64].

Dust accumulation was found to be the most significant factor affecting the efficiency of a PV module in interaction with environmental parameters as the relative humidity, temperature, wind speed, and wind direction [50], [65], [66], [51]. On the other hand, the accumulation rate of dust on the surface of the PV module increase over the time of exposition [67]. One of the pioneer studies on the early 1990s, El-Shobokshy and Hussein[68], [69] conducted a distinctive approach to study the impact of dust on the performance of PV panels. Precisely, the experiment was simulated with different nature of dust particulates (limestone, carbon, and cement) and halogen lamps. By varying the density of dust on the surface of the panel and keeping the light intensity constant the test was repeated for many times. Their studies reveal that the physical properties of dust (nature, size, and material) have a significant impact on the efficiency of the PV panels. However, the results show that for the same nature of dust fine particles have more degradation effect than coarser particles on the PV panel efficiency. The study also found the impact of cement particulates deposition to be more relevant on deteriorating the performance of the PV system of about 80% with a density of deposition of 73g/m². Although they have done a comprehensive study, since their experiment was conducted under limited indoor test conditions especially no wind effect was tested and reliance on artificial dust. One of rigorous experiment to investigate dust accumulation on glass transmittance. Hegazy[70] conducted an experimental study over a period of 1 year to investigate the effect of dust accumulation on the transmittance of a glass plates samples exposed in the Minia region, the middle of Egypt, known with his subtropical climate as the most regions of the North African desert. The experiment consisted of exposing glass plates samples for different tilt angle of 0°, 10°, 20°, 30°, 40°, 50°, 60°, and 90° for different periods of exposure 3, 10, 15, 18, 23 and 30 days. He reported that after 30 days of exposition the drop of transmittance was significant for the sample inclined with 10° with about 31% of reduction in comparison to the sample exposed vertically 90° with a drop in the range of 1%. Based on the obtained results, non-linear empirical model has been developed which correlate the glass transmittance decrease and the density of deposition taken in consideration the tilt angle and the days of exposure. The model has been proved to be accurate in the range of ±6%. As well in Dhahran, Saudi Arabia, the dust surface density has reached 6.2 g/m² for the period from February to December (10 months) [71]. In another studies, the accumulation rate of 132 mg/m²/day in Mesa, Arizona [72], and 1 to 50 mg/m²/day in Colorado [73], and 0.01 to

0.02 mg/cm²/ day has been recorded in Lahore, Pakistan for panels with a fixed tilt angle of 30° [74]. In Mediterranean climate, in Athens, Greece, the dust loading of 0.1 to 1 g/m² was recorded for a period of exposition of 2 to 8 weeks [75]. This accumulation rate is strongly dependent on dust particles concentration at the upper of the atmosphere and weather conditions of the local site [76]. In Zitouni et al. [77], they detected a daily soiling rate of 0.32%/day and 0.02%/day during the dry and the rainy periods respectively using a monocrystalline photovoltaic system. El-Nashar[36-37] evaluated the influence of dust deposition on evacuated tube collector field on the performance of a solar desalination plant located in Umm Al Nar Island, to the north-east of Abu Dhabi city. He concluded that dust deposition on the surface of the collectors reduce the transmittance of the glass tube from 0.98 to 0.70 (dusty collectors) which affect the efficiency of the system and subsequently decrease the distillation production of about 40% and increase the specific power consumption of the plant by about 38%. In Hassan et al. [80], the effect of airborne dust concentration on the efficiency of two different PV technology (amorphous and polycrystalline) was investigated in the Helwan area, Egypt for a period of 6 months. The results showed an efficiency decrease of 66% for the amorphous PV module for all the period of test without cleaning while it was about 9% for the polycrystalline in the summer months with a daily cleaning schedule. In Elminir et al. [81] experimental investigation on the influence of dust, different tilt angles, azimuth angles, and orientations on glass samples was carried out for a period of 7 months where the drop of glass transmittance was reported to be in the range between 12.38-52.54% for glass sample installed at a tilt angle of 90° and 0° respectively. On the other hand, the reduction in the transmittance samples has been found to be strongly dependent on dust density of deposition accordingly with tilt angle, as well as the orientation of the sample in conjunction with the dominant wind direction.

In reading the literature, several methods has been used to evaluate the effect of soiling and especially dust deposition on the performance of PV panels. In term of optical efficiency; the effect of dust on the transmittance of the front glass of the PV module has been widely used in order to evaluate the impact of dust deposition on the transmittance of light radiation with regard to the density of dust deposition[51], [70], [82]–[84]. Thus, will consequently reduce the incoming light to the PV cell and decrease the electrical output. However, the most reliable method is to assess the direct impact of dust deposition on the surface of PV module in term of the electrical parameters as the maximal power, short-circuit current, and the total energy production (in the case of a PV system). As dust deposits tend to attenuate short wavelengths with regards to the selective aspect of the spectral response of the PV cell, which explain the difference between light transmission loss and power loss [85].

Therefore, understanding the soiling mechanisms is highly crucial in order to develop optimized cleaning scenarios for dusty region.

I.5. Factors affecting soiling

The soiling is a phenomenon influenced by location-based meteorological factors and climatic conditions tilt angle, the sources [1]. Soiling may lead to partial shading of cells as the surface is covered with dust and thereby optical losses may occur. The different factors affecting soiling of PV panels are given in fig.1.28. It includes PV installation factors and environmental factors. The installation factors that affect soiling are height of installation, tilt angle, orientation, glazing characteristics, and PV technology used. The different environmental factors are wind speed, dust properties, ambient temperature, rainfall, humidity, and vegetation.

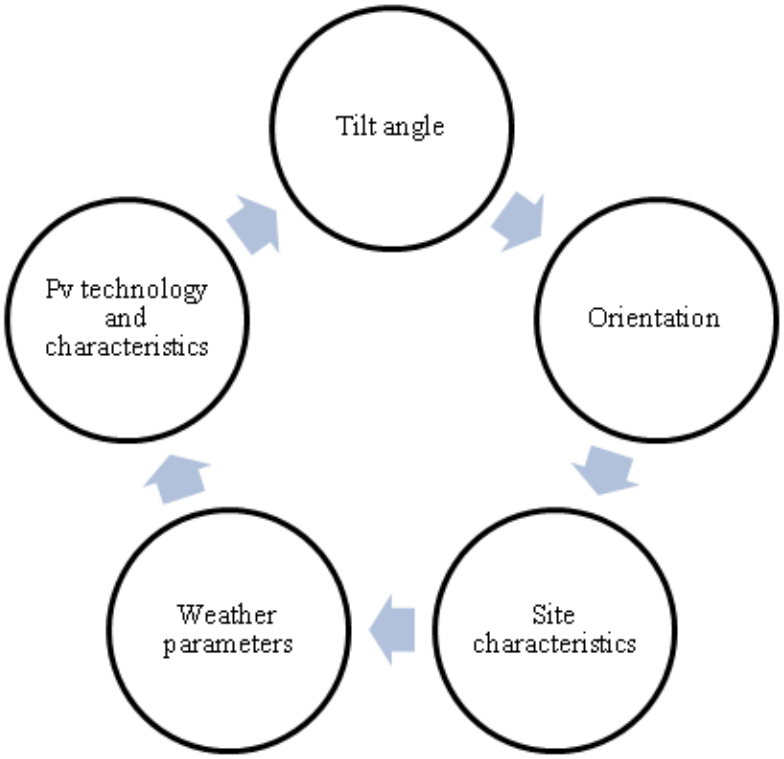

Fig.1.28. Factors affecting soiling of PV panels

I.5.1. Tilt angle and orientation

The dust particles may settle more on horizontal surfaces than the tilted surfaces [7]. The larger dust particles will roll down from top to bottom of a tilted PV module. Hence, the effect of gravitational force in dust accumulation increases as the tilt angle increases. The PV modules that are facing towards the wind will get the more influence in dust deposition compared to the PV modules kept far away from the direction of the wind. Hence, the orientation of PV panels is an important factor influencing the cleaning of panels by wind movement.

I.5.2. Ambient temperature, Pressure and humidity

Dust, humidity, and wind are the factors depending on the sun's radiation and the environment. At high ambient temperature and low relative humidity, wind carries the dust easily. The water vapor will condense and form water drops at low temperature [3]. High RH increases the dirt adhesion and forms a sticky surface over the solar panels [8]. This led to adhesive panel surface which attracts more particles from surroundings. When the airspeed is higher and there is low pressure, less soil accumulation occurs and vice-versa. The humidity changes with the irradiance in a non-linear manner and irradiance itself cause little variations in open circuit voltage and causes large variations in short-circuit current [3].

I.5.3. Site characteristics

The site characteristics involve the characteristic features of the location for PV panel installation. The area can be a metropolitan city or a village. The vegetation, natural habitats, pollution rate, pedestrian and vehicular traffic varies with location. Based on these variations, the soiling of solar panels varies as the dust pollutant types differ with geographic location.

I.5.4. Dust properties

The different properties of dust include chemical, biological, electro-static and physical properties.
The dust deposition will be different for different dust properties. The physical property of dust includes its size, shape, and weight. The small dust particles settle down more than that of the larger dust particles on the PV panel surface [2]. The different electrostatic property includes neutral,

positively charged and negatively charged particles. Generally, the charged particles cause more dust deposition than the neutral particles because the like charges attract and unlike charges repels.

I.5.5. Wind velocity

There are two effects of wind speeds on the dust settlement. In [5], it is claiming that the high wind velocities result in high soiling rate than the low wind speeds. But in other papers, the high wind velocity will clean the panels against soiling if it is oriented towards the wind movement. It is seen that the chances of dust settlement are more at light wind speeds. For the wind with high amount of airborne dust, the possibility of dust accumulation is more [3].

I.5.6. Glazing characteristics

The dust accumulation on PV panels varies with the property of panel surface. The surface texture and additional coating on the PV panels comprise the surface property. For plane surfaces, the dust accumulation is lesser. The textured panels have rough and irregular surfaces increase the soiling on panel surface [2]. A protective layer of glass on the PV module surface is less affected by dustdeposition.

I.5.7. Environmental effects

The environmental effects on soiling arise from the variations in atmospheric and climatic conditions.

The air borne dust concentration, probability of dust storm, the occurrence of dew, rainfall, volcanic eruptions, etc. contribute to soiling of PV panels.

I.5.8. PV technology and cell configuration

The soiling affects the different PV technologies differently based on the spectral transmittance. The PV technologies include monocrystalline PV panels and polycrystalline PV panels. The performance of PV panels varies with its technology.

I.6. Dust life cycle

Recently, many research studieshave been done on the processes governing the transport and deposition of dust in solar power plants [86], [87]. All these studies have concluded that the impact of dust on PV modules follows a cycle, which is called the life cycle of dust. This cycle contains four main stages (generation, deposition, adhesion and finally removal or elimination at the level of the panel) as indicated in Fig.1.29.

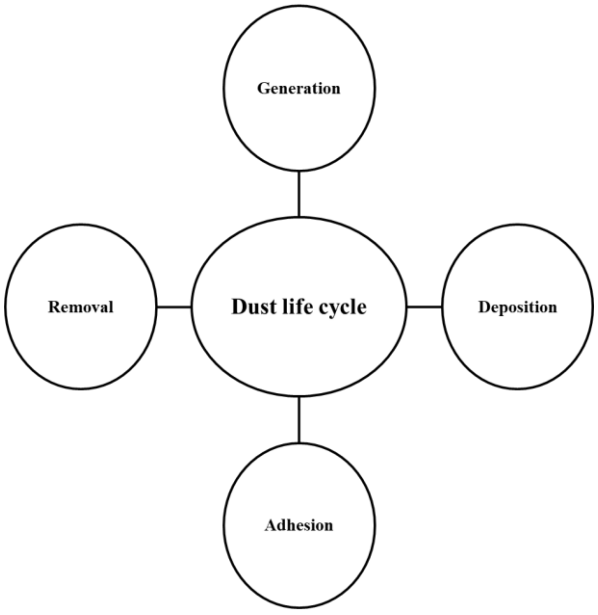

Fig.1.29. The dust life cycle.

I.6.1. Generation

The charging of the atmosphere with dust particles is mainly linked to soil erosion due to the wind [88], [89]. The wind emission produces when the wind has enough power to move the granular crushed material [90]; therefore the wind is the main phenomenon who allows raising dust to the atmosphere. We can distinguish three different modes of transport of particles by the wind speed, presented in Fig.1.30[89].

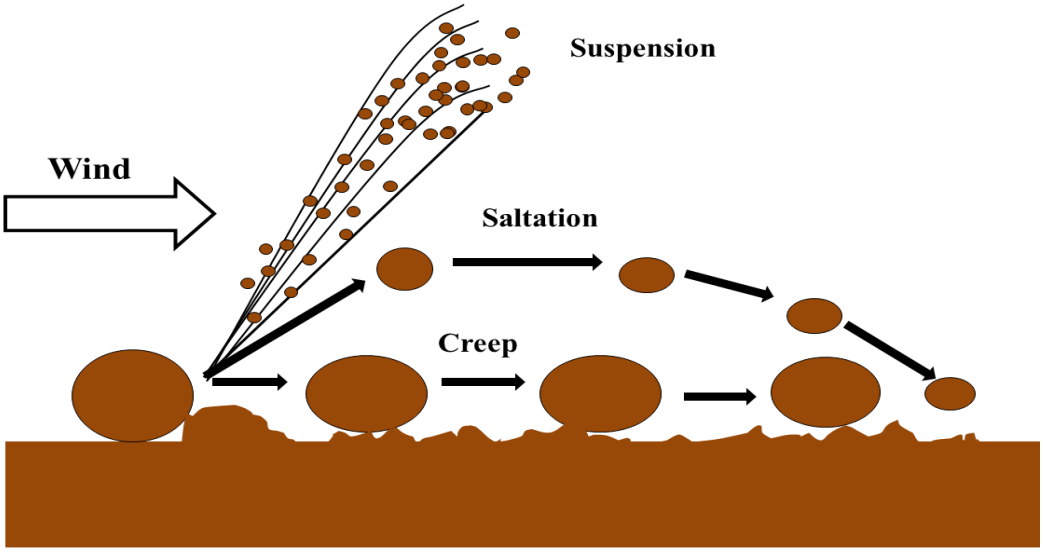

Fig.1.30. Modes of transport of particles by wind speed

Suspension: In general, fine dust can only be carried away if it has been thrown into the air by the impact of larger grains. Once in the turbulent layer, they can be lifted to great heights by ascending air currents and form dust clouds reaching altitudes of 3 to 4,000 meters. Their appearance can be impressive; the essential mechanism of wind erosion remains saltation, because without it such clouds could not occur.

Saltation: The initial movement of soil particles is a series of jumps. The diameter of the saltation particles is between 0.5 and 1.1 mm. After having jumped, the particles fall back under the action of gravity. The descending part of the trajectory is very inclined towards the ground and practically straight. Few particles reach an altitude greater than 1m and about 90% of them jump less than 30cm. The horizontal amplitude of a jump is generally between 0.5 m and 1m. The saltation phenomenon is essential to initiate wind erosion. It is the cause of two other modes of transport of soil elements by wind: surface crawling and air suspension.

Crawling: Larger particles roll or slide across the soil surface. Too heavy to be lifted, their movement is triggered by the impact of saltation particles rather than by the action of the wind. The particles which move in this way to a diameter of between 0.5 mm and 2 mm depending on their density and the wind speed.

I.6.2. Deposition

Once the dust particles have been assessed and suspended in the atmosphere. Many factors influence the deposition of dust on photovoltaic panels, two main types of deposit can be mentioned:

- Dry deposition: The desert aerosol cycle ends with the deposition of particles on the PV modules surfaces, under dry or wet atmospheric conditions. Dry deposition is mainly controlled by gravitational forces [91], which cause the particles to sediment. The particles dry deposition depends on several variables such as wind speed, friction speed, turbulence intensity and atmospheric stability [92].

  The sedimentation rate depends on the size of the particle. Sedimentation is a function of particle size, with the larger particles falling first and the smaller ones last. As a result, the larger and heavier particles will be deposited near the region of origin, while the smaller ones will be deposited farther away. Turbulence can also play a role, disrupting the flow of particles [93]. If the turbulence occurs near the surface, then the particles are deposited faster.

  The transfer of the dust particles to the surface of the panels is done through different mechanical processes as shown in Fig.1.31; sedimentation, Brownian diffusion, turbulent impaction and interception processes [94].

- Wet deposition: Wet deposition occurs when dusty air masses are mixed by convection with moist or cloudy air masses. Mineral particles can be captured directly by precipitation or by droplets within the cloud.

  The rate of wet deposition depends on the rate of precipitation and the rate of droplet fall. Particles between 0.1 and a few μm in size have the lowest sedimentation velocities, so they will be mostly deposited by wet deposition [86].

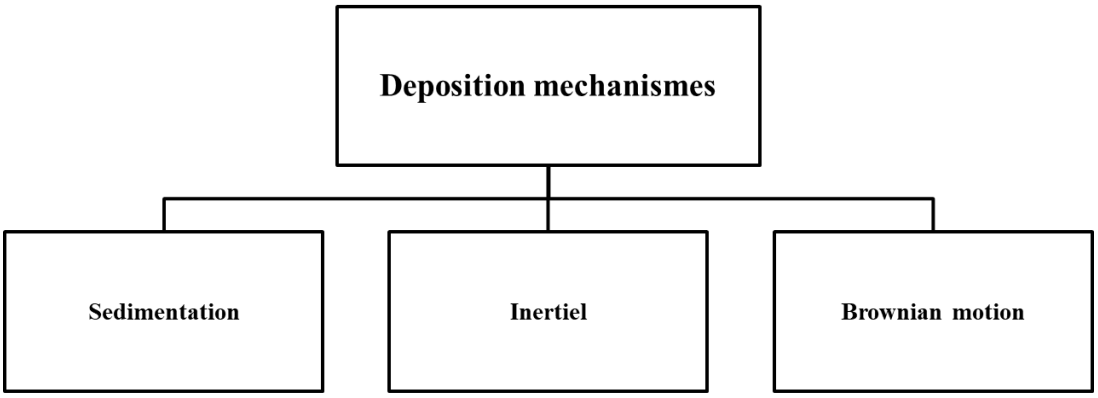

Fig.1.31. The depositionmechanisms

I.6.3. Adhesion

Dust is initially deposited on the surface of the photovoltaic panels, the adhesion forces such as van der Waals forces, electrostatic forces and capillary forces are the active forces that cause the particles to bind to the surface. The adhesion processes of these forces are described in Fig.1.32.[95].

- Due to the strength of van der Waals, small dry dust particles stick to a dry surface. This force is considered the dominant force between a solid platform and a dry particle under dry ambient conditions. The van der Waals forces are always present between the surface and the particles and act over a short distance since they originate from two surfaces that are in contact with interacting dipoles.
- The capillary force depends on both the air's humidity content (RH; relative humidity) and the surface. Capillary forces act when two moist bodies meet. The water vapor condenses into fine particles, thus enabling the gap between the dust particles and the surface of a PV module to be bridged leading to the adhesion.
- Electrostatic force causes adhesion in the presence of charges. Dust particles tend to acquire electric charges in the atmosphere by colliding with each other, and these charged particles tend to attract a positive charge to the surface, inducing a coulomb force.

All adhesion forces are active almost everywhere, but the extent of their adhesion is determined by the environmental condition and the property of the dust particles.

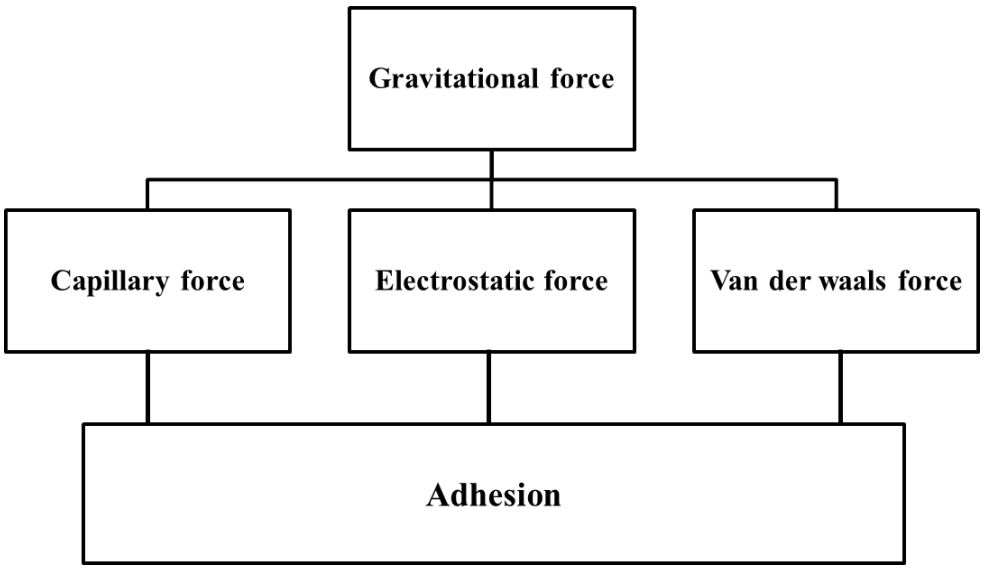

Fig.1.32. The adhesionmechanism

I.6.4. Removal

The elimination phase is the process of cleaning the particles from the surface. Basically, there are two types: Natural elimination and artificial elimination. The natural removal phase is when particles are removed by natural causes such as wind and rain. It consists of two phases: rebound and resuspension. However, artificial removal is done using specific tools to remove dust particles [96].

- Natural elimination : Two factors influence the natural cleaning process: the particles propreties (composition, number and size range) and the local weather conditions (frequency, intensity, rain and wind duration).

  The conditions taken into consideration for this process are : the alteration conditions, duration and the angle orientation of the surfaces (angle of inclination).

Consequently, it has been found that particles with a diameter of less than 10μm which are the most present on the surface of the panels,are eliminated by the natural cleaning forces.

- Artificial elimination: As regards artificial cleaning, they depend mainly on the type of contact device (brush and soft cloth), the quality of the water used (demineralized and tap water), the water pressure, additives and the state of the water (liquid and vapor).

Chapter: 2

Experimental investigation and modeling of photovoltaic soiling loss as a function of environmental variables: A case study of semi-arid climate

II.1. Introduction

The main objective of this chapter is to develop a prediction model of the soiling ratio as a function of the environmental variables (WS, RH, Tamb, WD, and precipitation) able to describe the SR evolution under semi-arid climate.

In this chapter, the impact of soiling on photovoltaic performance is assessed by calculating the soiling ratio, the energy difference, and the difference in performance ratio of an amorphous PV system over a period of one year of measurement at ground level.

After data collection, MLR, MLRWI, RSM, and ANN models are developed to predict the daily soiling loss using the environmental variables. As well, dust analysis is carried out by SEM, EDS, and XRF in order to define the mineralogy and morphology of the collected dust from the surface of the investigated PV plants.

II.2. Methodology and study protocol

The outdoor experiments were conducted at the Green energy park facility from August 21st, 2017 to July 30th, 2018. An amorphous PV system was installed at the platform with coordinates of 32°17’ N and 7°57’ W.

During the study period, a clean PV string was placed side by side to a no cleaning string (Fig. 2.1) under the same weather conditions to quantify the dust effect relatively. The modules specifications at standard conditions are listed in Table 2.1.

During the testing period, the electrical outputs (P_{MPP}, I_{MPP}, and V_{MPP}) of the dusty string and its clean reference were measured daily at the same moment for a systematic comparison.

Fig.2.1. The studied system.

Table.2.1.The main characteristics of the PV String at STC

Technology type	**Amorphous**
The nominal power (P_{max})	1080 W

The open circuit voltage (V_{oc})	490.4 V
The short circuit current (I_{sc})	3,41 A
The maximum voltage (V_{max})	376 V
The maximum courant (I_{max})	2,88 A

The meteorological data parameters were collected from a weather station installed at the same site using several sensors with high accuracy as described in Table 2.2.

Table.2.2. Meteorological station sensors.

Parameter	**Sensor**	**Spectral/Operating range**	**Accuracy**
Temperature	Campbell Scientific CS215	-40 °C to +70 °C	±0.3 °C at 25 °C ±0.4 °C over +5 °C to +40 °C ±0.9 °C over -40 °C to +70 °C
Relative humidity	Campbell Scientific CS215	0% to 100%	±2% over 10 to 90% ±4% over 0 to 100%
Wind speed	NRG #40CAnemometer	1 to 96 m/s	< 0.1 m/s over 5 to 25 m/s
Wind direction	NRG #200PWind vane	0° to 360°	< 1%
Tipping Bucket Rain Gauge (precipitation)	Young 52202 / 52203	Resolution 0.1 mm per tip	±2% up to 25 mm/h ±3% up to 50 mm/h

From the monitored data, the energy, the soiling ratio and the Performance Ratio (PR) were used to investigate the soiling impact on the string.
The PR is a parameter used for performance comparison defined as:

$$PR=\frac{Y_f}{Y_r} \quad (1)$$

where Y_f is the energy yield in [Wh/Wp] defined as:

$$Y_f = \frac{E}{P_n} \quad (2)$$

where E is the daily array DC energy output in [Wh] and P_n is the peak power at Standard Testing Condition STC in [Wp]. Y_r is the reference yield defined by the following equation:

$$Y_r = \frac{G_{poa}}{G_r} \quad (3)$$

where G_{poa} is the total incident irradiance at Plane of Array POA in [Wh/m²] and G_r is the irradiance at STC in [W/m²].

The soiling ratio in this study was quantified using the maximal current from both clean and dirty strings. The current has been often used in literature and is still considered as a good electrical parameter to estimate soiling loss [97].

Each daily average current (I_{max} (i)) considered in this work has been calculated as:

$$I_{max}(i) = \frac{\sum_{h=11}^{14} I_{max}(h)}{n} \quad (4)$$

where I_{max} (h) is the mean hourly maximal current measured per each string and n is the number of hours used for the daily average.

Data was collected as one min data and averaged into hourly values. Only data recorded between 11:00 AM and 2:00 PM and under clear sky conditions (irradiance ≥ 600 W/m²) were then considered for the calculation of the daily values.

The soiling ratio (SR) measures the ratio between the normalized maximal currents of soiled and cleaned PV strings for each day, as follows:

$$SR = \frac{I_{max\_d}}{I_{max\_c}} (5)$$

where (I_{max_d}) and (I_{max_c}) are the average daily maximal currents of the dirty and clean strings, respectively.

PV performance and weather data were convertedinto daily values.The quality of each dataset was independently checked and stored in the soiling stations.

II.3. Experimental results

II.3.1. Metrological data

Fig.2.2 presents the humidity and the temperature variation during the test period. From the figure, three periods can be observed: P1 (from August 18th to November 29th, 2017), P2 (from November 30th, 2017 to March 27th, 2018), and P3 (from May 03rd to July 30th, 2018). Considering P1, P2, and P3 respectively, the average daily temperature is 23 °C with 35.9 °C maximum and 14.2 °C minimum for P1, an average daily of 11 °C with 17.1 °C maximum and 4.9 °C minimum for P2, and an average daily of 21 °C with 29.2 °C maximum and 13 °C minimum for P3 respectively.

For P1 and P3 where higher temperatures (mostly from August to November and from May to July) are related to the lack of rainfall, while lower air temperatures in P2 (mainly from November to April) are related to a higher frequency of rainfall events.
For the relative humidity, it has an average of 46.3% with 75% maximum and 17% minimum for P1, an average of 77.3% with 94% maximum and 43% minimum for P2, and an average of 61.6% with 96% maximum and 35% minimum for P3.

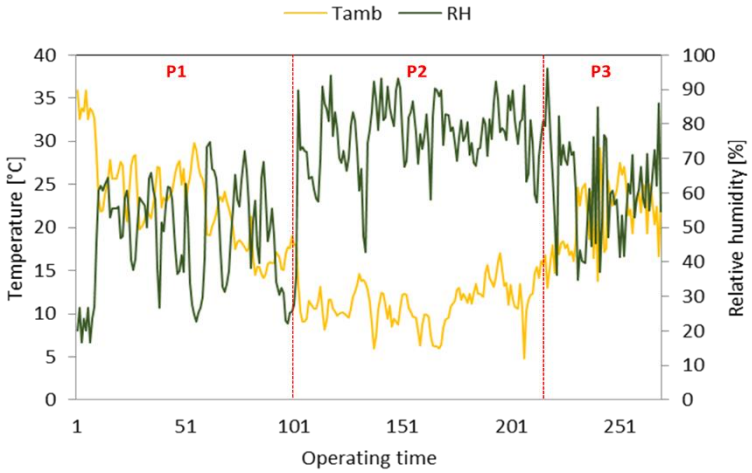

Fig.2.2.The daily ambient temperature (left y-axis) and relative humidity (right y-axis).

The wind speed and direction are presented in Fig.2.3, as can be seen, the speed is mainly between 0.9 m/s and 7.9 m/s, which are average values according to [98] and subject to dirt deposits.It should be noted that the wind direction blows mainly from the northeast and southeast which may influence the SR, because the PV modules are oriented towards the south.In addition, a higher wind speed is detected between the southwest and the northeast; this can also influence the dust deposition. In both cases, the concentration of particles may be dependent on the direction of the wind, it means that the number of particles can vary depending on the direction from where the wind blows [99], which is beyond the scope of this work.

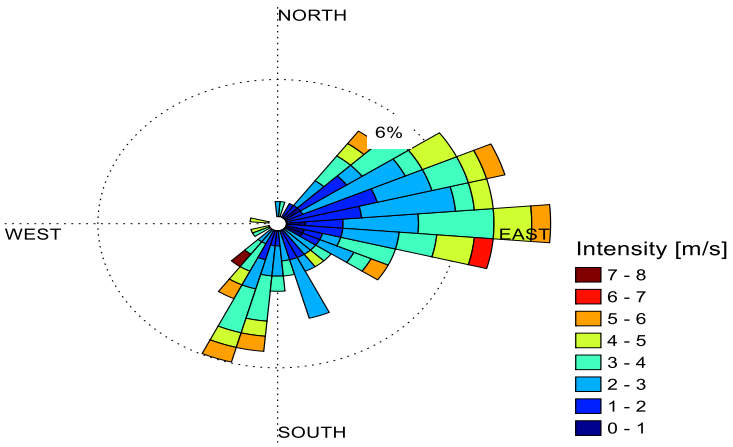

Fig.2.3. Wind Rose throughout the investigation period.

II.3.2. Dust analysis

Many researchers [100]–[102] have concluded that the physical and chemical properties of dust have a significant effect on the accumulation of dust particles which leads to a decrease in the performance of solar panels.

For this purpose, dust analysis was carried out by SEM, EDS, and XRF in two periods (December 2017 and June 2018) in order to define the mineralogy and morphology of our dust samples.

The EDS analysis of the dust was done in two periods; the results are displayed Fig.2.4. The results showthat there are major components present in the two periods as: oxygen (O), silicon (Si), calcium (Ca), aluminum (Al), iron (Fe),magnesium (Mg), potassium (K), and phosphorus (P).Nevertheless, some components were detected with low percentages, like titanium (Ti), sodium (Na), zinc (Zn), chlorine (Cl), and sulfur (S) were only seen in the December sample. Results show that around 80% of the major components of our samples are oxygen, silicon and calcium.

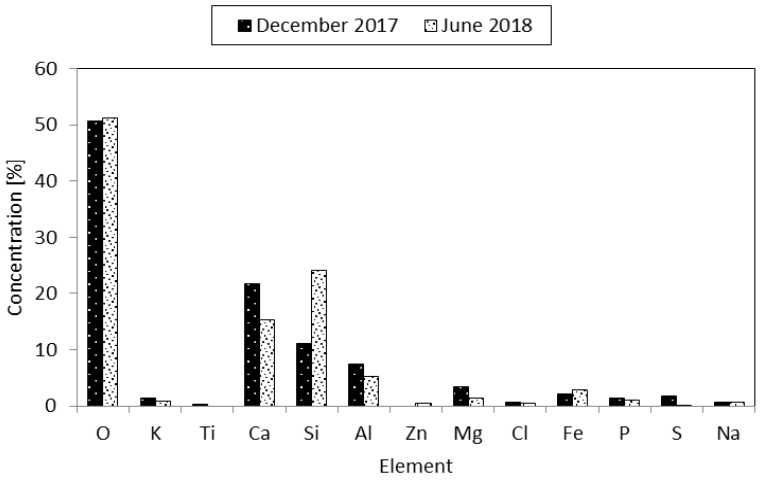

Fig.2.4. The EDS results of the local soil.

Fig.2.5 shows that silicon dioxide and calcium oxide represent the bulk of the accumulated dust in the two periods followed by Alumina. These components are generally extracted from calcite, dolomite, and quartz, which are attributed to construction activities in local urban areas as well in the semi-arid climate. The change in percentage for the two periods is due to the wind movements.

It has also noticed that for long exposition (June 2018), the presence of some components which were not present in the short exposition (December 2017) such as magnesium oxide, iron oxide and sodium oxide.

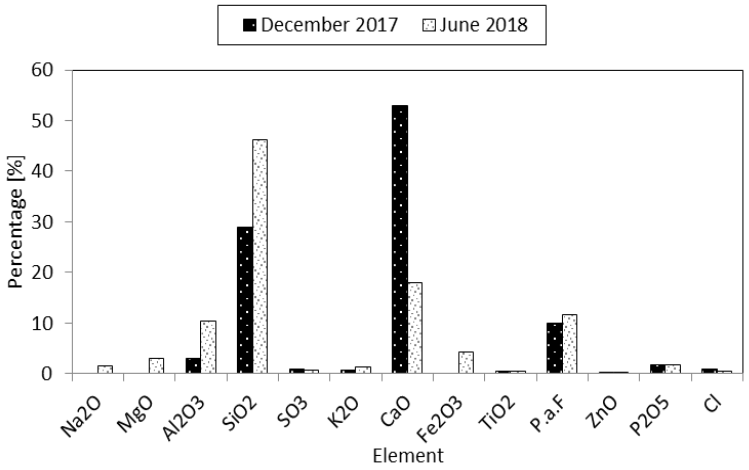

Fig.2.5. The XRF results of the local soil.

In order to define the morphology, a SEM micrograph of the dust particles was taken for the two periods as shown in Fig.2.6.

The results show different particle sizes with different morphologies. The larger particles of the order of a few tens of µm in diameter are more observed in Fig.2.6a (short exposition time). Although some particles have irregular shapes, the majority of the deposited dust particles have spherical shapes.

The morphology of dust particles changes with increasing exposure time. For a short exposure Fig. 6a, irregular shapes are found, while for a long exposure time Fig.2.6b, agglomerated particles are found.

The high proportion of smaller particles over a long period of accumulation is due to the natural resuspension processes in which larger particles were removed by wind or light rain.As reported in [45], that in addition to soluble materials on the surface, particles such as Na, Cl, K, S, C react with the moisture, which causes the grains to clump together, and consequently leads to the cementing of the dust particles with the surface of the PV module. Besides, they have observed that these elements (Ca, Si, Fe, Mg and Al) are present in all dust samples, and mostly associated with natural soil crust. Furthermore calcium from calcite was the most abundant element followed by silicon from quartz. The lower exposure times shows a presence of Na and Cl originating mainly from sea spray.

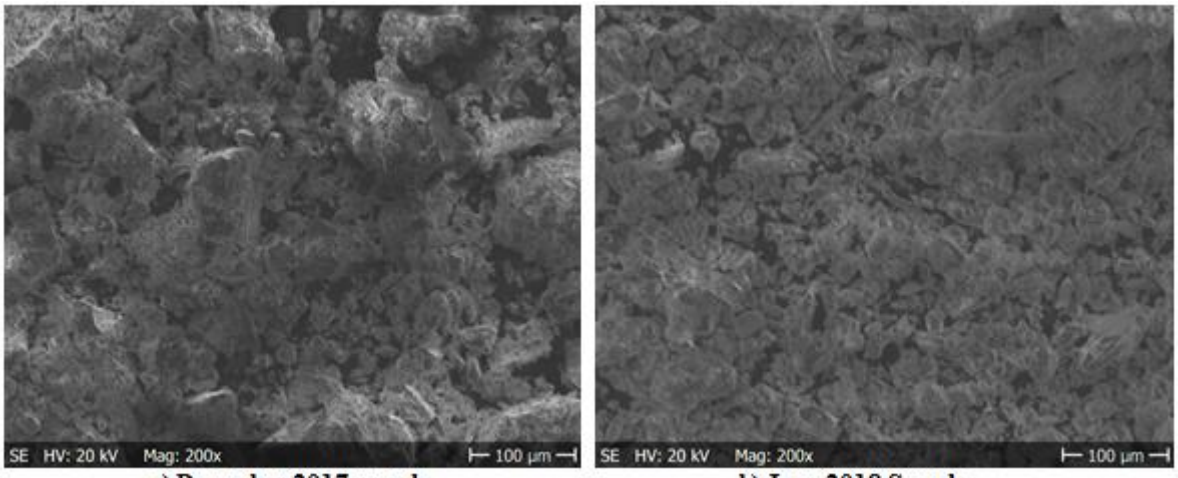

Fig.2.6. SEM micrograph of the dust samples

II.3.3. Soiling ratio

As mentioned above, the soiling ratio (SR) was calculated from Eq. (5) using the average of the current from 11:00 AM to 2:00 PM for the dusted and cleaned strings.Fig.2.7 shows the soiling rate with respect to the increase in the exposure time. We have also shown the precipitation data along with the exposure time. In fact, three periods can be observed P1 (from August 18th to November 29th, 2017), P2 (from November 30th, 2017 to March 27th, 2018), and P3 (from the May 03rd to July 30th, 2018), it is noted that the rate of soiling varies in a regressive way from 1 (clean state).

We notice that during P1 (dry period with one day of precipitation), the soiling ratio changes in a regressive way from 1 (clean state) to 0.83 (17% of performance loss) until October 9th. In October 10th the SR resumes the initial value (SR=1) due to precipitation and starts to decrease again until reaching 0.85 (15% of performance loss) in November the 29th. For the second period P2 (wet period), the soiling ratio values were around 1 (clean state) due to the presence of significant amount of precipitation (a total of 173 mm). Concerning P3 (dry period without precipitation), a cumulative soiling ratio of 0.72 (28% of performance loss) was reached. During the dry periods P1 and P3; the daily soiling ratio reaches an average of ~ 0.17%/day and 0.35%/day respectively. During the rainy period P2; the daily soiling ratio reaches an average of ~ 0.017%/day.

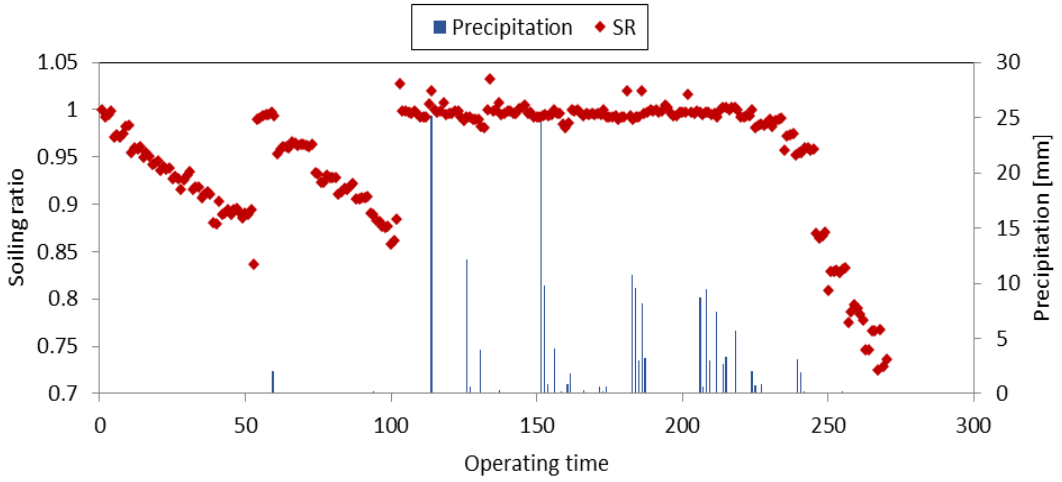

Fig.2.7. The soiling ratio as function of the precipitation.

II.3.4. Energy and performance ratio

The energy of cleaned and dusty strings is plotted in Fig.2.8 as a function of the difference in energy of the investigated strings. After evaluating the system data recorded from August 18th, 2017 until July 30th, 2018, it can be noticed that the production of the dusted string was always lower than the cleaned one during the dry period from August 18th to November 29th, 2017 and from May 1st until July 30th, 2018. Indeed, the maximum difference was obtained in (July 25th, 2018) where the energy produced by the cleaned string was about 7.11 kWh, while, the dusted one produced an energy of 5.16 kWh, which leads to a decrease of 1.9 kWh of the performance. However, during the rainy days the two strings have the same production (as in January 11th, 2018 for example) where the energy produced by the cleaned string was about 5.1458 kWh, while, the dusted one produced an energy of 5.1451 kWh.

In some days, it can be noticed that a decrease in the energy of both strings due to some specific events. In fact, in September 26th, 2017, October 10th, 2017, May 23th, 2018, and June 21st, 2018, the energy was lower due to a power outage. However, In the period from November 30th, 2017 until March 31st, 2018 the drop in energy is due to cloudy days. In October 11th, 2017 the energy difference drops from 0.73 kWh to 0.03 kWh due to rainfall.

During the dry periods (period P1 and period P3), the energy loss due to soiling reached 0.43 kWh/day and 0.61 kWh/day with a total of 43.91 kWh and 35.65 kWh respectively. As seen, the total energy loss is bigger for P1 because the exposure time was bigger. Regarding the rainy period from (period P2), the energy loss due to soiling reached 0.03 kWh/day and a total of 2.95 kWh.

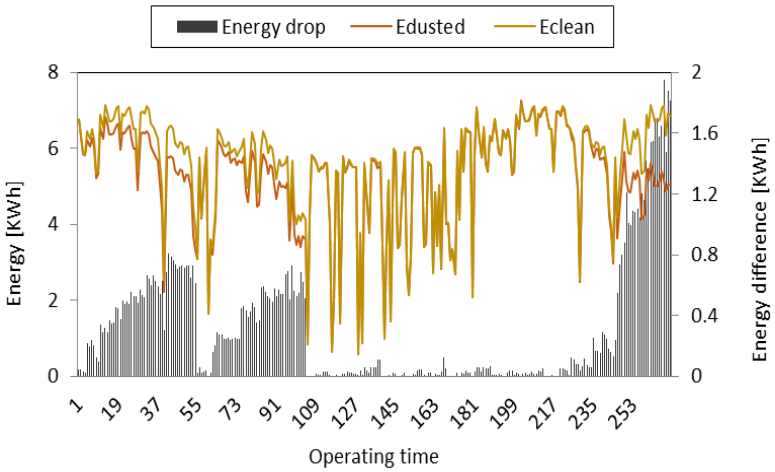

Fig.2.8. The energy of the dusted and cleaned strings in function of the difference in energy.

Fig.2.9 shows the Performance Ratio difference (ΔPR) between the soiled and the cleaned system. This parameter is calculated from Eq. (3).Similar to the soiling ratio, the PR drop increases with the absence of rain. In October 10th, 2017 the ΔPR decreases from 14% to 0.7% with the presence of precipitation.

During the dry periods P1 and P3; the daily performance ratio drop reaches an average of ~ 6.1%/day and 10%/day and a maximum of 14% and 26% respectively.

During the rainy period P2; the daily performance ratio reaches an average of 0.5%/day and a maximum of 1.6%.

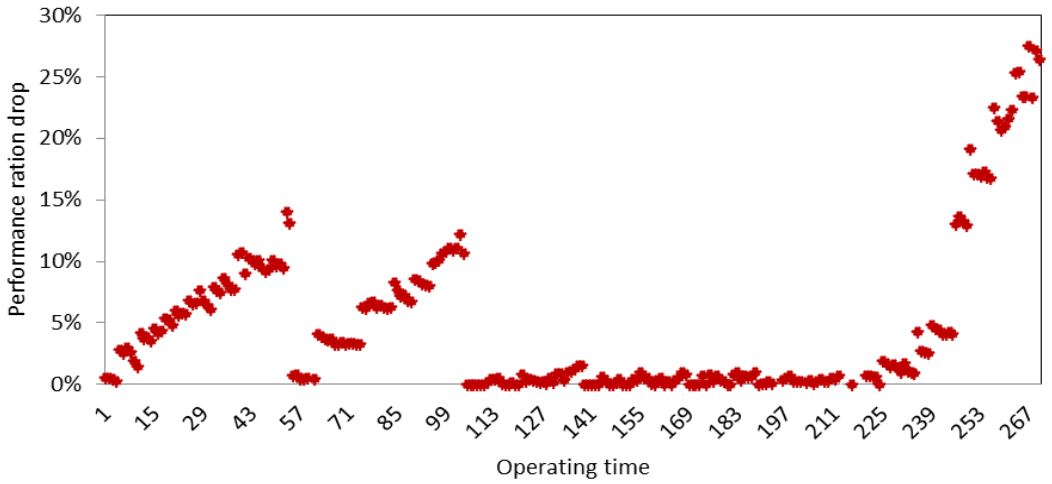

Fig.2.9. The performance ratio difference of the system.

II.4. Modeling results

Analysis of variance (ANOVA) has been applied to estimate the statistical parameters and to detect the correlations between the environmental variables (independent variables) and the soiling ratio (response). Two linear models as the multiple linear regression model (MLR) and multiple linear regression with interaction model (MLRWI), and the mathematical model generated by the response surface methodology (RSM) were developed for this analysis. The accuracy of the model prediction was evaluated by the coefficient of determination (R^2), adjusted R^2 (adj-R^2), and root mean square error (RMSE). Apart from this, an ANN model was set up to override the complexity of the PV soiling loss as a function of environmental variables.

II.4.1. Multiple linear regression models

Soling ratio is a parameter which is directly linked to the environmental data where the PV module is installed [99], [103].To understand how environmental data (ambient temperature, relative humidity, wind speed, precipitation, and wind direction) affects the variation of the SR, we have modelled soiling ratio as a function of environmental parameters. As a benchmark for modeling the SR [104], [105], a Multi-variable linear regression (stepwise method) model was implemented in this work. This model had been used to sets of data measured during one year of experiment as described above.

MLR models is based on statistical technique to predict the result of a variable based on the value of two or more parameters [106], [107]. The MLR allows analysts to determine the model variation and the relative contribution of each independent variable in the total variance. However, two types of MLR model are proposed, the simple regression and regression with interaction. Here is the equation of a simple regression:

$$Y_i = \beta_0 + \beta_1 x_{i1} + \beta_2 x_{i2} + \ldots + \beta_n x_{in} \quad (6)$$

where: β_0 , β_1, β_2 , … β_n are the model parameters.

The stepwise method begins with only a constant intercept and follows towards a linear model, by testing several variables combinations, and ends with the one that maximizes the adj-R^2.

Table 2.3 shows the details of the simple regression model. The inputs of the model are the ambient temperature, relative humidity, wind speed, precipitation, and wind direction. The MLR has the following statistical parameters: R^2 = 0.23, adj-R^2 =0.21 and RMSE = 0.0567. As it can be seen from the given results in the table, the ambient temperature has a great effect on the SR (p-value < 0.01) as well as the precipitation compared to the others parameters. However, the higher value of ambient temperature is linked to more soiling. So, it can be concluded that the higher ambient temperature is connected to summer days, which means that the soling ratio is seasonally connected.

Table.2.3. The ANOVA results for the simple regression model.

Parameters	**Coefficients**	**P_{value}**
Constant	1.025	-
Tamb	-0.0033	<0.01
RH	$9.44*10^{-5}$	0.7704
WS	-0.005	0.1426
Precipitation	0.003	0,0985
WD	$-4.07*10^{-5}$	0.2291

Multiple linear regression is not enough to explain the best interaction between the parameters data to predict correctly the soiling ratio. Thus, multiple linear regression with interaction (MLRWI) was used in order to have more ideas about the combinations between the environmental data. The MLRWI is given by the following equation:

$$SR = \beta_0 + \beta_1 x_1 \beta_2 x_2 + \ldots + \beta_{n-1} x_{n-1} \beta_n x_n \quad (7)$$

This model has the following statistical parameters R^2 = 0.48, adj-R^2 =0.46 and RMSE = 0.046. The MLR with interaction has a higher R^2 and adj-R^2 and lower RMSE compared to those of MLR model without interaction. The R^2 is improved from 0.21 to 0.48, which shows the importance of interaction terms. This latter has a real physical meaning in the description of soiling prediction as a function of environmental data. The terms in Table 2.4 with a P-value higher than 0.01 are not significant, which means that the interaction of these terms does not have an effect on the SR.

Table.2.4. The ANOVA results for multiple linear regression model with interaction.

Parameters	**Coefficients**	**P_{value}**	**Remarks**
Constant	1.0689	-	
Tamb	-0.0055	**< 0.0001**	Significant

RH	1^{22}	< **0.0001**	Significant
(Tamb-17,6015)*(RH-62,2344)	-0.0001	< **0.0001**	Significant
WS	-0.0038	< **0.0001**	Significant
(Tamb-17,6015)*(WS-2,87926)	-0.0035	< **0.0001**	Significant
(RH-62,2344)*(WS-2,87926)	-0.0012	< **0.0001**	Significant
Tamb-17,6015)*(RH-62,2344)*(WS-2,87926)	$-7.48*10^{-5}$	0.0036	
Precipitation	-0.0022	**0.00019**	Significant
(Tamb-17,6015)*(Precipitation-0,64259)	0.0008	< **0.0001**	Significant
(WS-2,87926)*(Precipitation-0,64259)	0.0092	0.0968	
(Tamb-17,6015)*(WS-2,87926)*(Precipitation-0,64259)	0.0009	0.2291	

II.4.2. RSM model

Response Surface Methodology (RSM) is a set of mathematical and statistical approach utile for modeling and analyzing problems in which a response of interest is influenced by different parameters where the objective is to optimize this response [108]. The underlying logic of the method is fitting a sequence of local regression; first, far away from the optimum or in a large area, the response surface is often fairly well described with a sample model as the first order model, where we only have the main effects part of the model, as described above the linear model has the form:

$$Y = \beta_0 + \beta_1 x_1 + \beta_2 x_2 + \cdots + \beta_k x_k + \varepsilon \quad (8)$$

Second, a quadratic model will be useful when we approach the optimum or in a smaller area, then a more complex model is often necessary to provide a good approximation of the underlying true surface. A second order model often provides a good approximation:

$$Y = \beta_0 + \sum_{i=1}^{k} \beta_i x_i + \sum_{i=1}^{k} \beta_{ii} {x_i}^2 + \sum_{i<j} \sum \beta_{ij} x_i x_j + \varepsilon \quad (9)$$

where β_0 represents the regression or the intercept coefficient; β_i, β_{ii}, and β_{ij} represent respectively the linear, quadratic, and interaction coefficients; x_i and x_j the coded values of the independent variable; and ε the random error.

As described above that the ANOVA is used to estimate the statistical parameters. The details of the regression analysis are given in table 2.5. The significance of the regression model and individual model parameters was performed based on the F-value and P-value (probability value) with a confidence level of 95%. The higher F-value and the lowest P-value (Prob.>F in Table 3.5) describe the significance of the corresponding parameter [109]. The F-value of 431.55 indicates that the ambient temperature (Tamb) is significant for the model. Additionally, with the adopted confidence level all the terms of the model are significant when the values of the Prob.>F are less than 0.05. In this case, the interaction between ambient temperature and relative humidity (Tamb*RH) is significant, also for the interaction between ambient temperature and wind speed (Tamb*WS), the interaction between relative humidity and wind speed (RH*WS), the interaction between ambient temperature and precipitation were significant. The quadratic term of wind direction was also significant with F-value of 128.03.

Table.2.5. The ANOVA results for the independent variables and significance to SR ($p<0.05$).

Source	Estimation	Standard error	Sum of squares	F value	Prob.>F (P value)
Constant	1.0930575	0.034604	--	--	--
Tamb	-0.006082	0.000926	0.09305595	431.552	**<.0001**
RH	-0.000602	0.000355	0.00620004	28.753	0.0912
WS	0.002994	0.003647	0.00145291	0.6738	0.4125
Precipitation	0.007512	0.007766	0.00201751	0.9356	0.3343
WD	3.68E-05	3.93E-02	0.00189489	0.8788	0.3494
Tamb*Tamb	-0.000213	0.000205	0.00232647	10.789	0.2999
Tamb*RH	-0.00032	0.000107	0.01915195	88.818	**0.0032**
RH*RH	-3.04E-02	1.83E-02	0.00598744	27.767	0.0969
Tamb*WS	-0.002853	0.000876	0.02285370	105.985	**0.0013**
RH*WS	-0.001112	0.000292	0.03132041	145.250	**0.0002**
WS*WS	-0.000355	0.001712	0.00009257	0.0429	0.8360
Tamb*Precipitation	0.001712	0.00044	0.03262056	151.280	**0.0001**
RH*Precipitation	1.66E-01	0.000269	0.00000823	0.0038	0.9508
WS*Precipitation	0.002004	0.00198	0.00220921	10.245	0.3124
Precipitation*Precipitation	-0.000142	0.000196	0.00113377	0.5258	0.4691
Tamb*WD	-2.07E-03	9.83E-03	0.00009575	0.0444	0.8333
RH*WD	2.74E-03	3.31E-03	0.00001479	0.0069	0.9341
WS*WD	2.17E-01	2.88E-02	0.00122610	0.5686	0.4515
Precipitation*WD	5.20E-01	4.31E-02	0.00313088	14.520	0.2294
WD*WD	-1.17E-03	3.28E-04	0.02760679	128.028	**0.0004**

The correlation between the measured and the predicted soiling ratio SR is shown in Fig.2.10. The R^2 and the adj-R^2 are found to be respectively 0.51 and 0.47. The value of R^2 describes that the model explain 51% of the data which is much higher than the ones found in [104], using an artificial neural network model with five and eight variables. The RMSE for the model was 0.0464, which is lower than the MLR and the MLRWI models.

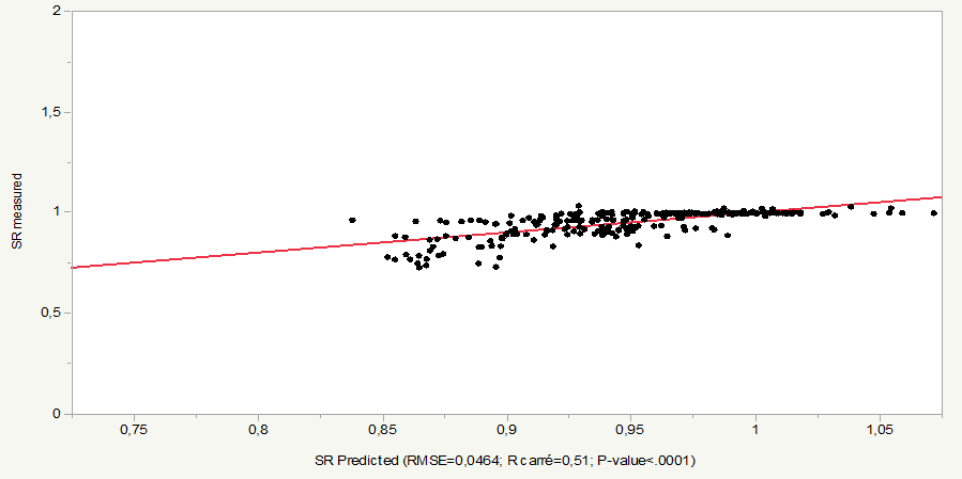

Fig.2.10. The correlation plot of the predicted and the measured soiling ration SR.

The results of the effects of different parameters used in this study on the soiling ratio SR, corresponding three dimensional response surface plots are shown in Fig.2.11, Fig.2.12, Fig.2.13, Fig.2.14, and Fig.2.15.

A weak correlation of the SR with WS or RH was illustrated when analyzed individually with relatively high significance for WS. This weak correlations were also reported by other researchers [99], [104], suggesting that there are interaction between the different parameters.We have also shown, the correlations on the two-dimensional surface of WS and RH in Fig.2.11.

In Fig.2.11, it can be seen that for high WS (> 6 m/s) the soiling ratio was high especially when coincides with a low RH (< 40%), which makes dust particles less sticky and more susceptible to be easily re-suspended by the wind [99], [110]–[112]. In contrast, with high RH (> 80%) and despite the high average of wind speed, the soiling ratio was very low and varies between 0.2 and 0.5, which emphasizes the fact that relative humidity affects the threshold wind speed by increasing the energy required for dust particles resuspension [54–56]. On the other hand, on days with moderately high RH (> 80%) and low WS (< 2m/s), the soiling ratio was in the range of 0.8, which could be explained by water condensation (dew droplets formation) on the surface of the PV modules during the night and the early morning and lead to partial cleaning [104], [116].

Moreover, ambient temperature (Tamb) as an individual parameter and in interaction with the other parameters as WS, RH, and precipitation had significant ($p < 0.05$) effect on model performance. This parameter was found to have seasonal effect of the soiling on solar reflectors, in which the high temperatures are connected to summer season, while lower values are associated to fall season [105].

Examining the Fig.2.12, it is apparent that the interaction between Tamb and WS could be simulated to the interaction between the RH and WS. Once it can be noticed, that the soiling effect decrease with the increase of WS and the decrease of the Tamb. This could be explained by the removal of dust particles in the presence of high WS (> 4 m/s) and the presence of dew during the night especially during the Fall season (low temperature values), which allow a partial surface cleaning. However, the soiling ratio was very low for high temperature values (> 35 °C) despite the presence of high WS values (> 4 m/s), which describe the summer days with high airborne dust concentration when coincided with a significant WS. This negative impact of Tamb is due to the dry deposition of dust on the surface of the PV panel with high concentration.

The effect of Tambcanbe seen also in Fig.2.13 with interaction of RH, which emphasizes the seasonal effect of this parameter where the soiling ratio is seen to be significantly higher for higher Tamb and RH. On the other hand, high Tamb and low RH (<20%) resulted in positive impact with high soiling ratio, the same pattern was found with the increasing RH and decreasing Tamb. This positive impact of high RH on soiling ratio, which is generally representing the climate conditions during the fall and winter seasons. This way, dew formation with remarkable amounts and with low Tamb (< 25 °C) will not dry that fast that lead to partial cleaning. Also, the soiling ratio is in the range of 0.8 for low Tamb (< 15 °C) and RH (< 20%); at the same range the soiling ratio is seen for moderate Tamb (< 30 °C) and RH (< 75%) levels.

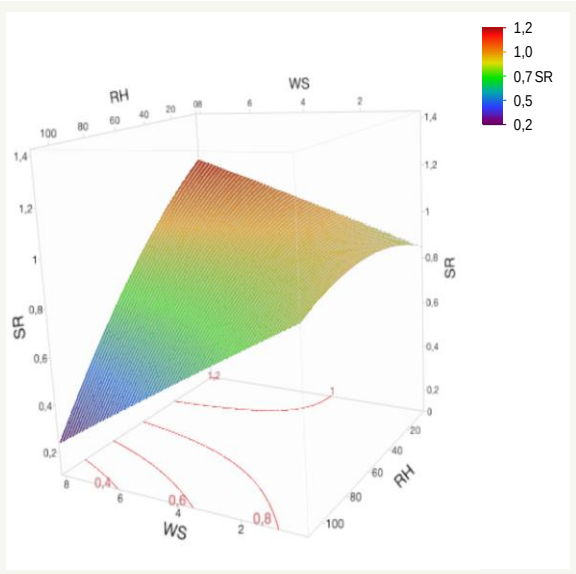

Fig.2.11. Combined effect of relative humidity (RH) and wind speed (WS) on soiling ratio SR.

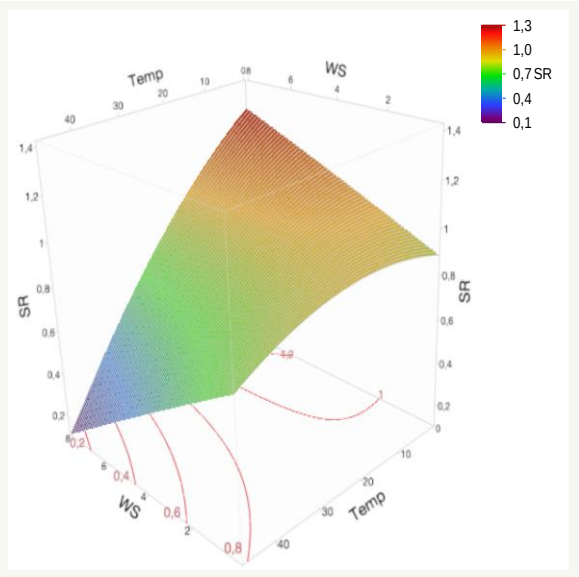

Fig.2.12. Combined effect of ambient temperature (Tamb) and wind speed (WS) on soiling ratio SR

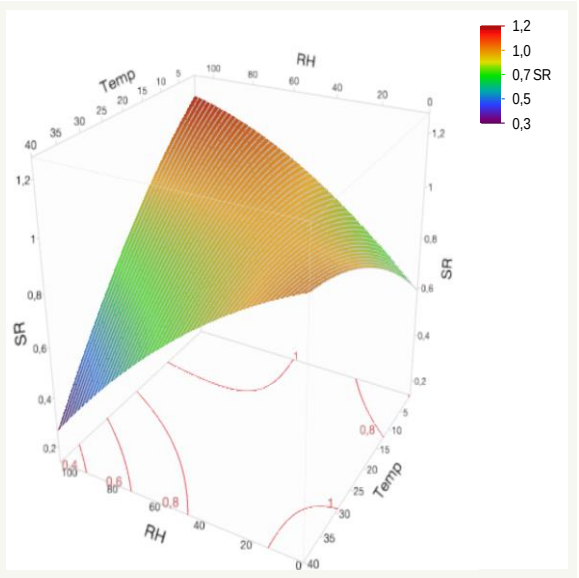

Fig.2.13. Combined effect of ambient temperature (Tamb) and relative humidity (RH) on soiling ratio SR.

The interaction between Tamb and precipitation is found to be relevant to the model prediction ($p<0.05$). The precipitation parameter has been described as a cleaning agent in many research studies [58,59], and that his pattern is strongly correlated to the soiling in interaction with the particulate matter concentration [119]. In previous relevant studies, periods with precipitation were removed from the data of the prediction model as they consider that the precipitation parameter has a cleaning effect, especially in a region with significant rainy days [105]. In addition, in a region with long dry months in the Middle East desert, the precipitation parameter was not that much relevant in comparison to the other parameters, like particulate matter concentration, wind speed

and wind direction, and relative humidity [104]. In the context of this study, the precipitation parameter has been included on the prediction model as the rainy period was much significant during the experiment.

From Fig.2.14, the soiling ratio was high for periods with high Tamb (> 30 °C) and high amount of precipitation (> 15 mm). This could be due the cleaning effect of precipitation especially during dry season period (high Tamb, and low RH that makes dust particles less sticky), which promote the cleaning of the surface of the PV panel in the presence of high amounts of precipitation. On the other hand, the soiling ratio decreases with decreasing precipitation under high Tamb, which can be clearly seen during the dry period of the year. This reflects the fact that higher Tamb connected to Summer days, where high airborne dust concentration can be detected, will enhance the PV soiling loss if they coincide with light precipitation, this is also referred as the red-rain phenomenon [59,61].

Wind direction was also found to have a significant impact on the prediction model as a quadratic term as of the linear and the interaction terms. This parameter has been found to have a complex relationship with soiling individually [99]. The authors found that the soiling loss increases when the winds are northwesterly between 270° and 330°. They found that the prevailing wind direction was related to high wind speed, which emphasizes the interdependency of this parameter to the other climate parameters as wind speed and particulate matter concentration. In another work [104], the authors highlighted the impact of wind direction on RH, WS, and particulate matter, which thereby affect indirectly the daily soiling loss.

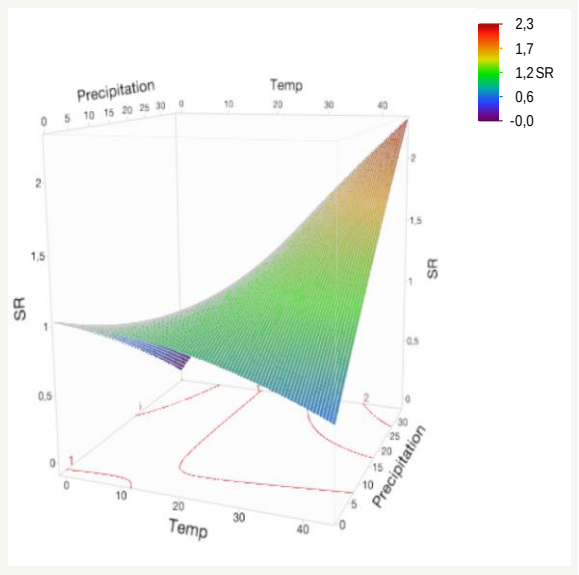

Fig.2.14. Combined effect of ambient temperature (Tamb) and precipitation on soiling ratio SR.

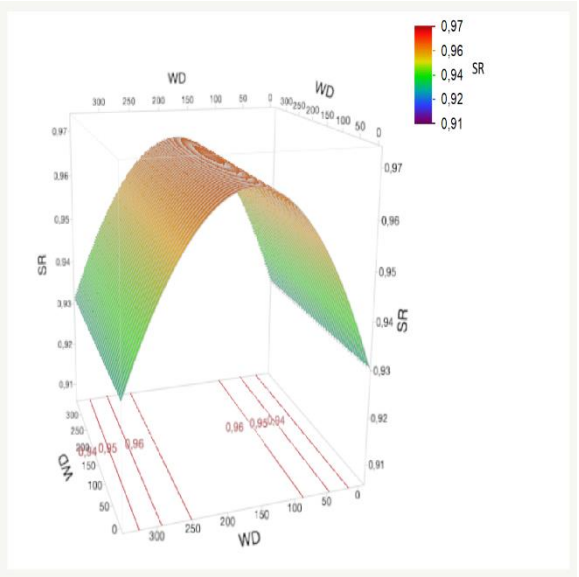

Fig.2.15. Quadratic effect of wind direction on soiling ratio SR.

II.4.3. ANN model:

Artificial Neural Networks (ANNs) are powerful mathematical frameworks, inspired by the functioning of the nervous system. They are used to model complex systems which can establish complex relationships between inputs and outputs. They are based on interconnected units, called neurons, and they use a connectionist approach to compute when processing information. The robustness of these models is manifested in the modelling of very complex systems, for which there is not yet an analytical solution and even these do not require knowledge of the phenomenon. For this reason, ANNs have been vastly used for a variety of applications in the last three decades [121]–[125]. The ANN architecture is usually divided in three main parts: an input layer, the hidden layers, and an output layer connected with nodes as shown in Fig.2.16, in which for each layer, a transfer function is affected. It is essential to evaluate several ANN architectures in order to find out a reliable model and estimations. ANNs are subjected to an iterative process called training that uses specific and complex mathematical algorithms to solve nonlinear multivariable phenomena.

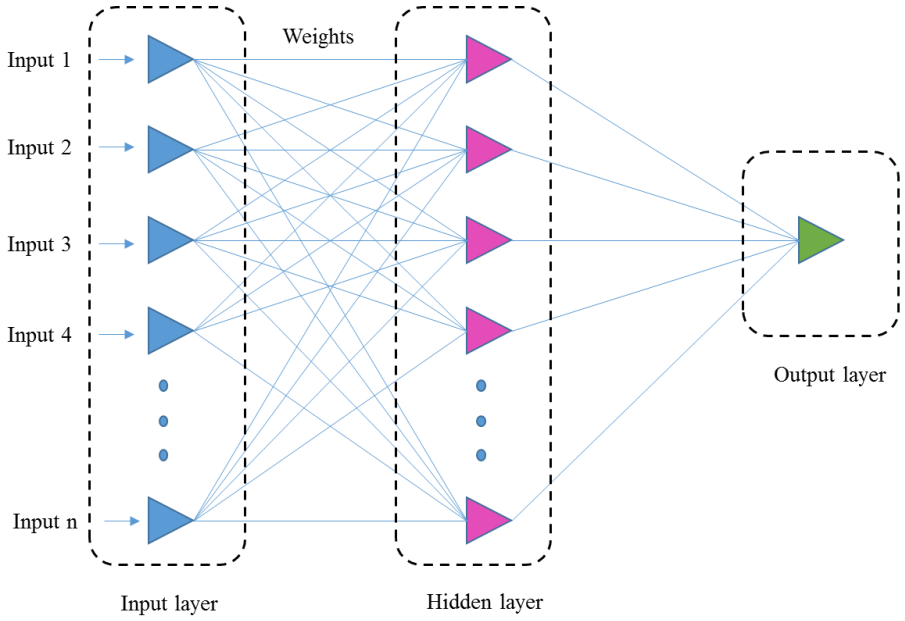

Fig.2.16. Artificial Neural Network architecture.

In this work, a multilayer perception with one hidden layer was adopted for the ANN model. Many training algorithms were tested and evaluated in order to carry out the one that fit the soiling phenomena and provide good performances, thus, the Keras training algorithm was chosen [126]. The ANN model used was composed of an input layer, a hidden layer, and an output layer. Moreover, the sigmoid transfer function was used in the output layer, especially the predicted soiling ratio is between 0 and 1, while the hyperbolic tangent transfer function was selected for both the input and hidden layers. The input layer was composed of 6 neurons representing the environmental variables: ambient temperature, relative humidity, wind speed, wind direction, precipitation, and the previous day values of the soiling ratio. Regarding the number of neurons in the hidden layer, several cases were tested and evaluated by varying the number of neurons from 3 to 12 neurons with randomly initialized weights in order to come up with the optimal one, and avoid over fitting. In addition, the ANN model was trained and evaluated 10 times for each number of hidden layer neurons to get the best results and performances [127]. The ANN model with 10 neurons in the hidden layer presented the best results, and it was used then for generating the model outputs. The dataset was divided into 80% for training, and 10% each for validating and testing.
Additionally, four main statistical error indexes were used to determine the accuracy level and to evaluate the performance of the developed model: Root Mean Square Error (RMSE), Mean Square Error (MSE), Mean Absolute Error (MAE), and regression coefficient (R^2). The statistical formulas of these indexes can be found in [68,69]. High accuracy is achieved when these errors are closer to zero, while R^2 parameter is closer to 1, best model performance is obtained. The dataset considered in this modelling were conducted for the period from August 18, 2017 to July, 30, 2018 (with 271 observations) and were used in this model to predict the soiling ratio taking into account the corresponding environmental variables. Table 2.6 presents the main obtained results using the ANN model described above. It can be observed that the proposed ANN model gives a good fit and can

explain approximately 81% of the data set ($R^2 = 0.813$, $p < 0.05$). This explain that the ANN model can adequately understand the interaction between the input variables and therefore predict the daily soiling ratio values with smaller biases in comparison to the MLR model.

Moreover, the accuracy evaluation of the proposed ANN model in term of statistical indicators shows that the RMSE is significantly smaller than the MLR model. The RMSE of the ANN model has decreased more than 50% (RMSE = 0.0268) in comparison to the MLR model (RMSE = 0.0567).

Fig.2.17 illustrates the regression plots of the proposed model. Following, the ANN model is a fast process and gives better accuracy and results comparing with linear models.Therefore, the ANNs appear to be a promising tool to solve complex problems and achieve higher R^2 values. However, defining a robust ANN architecture, pre-processing, increasing the dataset, and other relevant variables are very essential. These parameters must be considered with high attention in order to achieve a high accuracy model (which also does not overfit the model).

Table.2.6. Statistical error indexes of the proposed ANN model.

Parameter	**Data size**	**MAE**	**MSE**	**RMSE**	**R^2**
Training + Validation	80% + 10%	0.020964	0.000763	0.027625	0.817143
Test	10%	0.015883	0.000348	0.018664	0.872404
All data	100%	0.020431	0.000720	0.026826	0.813081

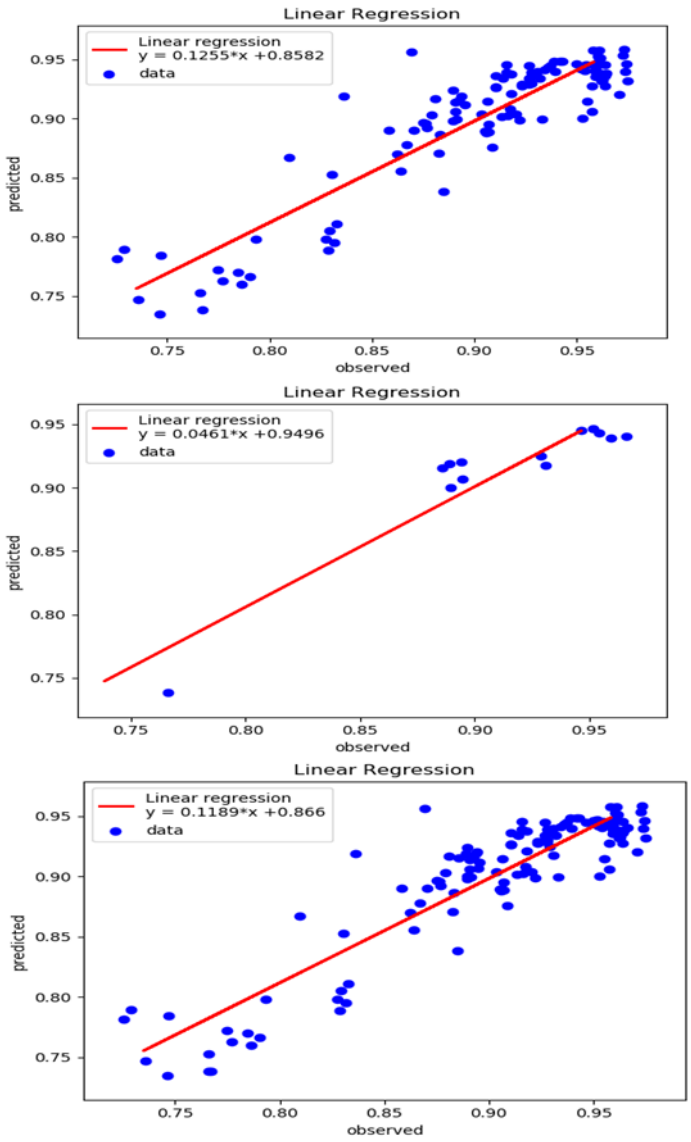

Fig.2.17. Regression plots of the proposed ANN model, Top: Training and validation dataset, Middle: Test dataset, Bottom: All data.

II.5. Conclusion:

In this chapter, the effect and prediction of soiling rate on the performance of the PV panels in the semi-arid climate were investigated using an amorphous PV system.

The objective of this work was to predict the effect of soiling on the performance of the PV panels by using one year of experimental results and three modelling methods. The main conclusions of this work are summarized as follows:

- The major components of the local dust are silicate, calcium, aluminum, and iron.
- The morphology of the dust particles changes with increasing exposure time.
- The accumulated soiling losses reached 28% by the end of the test.
- The daily soiling ratio reaches an average of 0.35%/day and 0.017%/day in the dry and rainy periods respectively.

- The total energy loss throughout the test period was 82.5 kWh.
- The energy loss due to soiling effect reached 0.61 kWh/day and 0.03 kWh/day during the dry and rainy periods respectively.
- The MLRWI has a higher R^2 and adj-R^2 and lower RMSE compared to those of a simple regression MLR model.
- The statistical parameters obtained are $R^2 = 0.23$, adj-$R^2 = 0.21$ and RMSE = 0.0567; $R^2 = 0.48$, adj-$R^2 = 0.46$ and RMSE = 0.046; $R^2 = 0.51$, adj-R^2 =0.47 and RMSE = 0.0464; $R^2 = 0.813$ and RMSE = 0.026 for the MLR, MLRWI, RSM, and ANN models respectively.
- The soiling ratio is high for periods with high Tamb (> 30 °C) and high amount of precipitation (> 15 mm).
- The ambient temperature Tamb as individual parameter and in interaction with the other parameters as WS, RH, and precipitation has a significant ($p < 0.05$) effect on model performance.

Chapter: 3

Development of a method for calculating the soiling rate on photovoltaic modules

III.1. Introduction

In this chapter we have presented the different components of the soiling rate calculation system, as well as the programming of the data acquisition card used (raspberry pi) and the results of the simulation.

We were interested in this work in the evaluation of the electrical performance of PV modules. Under the effect of soiling and natural aging, as well as the development of a method for calculating the soiling rate on the various photovoltaic modules.

III.2. Operating principle of the proposed system

To calculate the fouling rate, our system compares the power outputs of two identical PV panels mounted side by side one of which is clean and the other naturally soiled, so the fouling rate will be calculated according to the following equation:

$$SR = \frac{\mathrm{Ps}}{\mathrm{Pp}} \qquad (1)$$

With:

- Ps: The power supplied by the dirty panel.
- Pp: The power supplied by the clean panel.

For this, we put a variable resistor across each panel, current and voltage sensors to calculate the power.

This system will be programmed to take measurements once every 10 minutes from 6 a.m. to 8 p.m. These measurements will be saved in text files that can be retrieved remotely using SFTP protocol. And via a web interface, we visualize the fouling rate in real time, its maximum and minimum value, as well as its evolution throughout the day.

Our system must be autonomous. To achieve this goal, a battery has been added which will be charged by the clean panel for 10 minutes with the closing of a relay on the battery side and opening of the relay on the load side in order to keep the same conditions for both panels.

The clean panel is equipped with a pump, a water tank, and a spray jet that directs the liquid to this reference module for automatic cleaning. The cleaning is done every morning before starting the power measurement.

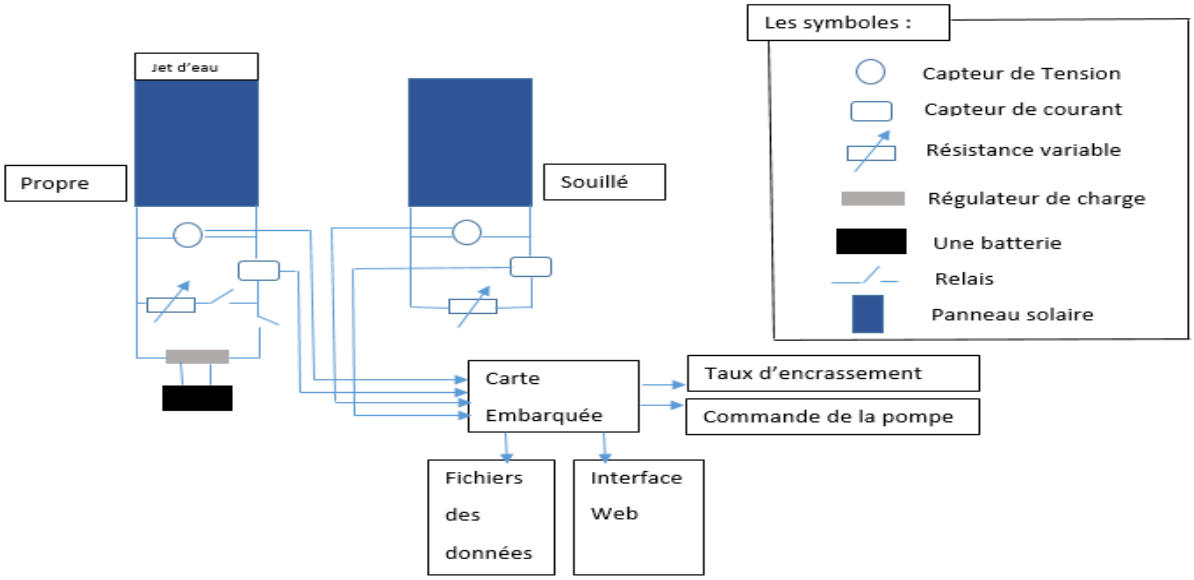

Fig.3.1. System concept

III.3. Presentation of materials

III.3.1. Photovoltaic module

A solar panel is a device that converts part of solar radiation into electrical energy. We need two 12V 5A solar modules, one will be cleaned and the other fouled to ignore the factors that permanently degrade solar panel performance. The price of this panel is 677dhs [129].

Fig.3.2. Polycrystalline VICTRON solar panel

III.3.2. Current sensor: ACS712 sensor

The ACS712 Allegro device provides an economical and accurate means of detecting AC and DC currents. This Allergo ACS712 current sensor is based on the principle of the Hall Effect. This sensor has the following characteristics [130] :

- Dimensions: 31 * 13 * 15mm.
- Measured current range: -30A to + 30A.
- Vref at 0V: Voc / 2 or 2.5V.
- Sensitivity: 66mV / A.
- Consumption: 10mA.
- Power supply: 5V.

- Weight: 2g.
- Price: 40dh.

Fig.3.3. ACS712 current sensor

III.3.3. Voltage sensor : RB-Oel-88 sensor

- 100% compatible with Raspberry pi.
- Operating output voltage: 3.3V-5V MAX.
- Input voltage range: 0.0245 V ~ 25 V MAX.
- Analogue input.
- Price: 60DH [131].

Since we are going to adopt the Raspberry pi board as a data acquisition board which has only digital inputs, we must add an analog-to-digital converter to these sensors.

Fig.3.4. Capteur de tension RB-Oel-88

III.3.4. Analog to digital converter: mcp3208

The MCP3208-CI / P is an Analog to Digital Converter (ADC) with 12 bit resolution. This ADC combines high performance and low power consumption in a small package, making it ideal for on-board control applications. The MCP3208 has a SAR (Successive Approximation Register) architecture, with a built-in sample-and-hold which allows 12-bit A / D conversion capability to be added to all PIC microcontrollers.

Fig.3.5. MCP3208 converter

It is programmable to provide four pairs of pseudo-differential inputs or eight single-ended inputs. Communication with peripherals is carried out using a simple serial interface compatible with the SPI protocol. Its low current design allows for typical standby currents of 500nA (2µA maximum) and active currents of 320µA (400µA maximum), and it is available in 16-pin PDIP and SOIC packages. Applications of the MCP3208 include data acquisition, instrumentation and measurement, multi-channel data loggers, industrial PCs, robotics, smart sensors, automation, and home medical devices [132].

The main features of MCP3208:

• Analog inputs programmable as single-ended or pseudo-differential pairs

• Works with a simple 2.7V to 5.5V power supply

• Maximum sampling rate of 100KSPS at VDD = 5V

• Maximum sampling rate of 50KSPS at VDD = 2.7V

• Low consumption CMOS technology

• Industrial temperature range from -40 ° C to 85 ° C

• Price: 19dh.

Fig.3.6. 12V-5V USB step-down module

The specifications of this module are as follows:

• Input voltage: 6-32VDC

• Output voltage: 5VDC by default, automatic adjustment between

• 3V-12V after rapid trigger charging

• Output power: Max.24W (5V to 3.4A, 9V to 2.5A, 12V to 2A)

• Conversion efficiency: 90% ~ 97%

• Reverse input protection: No

• Input undervoltage protection: Yes

• Input overcurrent protection: yes

• Output short-circuit protection: Yes

• Overheating protection: yes

• Weight: about 15g.

• Price: 70.84dhs.

III.3.5. Raspberry pi 3 board

The Raspberry Pi (pronounced as "Raze" "Berry" "Straw" in English) is a small computer the size of a credit card. Is an ARM-based single-board nanocomputer designed by video game creator David Braben, as part of his Raspberry Pi 3 foundation [133].

This computer, which is the size of a credit card, is intended to encourage learning of on-board computer programming; it allows the execution of several variants of the free operating system GNU / Linux-Debian and compatible software.

Pi is because originally we were going to produce a computer that could only really run Python. So the Pi is here for Python.

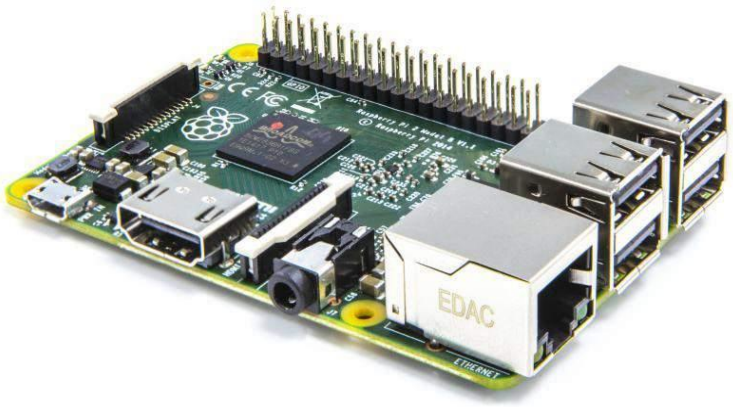

Fig.3.7. Raspberry Pi 3 model B board

✓ Components of the Raspberry Pi board

The raspberry pi nano-computer is an on-board target that features a Linux operating system. It serves as our brain within our system. Composed of the peripherals essential for the installation of an operating system and for communication with the external environment.

• Clocking: 1.2 GHz

• Chip (SoC): Broadcom BCM2837

• Processor: ARM Cortex-A53 64 bits quad core

• Graphics processor: Broadcom VideoCore IV dual-core (OpenGL ES 2.0, H.264 Full HD at 30 fps)

• Memory (SDRAM): 1GB LPDDR2

• Number of USB 2.0 ports: 4

• Extension port: 40 pins GPIO

• Video outputs: HDMI and RCA, plus 1 CSI camera connector

• Audio outputs: 3.5mm stereo jack or HDMI

• Data backup: MicroSD card

• Network connection: 10/100 Ethernet, WiFi 802.11n and Bluetooth 4.1 (BLE - Low Energy)

• Peripherals: 17 × GPIO

• Power supply: 5v 2.5A via micro-USB

• Dimensions: 85.60mm × 53.98mm × 17mm

• Weight: 45 g [133].

Advantages and disadvantages of Raspberry Pi :

• Small in size

• Cheaper / Low cost

• Lots of inputs / outputs (40 GPIO pins)

• Can be used as a Super Computer.

But the major downside of this card is that it has a low CPU and cannot run X86 operating systems.

III.3.6. Two relay modules

The two-direction dual relay module allows the equivalent of two-direction single-pole switches to be independently and easily controlled from a low-voltage, low-current control signal. These relays are called "SPDT" [134]. This module is very usable in projects, it can be controlled by microcontrollers (arduino, raspberry, pic,…).

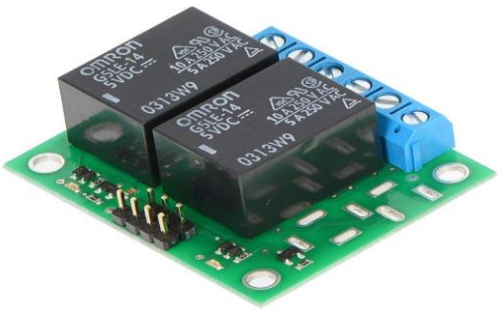

Fig.3.8. Two relay module

Among its characteristics we will have:

• Compact module.

• LEDs indicating the status of the relays.

• Use of Zener diode to decrease the current in the coils more quickly.

• With a relay supply VDD = 5V

• Activation current with 5V signal = 0.040mA

• Activation current with 3.3V signal = 0.030mA

• Withstand a current of 10A and a voltage of 30V

• The price of this module: 125.70 dhs.

III.3.7. Integrated circuit: L298N

The L298N can control 2 continuous motors or 1 stepper motor. It can run motors in continuous speed or in PWM. In addition, it includes diodes to protect the circuit, pull-up resistors and a heat sink in case of heavy load.

The L298N is a double H-bridge, that is to say it allows the motors to turn in one direction or the other without having to modify the connections, it also allows to vary the speed of the DC motor. This module can control motors with voltage up to 50V and current of 2A (3A at max), and it is compatible with 3V and 5V logic circuit (e.g. Raspberry pi board), and it can withstand temperature of -25 up to 130 ° C [135].

Fig.3.9. L298N module

1: Positive + of motor 1

2: The mass of motor 1

3: 12V jumper to disabled if the voltage is greater than 12V. It powers the internal 5V regulator

4: Power supply + up to 35V

5: the ground is connected to the raspberry pi board

6: 5V output

7: ENA motor 1 to be connected to PWM of Raspberry pi to manage the speed of the motor

8, 9: The motor 1 control (direction of rotation)

10, 11: Motor 2 control (direction of rotation)

12: ENA motor 2

13: Positive + of motor 2

14: The mass of motor 2

The price of this module: 69dhs.

III.3.8. Cleaning system: Pump

This diaphragm water pump is made of high-quality material, with smooth rotation, low noise and long service life.

Fig.3.10. Pump

The characteristics of this pump are as follows:

- This pump can withstand a temperature of 80/167 ° C.
- Compact size and strong structure, easy to install and maintain.
- The pump body is sealed to prevent ingress of moisture and dust. It is characterized by corrosion resistance and high reliability.
- Working voltage: 12V.
- Working current: 0.5-0.7A.
- Flow rate: 1.5-2L / min (approximately).
- Maximum suction range: 2m.
- Maximum hydraulic head: 3m.
- Lifespan: 2500h (maximum).
- Weight: approx. 110g.
- Size: approx. 10 × 6 × 3.5cm / 3.9 × 2.4 × 1.4inch.
- Price: 149.70dh.

III.3.9. Water jet

This device is attached to the pipe outlet. It is adjustable, allows to increase the water pressure drawn by the pump in order to clean our mini-module, it is made of metal, Not very expensive (18dhs).

Fig.3.11. Spray jet

III.3.10. Variable resistance

The Rheostat of 100 Ohms and 100W, allows to control the electrical resistance of a circuit without interrupting the flow of current. This rheostat is widely used as light dimmers and motor speed control, it is applicable to arc lamps, pumps, ventilators and respirators. Its price is 113dhs.

Fig.3.12. Potentiometer

III.3.11. MPPT regulator

The use of an MPPT (Maximum Power Point Tracking) solar regulator will optimize the electrical operating parameters between the photovoltaic panels and the battery.

The function of the charge regulator is to protect the batteries from overcharging or deep discharging and thus ensure that all the energy produced by the photovoltaic panels is stored more efficiently in the batteries. The price of this regulator is 898 dhs [29].

Fig.3.13. Victron Energy MPPT Charge Controller

III.3.12. Battery

The battery is a system component for storing the energy of the solar panel to power our system continuously. We have used the battery of 22Ah capacity and 12V voltage.

III.4. Card programming

The raspberry pi card is programmed using many languages such as C, C ++, JAVA, PYTHON, etc. We have chosen to program our card using python language which is part of the category of interpreted programming languages.

III.4.1. Organizational chart

A programming flowchart is a standardized graphical representation of the sequence of operations and decisions carried out by a computer program.

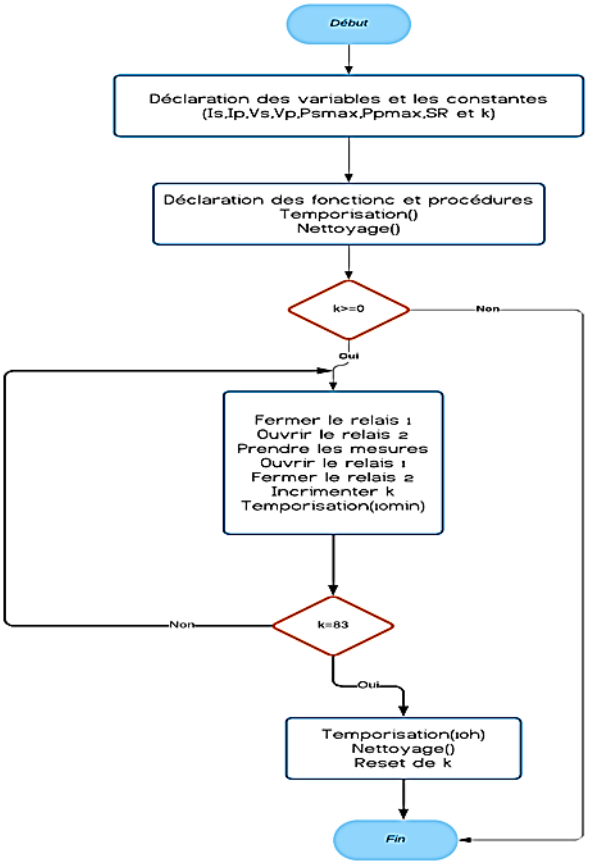

Fig.3.14. Principal flowchart

III.4.2. Programming

Programming, also called coding, is the set of activities that allow the writing of computer programs (annexs 1 and 2). We present to you the most important functions of our main program.

Pin configuration:

GPIO (General Purpose Input / Output) or input / output ports are ports that are widely used in the world of microcontrollers, particularly in the field of on-board electronics. Depending on the configuration, these ports can operate both as an input and / or as an output.

```
#Setup
GPIO.setmode(GPIO.BCM)
GPIO.setwarning(False)
GPIO.setup(EN,GPIO.OUT)
GPIO.setup(IN1,GPIO.OUT)
GPIO.setup(IN2,GPIO.OUT)
GPIO.setup(Relais_1,GPIO.OUT)
GPIO.setup(Relais_2,GPIO.OUT)
```

Fig.3.15. Pin definition

Reading sensor values:

The recovery of the values measured by the analog sensors with the Raspberry on-board card, requires an analog / digital converter, because it only contains digital inputs / outputs which uses the SPI (Serial Peripheral Interface) protocol.

```
#Fonction de lecture du MCP3208 via SPI
def ReadChannel(adcnum):
    if (adcnum>7) or (adcnum<0):
        return -1
    adc=spi.xfer2([4 | 2 | (adcnum >> 2),(adcnum & 3)<<6,0])
    data=((adc[1] & 15) << 8) + adc[2]
    return data
```

Fig.3.16. MCP3208 measurement reading function

Cleaning:

Cleaning the photovoltaic module is the operation of removing dirt in order to ensure the cleanliness and proper functioning of the solar panel (yield, maximum power, etc.).

```
def nettoyage(delay):
    GPIO.output(IN1,GPIO.HIGH)
    GPIO.OUTPUT(IN2,GPIO.LOW)
    time.sleep(delay)
    GPIO.OUTPUT(IN1,GPIO.LOW)
    GPIO.OUTPUT(IN2,GPIO.LOW)
```

Fig.3.17. source code of the cleaning function

III.5. Data acquisition

III.5.1. Creating a graphical interface

A web server is a computer connected to the Internet and on which websites composed of HTML pages are hosted. The Raspberry Pi can be configured as a web server, for this we used the Flask tool which facilitates the creation of web application in Python, which will provide us with information on the instantaneous fouling rate and its variation during the day in a web interface. In this part, we present the basics and the different stages of the application development.

Web server:

A "web server" can refer to software components or hardware components or software and hardware components that work together.

At the hardware component level, a web server is a computer that stores the files that make up a website (e.g. HTML documents, images, CSS stylesheets, JavaScript files) and sends them to the web device. user who visits the site. This computer is connected to the Internet and can usually be accessed through a domain name such as mozilla.org [30].

At the software component level, a web server contains various fragments that control how users can access hosted files. There will be at least an HTTP server.
An HTTP server is software that understands URLs and the HTTP protocol (the protocol used by the browser to display web pages) [30].

At the simplest level, whenever a browser needs a file hosted on a web server, the browser requests the file over HTTP. When the request reaches the correct web server (hardware), the HTTP server (software) returns the requested document, also using HTTP.

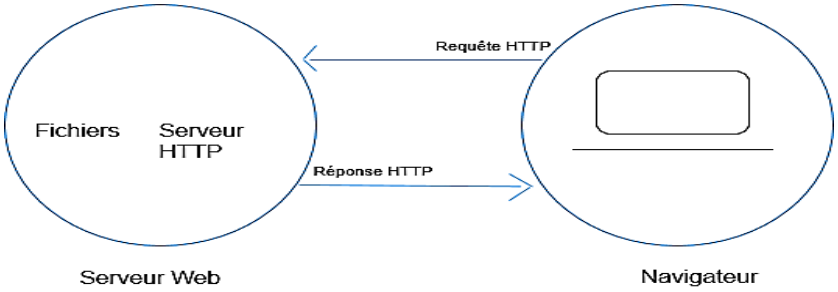

Fig.3.18. Principle of the web server

- **The HTTP protocol**

Hypertext Transfer Protocol (HTTP) is a client-server communication protocol developed for the World Wide Web. HTTPS (with S for secured, or "secure") is the variant of HTTP secured by the use of SSL or TLS protocols [31].

HTTP is an application layer protocol. It can work on any reliable connection, in effect TCP is used as the transport layer. An HTTP server then uses port 80 by default (443 for HTTPS).

The most well-known HTTP clients are web browsers that allow a user to access a server containing the data. There are also systems for automatically retrieving content from a site such as website crawlers.

In the HTTP protocol, a method is a command specifying a type of request, that is, it requests the server to perform an action. In general, the action concerns a resource identified by the URL following the name of the method.

There are many methods, the most common being GET, HEAD, and POST:

GET: It is the most common method to request a resource. A GET request has no effect on the resource, it must be possible to repeat the request without effect.

HEAD: This method only requests information about the resource, without asking for the resource itself.

POST: This method is used to transmit data for processing to a resource (most often from an HTML form). The supplied URI is the URI of a resource to which the sent data will apply. The result can be the creation of new resources or the modification of existing resources. Due to the poor implementation of HTTP methods (for Ajax) by some browsers (and the HTML standard which only supports GET and POST methods for forms), this method is often used as a replacement for the PUT request, which should be used for updating resources.

Flask:

Flask is an open-source Python web development framework. Its main goal is to be light, in order to keep the flexibility of Python programming, associated with a system of templates [32].

Creation of web interface:

First, we will have to install the flask library which will allow us to make our Raspberry Pi a web server. Just enter the following command in the terminal:

pip install flask

After installing this library, we start writing our flask code, here are the main lines of code:

- from flask import Flask: we imported the Flask object from the flask package.
- app = Flask (__ name__): We created our Flask application instance with the name app. We passed the special variable __name__ which contains the name of the current Python module. It is used to tell the instance where it is.
- Once you have created the application instance. It is used to process incoming web requests and send responses to the user.
- @ app.route ("/ graphSR"): @ app.route is a decorator that turns an ordinary python function into a Flask display function, which converts the return value of the function to an http response to be

displayed by an http client, such as a web browser. We pass the value '/ graphSR' to @ app.route () to indicate that this function will respond to web requests for the URL / graphSR, which is the primary URL.

- render_template: Flask provides this function which makes it possible to render the HTML template files that exist in the template folders. It takes as argument the name of the template (graphSR.html in our case) and the variables we want pass to the model engine as keyword arguments.
- app.run (host = '0.0.0.0', port = 5000, debug = False): host = 0.0.0.0 this makes our application accessible by machines that are in the same network as Raspberry Pi.

The fouling rate is recorded at a regular time interval (10min) in a text file which is saved under the name of the day, and these files are saved in a folder whose name refers to the year as shown in fig.3.19.

Fig.3.19. Data file

It is enough to recover this data and to insert it in a graph. For this part, we will use a tool developed by Google: Google Charts; allows you to quite easily create a bunch of graphs of all types: Circulars, histograms, maps, curves… For our project, we are going to use the curves module: Line Chart.

To begin with, we will create a file-to-list (file-path) function which will transform the lines contained in the fouling file into two lists which will be used to draw the curve.

Here is the body function:

```
def  fichierversliste(cheminfiche):
    f=open(cheminfiche, "r")
    points=[]
    soilingratio=[]
    for line in f:
        points.append([line[0:2], line[3:5], line[6:len(line)-1]])
        soilingratio.append(float(line[6:len(line)-1]))
    f.close
    return [points, soilingratio]
```

Fig.3.20. Source code of transform files to list function

We will now use all this by creating the graphSR (date) function which will return to the HTML page, this one will load to draw the graph.

To change the writing style, we used a style.css file saved in a folder named static which contains some modifications (type of writing, size ...), and to link the HTML & CSS documents with Flask, we added this line in the <head> tag of the HTML code: <link rel = styles 'stylesheet' 'type =' 'text / css' '' href = '' {{url_for ('static', filename = 'style.css')}} '' />

After we've finished programming our script, we save it and go to the terminal to run it.

Before running our web application, we specify the development mode with the environment variable FLASK_ENV. Then, we must tell Flask where to find the application (the code_ui.py file in our case) with the environment variable FLASK_APP.

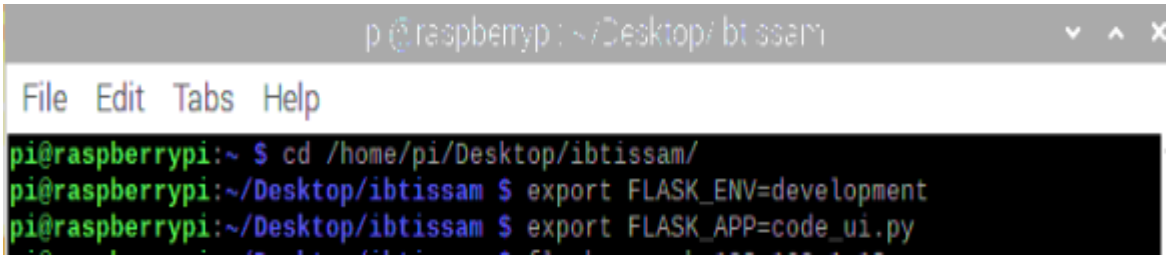

Fig.3.21. Steps to launch FLASK

Finally, we run the application using the following command:

Flask run -h 192.168.1.12

Once the application is launched, the output will be as follows:

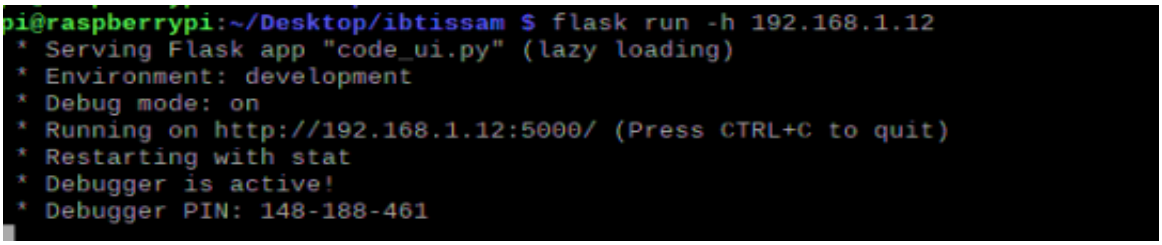

Fig.3.22. Running FLASK

The previous output contains several pieces of information, such as:

- The name of the application we are running (code_ui.py).
- The environment in which the application is run (development).

- Debug mode: we mean that the Flask debugger is running. This is useful in development as it gives us detailed error messages when things go wrong, making troubleshooting easier.
- The application runs on the URL http://192.168.1.12:5000/, 192.168.1.12 is the IP address that represents the local host of raspberry and: 5000 is the port number.

We open a browser and we type the URL: http://192.168.1.12: 5000 / graphSR,

We receive this web interface:

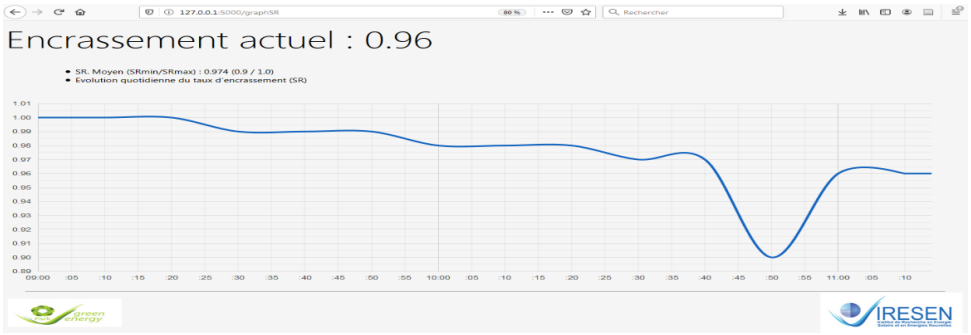

Fig.3.23. WEB Interface

III.5.2. Automating Script Execution

In this system, the execution of the two scripts should be scheduled as follows:

- Running the measurement script on a regular basis (every 10 min) every day from 6 a.m. to 8 p.m.
- Run cleaning activation script every morning at 5:55 am.

For this we have adopted the crontab tool. It is a mechanism for configuring scheduled tasks on systems. It is used to schedule commands or scripts to be executed periodically and at fixed intervals. https://www.raspberrypi.org/documentation/linux/usage/cron.md

The crontab –e command modifies the list of scheduled tasks. Adding a task is done as follows:

m h j M dd Order

With:

- ✓ **m**: minutes (00-59)
- ✓ **h**: hours (00-23)
- ✓ **j**: day of the month (01-31)
- ✓ **M**: month (01-12)
- ✓ **jj**: day of the week (1-7)
- ✓ **Command**: the task to be executed

In our case, we added two commands. (Annex 3)

4.5.3. Remote Raspberry Pi File Recovery

To get our files remotely for processing, we used the SFTP protocol. SFTP (SSH File Transfer Protocol) is a secure file transfer protocol. It runs over the SSH protocol. It supports all security and authentication features of SSH.

The SFTP port number is SSH port 22. This is basically an SSH server. It is only after the user has logged into the server using SSH that the SFTP can be initiated.

To establish communication between two devices via the SFTP protocol, two main elements are needed: SFTP server and SFTP client.

An SFTP client is a software that allows you to connect to a remote server in order to view, modify, drop or check out files. There are several free SFTP clients such as:

- Filezilla, compatible with Linux, Windows and Mac.
- Cyberduck, Windows and Mac compatible.
- WinSCP, Windows compatible.

For the SFTP server, it is already included in the SSH server because SFTP is an overlay of SSH.

The steps to establish remote communication between Raspberry Pi and our PC are as follows:

✓ Enable Raspbian's SSH access:

Using the secure SFTP connection, there will be no FTP server to install or update (which is always a potential security breach).

On Raspbian it can be activated from the Raspberry pi control panel which is in Menu -> Preferences. Then in the interfaces tab, we enable SSH. We must restart the Pi for the modification to take effect.

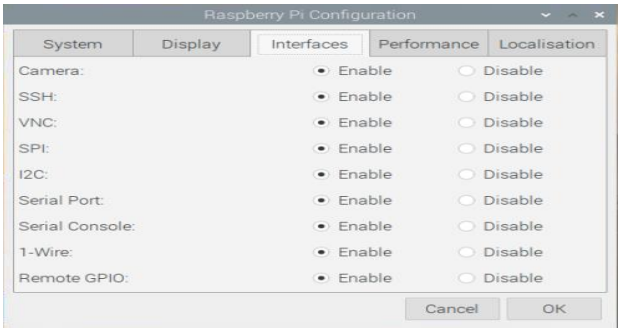

Fig.3.24. SSH activation

✓ Install the SFTP client on CP:

FileZilla is the best known solution. It is free and easy to install software, and it is available for MacOs, 32-bit Windows, 64-bit Windows, and Linux.

Once installed on the computer, we start FileZilla, and configure the connection like this:

- Host: The IP address of the Raspberry pi is obtained through the terminal via the command: **ifconfig**

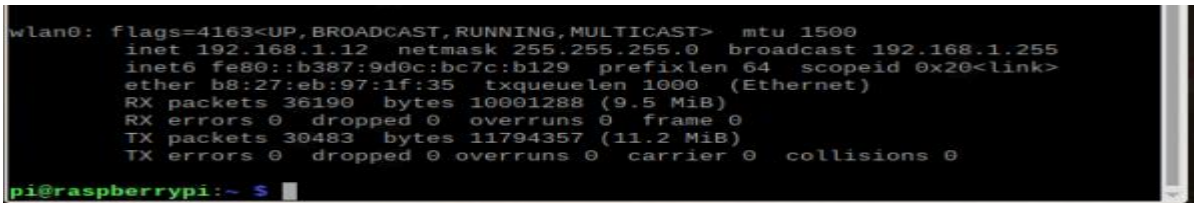

Fig.3.25. FileZella configuration

- Username: pi
- Password: t
- Port: 22 (the port of SSH)
- Press quick connection

Fig.3.26. Filling in FileZilla fields

After a few seconds, we are connected to our Raspberry and we can see its files in the right part. This means that we are allowed to do whatever our Raspberry Pi can do on the server. This makes it easy to transfer files between Raspberry and the computer with simple drag and drop.

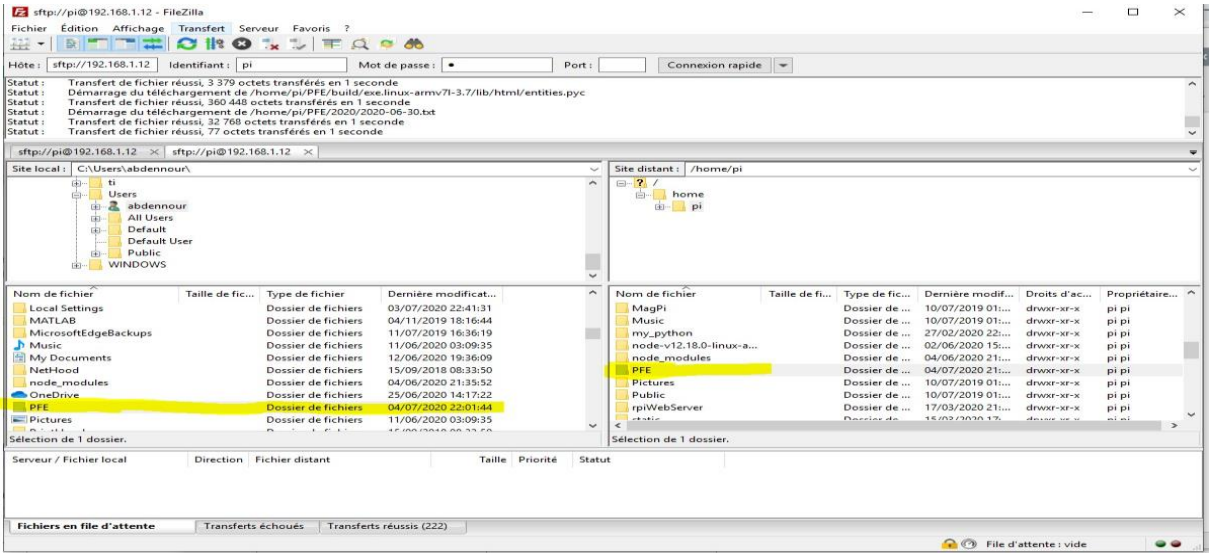

Fig.3.27. FileZilla window

III.6. Simulation and results

Simulation is the execution of a program on a computer or network in order to simulate a real and complex physical phenomenon. It is part of a stage of verifying the functioning of electrical and electronic circuits. The simulation is done from software such as ISIS PROTEUS in our case.

Isis Proteus is software for application development and simulation via a simple and interactive graphical environment.

We have translated our program instructions into blocks within the main function main, this is what we will present in the figure below.

It is made up of two essential parts:

- Setup: dedicated to configuring the card pins (input / output) and their initializations.
- Loop: consists in describing the state of each pin (0 or 1) as well as the timing subroutines which will run infinitely.

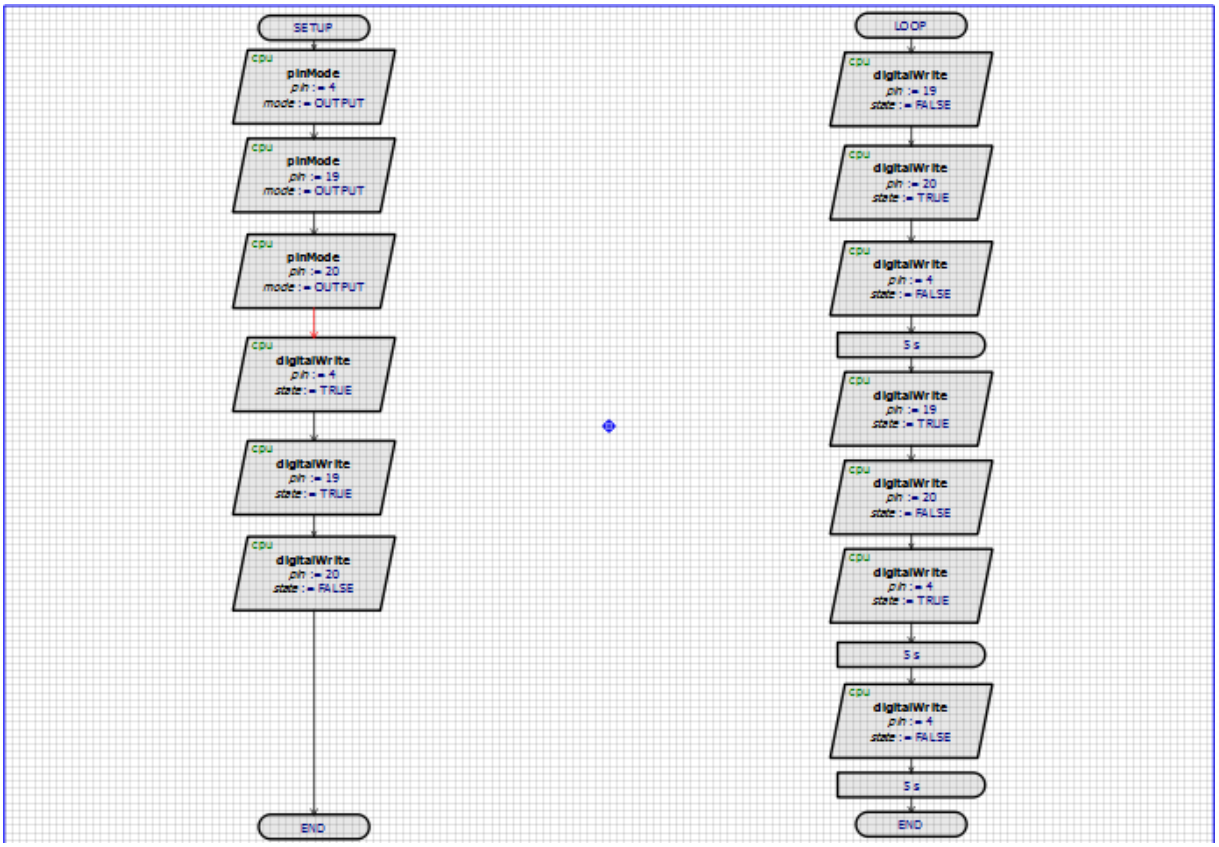

Fig.3.28. Block code on ISIS

After having a main hand we illustrated the diagram of our system using the software library to recover its different components, and launched the simulation of the system in order to visualize the evolution of the commands which come from the onboard raspberry pi board (controllable relays and cleaning pump).

The figure below shows the verification of the program for example, that the two relays are conjugated between them every 5 seconds and the motor turns 10 seconds while it takes one minute at rest.

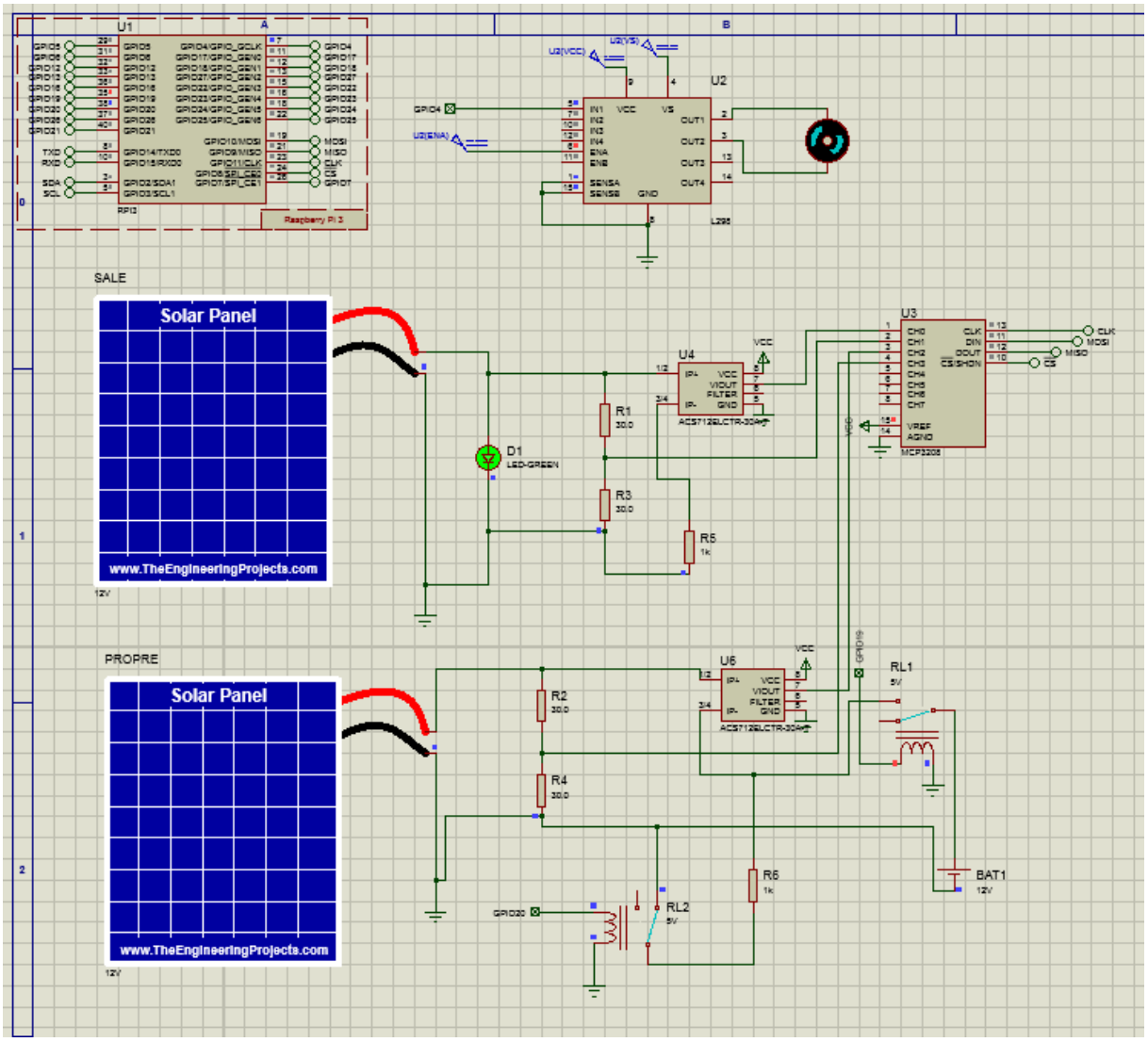

Fig.3.29. System simulation

III.7. Conclusion

Throughout this chapter we have proposed a solution that aims to fully calculate the soiling rate and automate the cleaning operation of photovoltaic panels, which results in less involvement of the human factor and will be economical in terms of resources, precise and effective.

The system developed met the specifications of this project in terms of several criteria, among them:

- Autonomy.
- Data acquisition.
- The ability to adapt the system to a wide range of PV technologies.

In this chapter, we have presented the different hardware of the system, the programming of the Raspberry pi onboard board using the interpreted python language, thus creation of a Flask interface and the FTP (File Transfer Protocol) used to transfer files between a Raspberry Pi and another computer connected to the same network of the card, and finally the simulation of the system under ISIS PROTEUS software.

Chapter: 4

Design of an efficient and intelligent cleaning system for Photovoltaic modules

IV.1. Introduction

In this chapter, we will present the design of a stand-alone photovoltaic module cleaning system, which uses the cleaning mechanism with water, using a rotating cylindrical brush and water injected by a pump.

IV.2. Cleaning techniques

To avoid the soiling problem, the use of cleaning systems is mandatory in order to remove the dust accumulation on the front surface of PV panels and increase its efficiencies. In this since several cleaning systems has been developed like natural method, manual cleaning, electrostatic method, self-cleaning nano-film and automatic cleaning system as presented in fig.4.1.

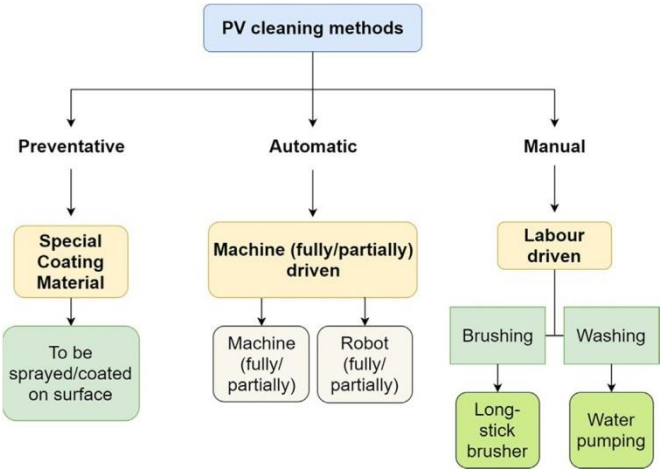

Fig.4.1. Classification of cleaning method

IV.2.1. Natural cleaning

The natural cleaning process is a method that uses nature as its cleaning tool. Among these natural tools, we find wind speed, rainwater as well as the earth gravitation. The high wind speed or a water droplet can remove or roll-off the dust on the PV panel surfaces. However, less gravitational occurs at night and early morning can float the dust naturally onto the surface of PV panels.

Gair et al [136]reported in their study that dust removal can be done easily if we turn the PV panels to a vertical position during rainy day, evening night, and early morning. This method has as advantages, low cost, and clean energy for the environment. However, the problem of this technic is the tilting rotation of PV plants on a large scale and not operational for high humidity climate.

IV.2.2. Manual cleaning

This method is the same as the one used in the cleaning of high-rise building windows. Dust particles are removed by special brushes equipped with bristles to avert any scratches on the glass of the PV module. These brushes are connected with a water supply that enables washing. The uneven movement of brushes over the PV module surface leads to a risk of abrasive effect. This latter can be minimized soft cleaning cloth or brush with soft bristles[137], [138]. The cleaning brush is used with a water pressure of 100 to 160 bar which allows easy manual cleaning. For high dirty surfaces, a cleaning product is added to the water to remove easily dirt. Then the surfaces are

rinsed with demineralized water. This cleaning system is recommended for small areas of 150 to 300 m².

To clean the solar panels, we need a bucket of warm soapy water, a dry cloth and a rubber squeegee. The surface of the panel is washed with soap water and a cloth to remove dust, debris, and water spots. A squeegee is used to remove excess water. This method has the advantage of being simple and less expensive, on the other hand, it has many disadvantages: it is not suitable for large areas, it uses large quantities of water which is not compatible with desert areas, it leads to a degradation of the PV modules surface (appearance of micro-scratches under the effects of friction), and finally it has a direct impact on the damping time of the installation.

Manual cleaning is usually used for cleaning small facilities or domestic solar panels [139], [140]. This cleaning methods is expensive and requires skilled labor to clean off soiling onto the PV plants. However, fully automated systems can bring flexible cleaning. At the level of our research facility [141], we use manual cleaning since we dispose of PV plants with small scales that are dedicated to research and development.

IV.2.3. Electrostatic cleaning

The electrostatic method is based on an electrostatic charge (from the electric curtain on the PV panel) to remove dust on the surface of the PV panel. This latter has been developed at NASA in 1967 [142].The action of electrostatic and dielectrophoretic forces to remove the dust has been studied by Calle et al [143]. In order to generate electrostatic and dielectrophoretic force, the electrodes have been used to transport charged and uncharged particles on the PV modules surface. Stable electrostatic force occurs, which makes to unbalance between charged particles and surface, this phenomena deal with the particles to create their own force. This kind of force generates a movement of a dust particle on the PV module surface which called dielectrophoretic forces.

IV.2.4. Self-cleaning Nano film

The Self-Cleaning Nano film method is the method that uses the coating process to add a Nano film layer on the PV panel surface. Several coating processes have been innovated by researchers such as chemical vapor deposition (molecular beam epitaxy, electrostatic spray assisted vapor deposition, vapor deposition, chemical and electrochemical technique, physical vapor deposition, plasma spraying, roll-to-roll coating process, spin-coating, and dip coating. This method deals to modify the normal PV module surface by turning it to superhydrophobic surfaces and superhydrophilic surfaces using a special nano-film coating characterized by superhydrophobic and superhydrophilic proprieties[144]–[149].

IV.2.5. Automatic cleaning system

Robotic systems have emerged as an attractive solution for cleaning the dirty surfaces of photovoltaic module [150]. Besides and depending on geographical land and area of application, existing solutions can be further compared based on the capital costs and performance ratio.

PV module cleaning robot comprises a mobile robot that carries the cleaning payload and cleaning tool, which performs the cleaning work [150].

Serbot Swiss Innovations has developed a robotic cleaning system called ‘Gekko Solar’ and ‘Gekko Solar Farm’ in order to be used for mobile deployment onto PV plants [151]. This latter uses the rotating brush and demineralized water to clean the PV modules surface. The movement of this system is based on feet with vacuum technology enabling the robot to astonishing flexible movement in every chosen direction.

Raybot is an eco-friendly robot designed to clean solar panels [152]. It can move on surfaces with a slope of up to 65 degrees using suction cups without risk of damaging them. It can clean around five solar panels per hour and in most cases, it is enough to use it at the end of two months. The robot safely sweeps surfaces that are often characterized by difficult access. Raybot is an eco-friendly robot designed to clean solar panels. It can move on surfaces with a slope of up to 65 degrees using suction cups without risk of damaging them. It can clean around five solar panels per hour and in most cases, it is enough to use it at the end of two months. The robot safely sweeps surfaces that are often characterized by difficult access. By sweeping, blowing, and vacuuming, it removes the dust and dirt that naturally settles on the solar panels. Using several sensors, Raybot mobilizes without any risk of falling. In addition, to carry out its task, it is equipped with an interchangeable battery that allows it to resume work without the need for a charging station.

The HYCLEANER black SOLAR allows simple, quick, and economical cleaning [153]. This robot allows optimal cleaning with its mechanical power and low water consumption. It works with radio control, which helps the user to not need to walk, either on the roof or on the solar surface. Lithium batteries guarantee electric drive, so a power outlet near the work area is not mandatory.

Ecoppia’s E4 is a robot that operates during the night to maintain maximum energy production at all times [154]. It operates at a cleaning rate of 54 square feet (approximately 5 m) per 30 seconds. The robot moves along a rigid aluminum structure, its wheels are covered with polyurethane to ensure that the movements are light without carrying a load on the solar panel surface. This robot is fully autonomous and independent of energy, it has its own solar panel for self-loading and its self-cleaning mechanism. The robot recovers energy during its descent along with the solar panel, which will be reused in the next cleaning cycle, which optimizes the robot's performance.

SOL BRIGHT developed a cleaning robot that eliminates 99% of dirt and pollution on photovoltaic panels. Tested in large solar power plants, the robots improve their electricity production rate by 7 to 15%. The robot operates at night using its own photovoltaic module as an energy source, without interrupting the conversion of solar energy during the day. The cleaning robot is equipped with a roller brush, which is not supplied with water, which helps to save energy and protect the environment.

Table 4.1 gives a summary of the different robotic cleaning technologies described above.

Table 4.1. Comparison of the presented robotic cleaning systems.

Robot	**GEKKO**	**RAYBOT**	**HYCLEANER**	**ECCOPIA**	**SOLBRIGHT**
Tilt	45°	65°	35°	Adaptable to	Adaptable to

				anyinclinati on	anyinclin ation
Cleaningtechnol ogy	By heated deminer alized water and pressuri zed.	Dry	Wet	Dry	Dry
Cleaningequipm ent	Polyami de12 nylon brush with a rotation speed of 350 rpm	Brushes, vacuum cleaners and fan	Brush	2 microfiberb rushes	Roller brush
Displacementme chanism	By suctionc ups	• By suctionc ups • By lengthen ing and shrinkin g of his body	By strap	By rail and polyurethan e wheels.	Roll along the chassis of the PV panels
Moving speeds	4m/min	---------- -------	25m/min	---------- --	10 to 20m/min
Course control system	By remote control	By position sensors	By radio control	Remote control by masterE4 application	Using intelligen t control software.
Yield	300-400 m²/h	5 panels/h	400-800m²/h	600m²/h	1800-3600 m²/h

IV.3. New cleaning system

IV.3.1. Robot design and functionality

Based on the investigations and the obtained results discussed in the previous sections, and in order to increase the PV plants efficiency by continuous cleaning activities, an autonomous cleaning robot is proposed. The proposed system can maintain high efficiency of the solar panels by ensuring a continuous cleaning without the need for any guide or human intervention (self-guided robot). In addition, the robot can be monitored and controlled in real time through a web link application. Users can easily monitor the robot status (ON or OFF), battery charge, water level, and can also set

a schedule with a specific time for cleaning. The proposed robot is designed to be mounted and adapted to all PV systems and technologies by adjusting only the vertical supports (over the PV system width). In addition, system flexibility is the main advantage of the proposed system. The robot can be controlled by three modes: a manual mode that the operator can immediately turn on/off the robot, the robot can also move to a specific position via this mode; following, users can control the time or frequency of cleaning using the web link application; the third mode is used to communicate with other electronic devices by receiving a digital signal to start the cleaning process (the user sets a default time to start cleaning when a signal is received, 6 pm. for example). For instance, an electronic device that calculates the soiling ratio or the PVP efficiency. In addition, the robot is designed to be lightweight and small to facilitate installation and maintenance and also to reduce the cost of the system by minimizing mechanical structures and motors torques. The proposed solution uses also a low number of electronic sensors and motors to minimize even more the robot cost and reduce its maintenance (details can be seen in Fig. 4.2).

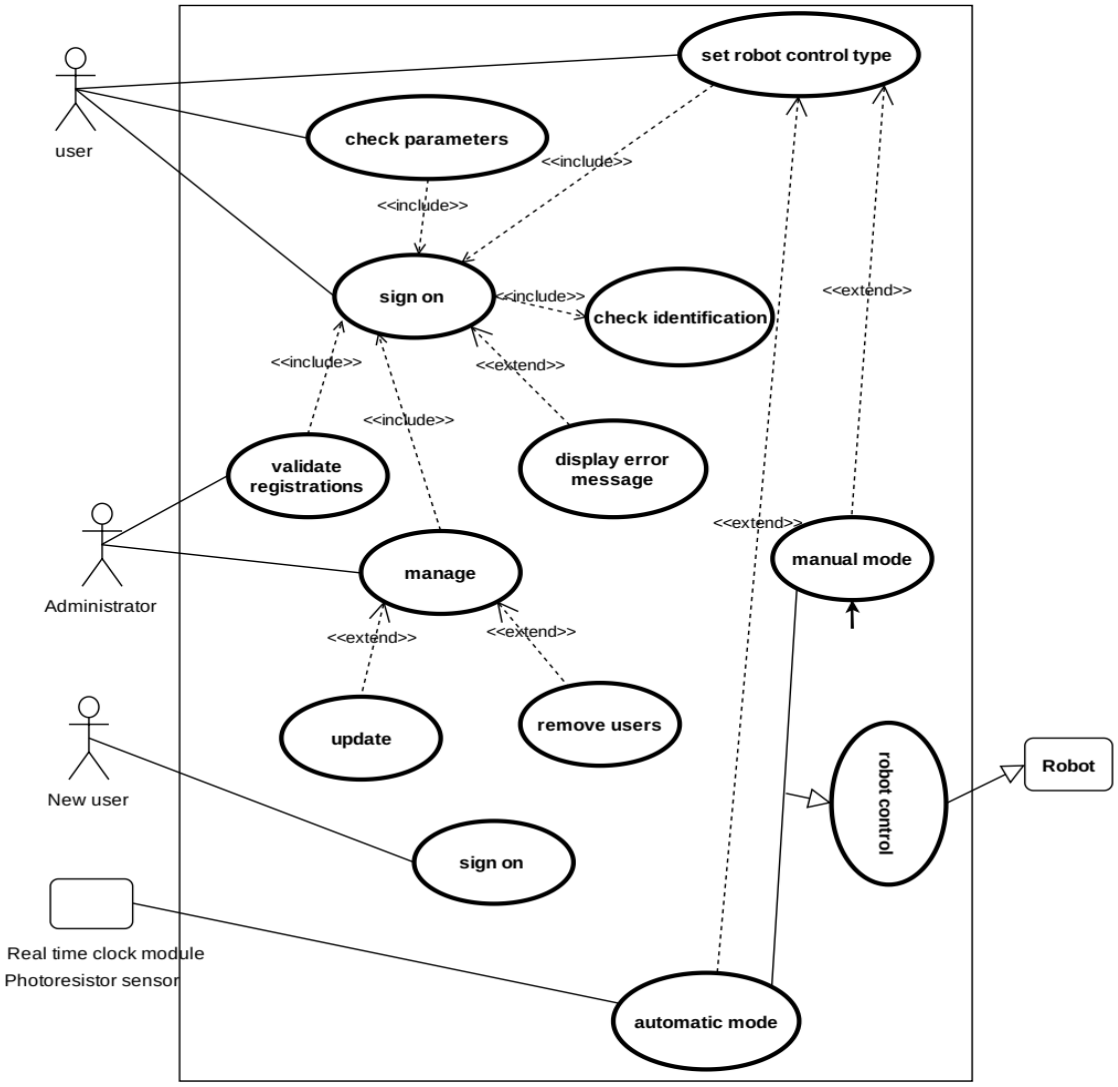

Fig.4.2. Use case diagram of the proposed robot cleaning.

IV.3.2. Mechanical robot design

The mechanical design and simulation were done using CATIA V5. All the robot components were designed and simulated in order to establish an optimal design and to study all the mechanical aspects and uncertainties that may occur in real working conditions. For this reason, mechanical design and modeling address to the following technical issues: to choose the optimal material and size for each block; to better distribute the robot and supports mass on the solar panels; to size the electrical motors for brush rotation and robot movement; to minimize the possibility of robot slipping or sliding.

The proposed robot is divided into two main systems. The first system performs a horizontal movement along the PV system length (see Fig.4.3-(a)). This system is made up of mechanical supports and wheels grip the frame of the panels in order to avoid any scratch on the PVP surfaces. Furthermore, the battery and water reservoir are mounted in this frame, in which the weight is shared between the top and the bottom. Two windshield wipers are used at the front and rear of the system to remove any water or sand that can propagate or re-deposition on previously cleaned panels. The main advantage of this system is its flexibility, it can be adapted to any length or technology. The second system represents the cleaning unit and ensures the vertical movement over the entire PV system width (see Fig.4.3-(b)). It is composed of a mechanical frame, which moves vertically using four wheels and contains a cylindrical brush in the middle. The vertical movement is ensured by a belt pulley system.

To summarize, the proposed robot is made up of two systems or frames: the main frame used to move horizontally using wheels, which grip on the panels frame. The second frame, composed of one cleaning and rotating brush, moves up and down along each PV system column. The material used for supports and frames design is the Aluminum 7075 due to its high resistivity and good density. The weight of the main frame is 21 Kg including wipers, motors, battery, water reservoir, and others. The weight of the cleaning frame is 4 Kg including brush, DC motor, wheels, and belt pulley system. Therefore, the total weight of the robot is 25 Kg.

(a)

(b)

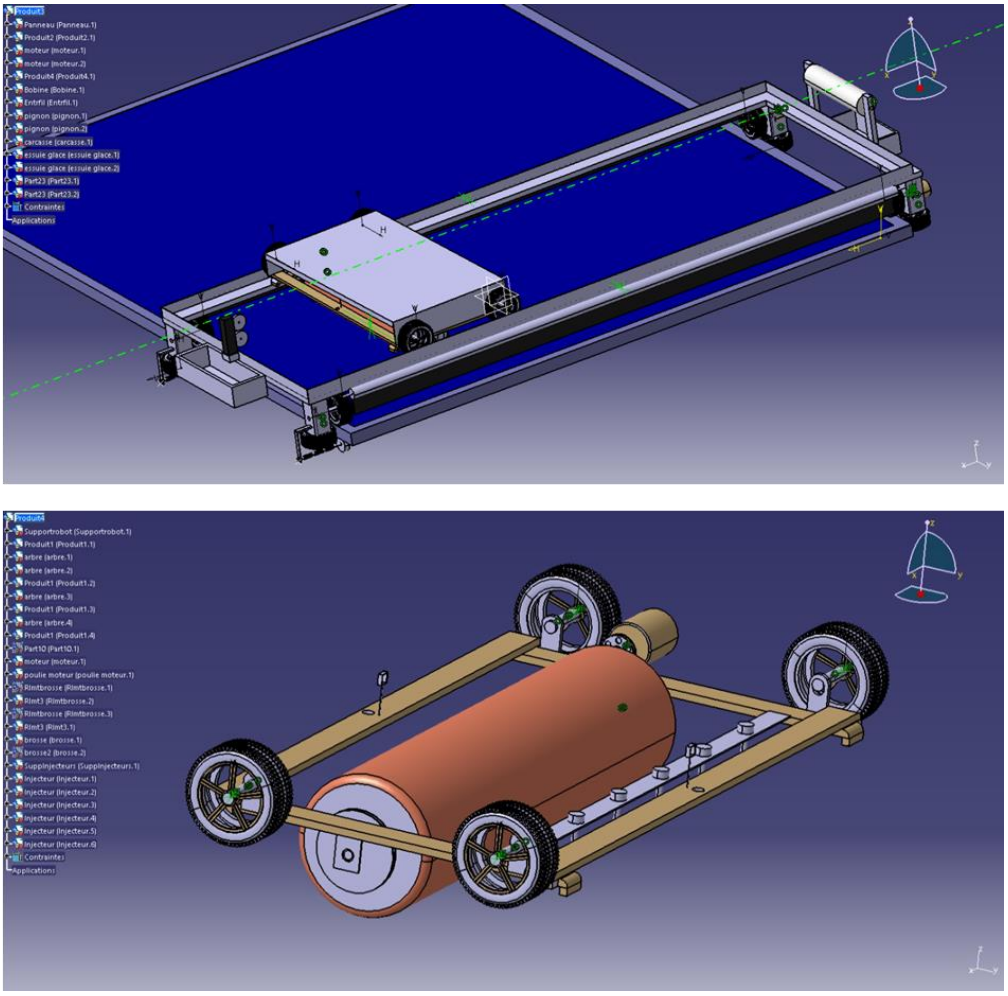

Fig.4.3. Robot design (a) main frame (b) second frame.

IV.3.3. Electronic control and powering system

The overall electronic devices are mounted inside the robot and powered by a small PV panel. The electronic circuits developed are designed and simulated using Isis Proteus and the Arduino software (IDE). The on-board control system uses Arduino Mega 2560 based on ATmega2560 microcontroller. After establishing the total energy consumption of the robot including all the electronic devices, the robot is powered by 12 V DC, 12 Ah. For this, the appropriate PV panel is dimensioned and fixed to a 25W monocrystalline panel with a PWM regulator. In addition, the motors' torque is determined to ensure the movement of the robot and the rotation of the brush as a function of the weight of each corresponding frame. For the main frame (horizontal movement), the Nema 11 (MS14HS1P4024) is used. Regarding the second frame (vertical movement), the Nema 24 (MS24HS5L4420) is employed. In addition, the SPOMHNK3054 motor is used for rotating the brush. Both horizontal and vertical movements are driven by stepper motors because of their precise positioning and controlled by PWM based signals given by Arduino Mega 2560 board, while a DC motor is used for rotating the brush with high speed and simply activated or deactivated by digital signal generated by the board. Two servo motors are used to lift the wipers because of their ability to hold the position (DS04-NFC). Furthermore, four high resolution ultrasonic sensors (HC-SR04)

are used to detect the real time current position of the robot as well as to adjust its direction and speed. These sensors are mounted on the four corners of the robot, powered by +5V DC, and connected to Arduino Mega 2560 inputs. The water reservoir is also measured in real time by the ST045 sensor. Finally, The ESP8266 integrated circuit allows the connection via WIFI and widely used to control devices over the Internet (a GSM module can also be used in this sense). This integrated circuit communicates and transfers data in real time with the web application. Users can monitor and visualize the robot status, battery charge, water reservoir level, and can also control or schedule a cleaning time. Fig.4.4 illustrates the interne bloc diagram of the proposed robot and describes the interactions between blocs.

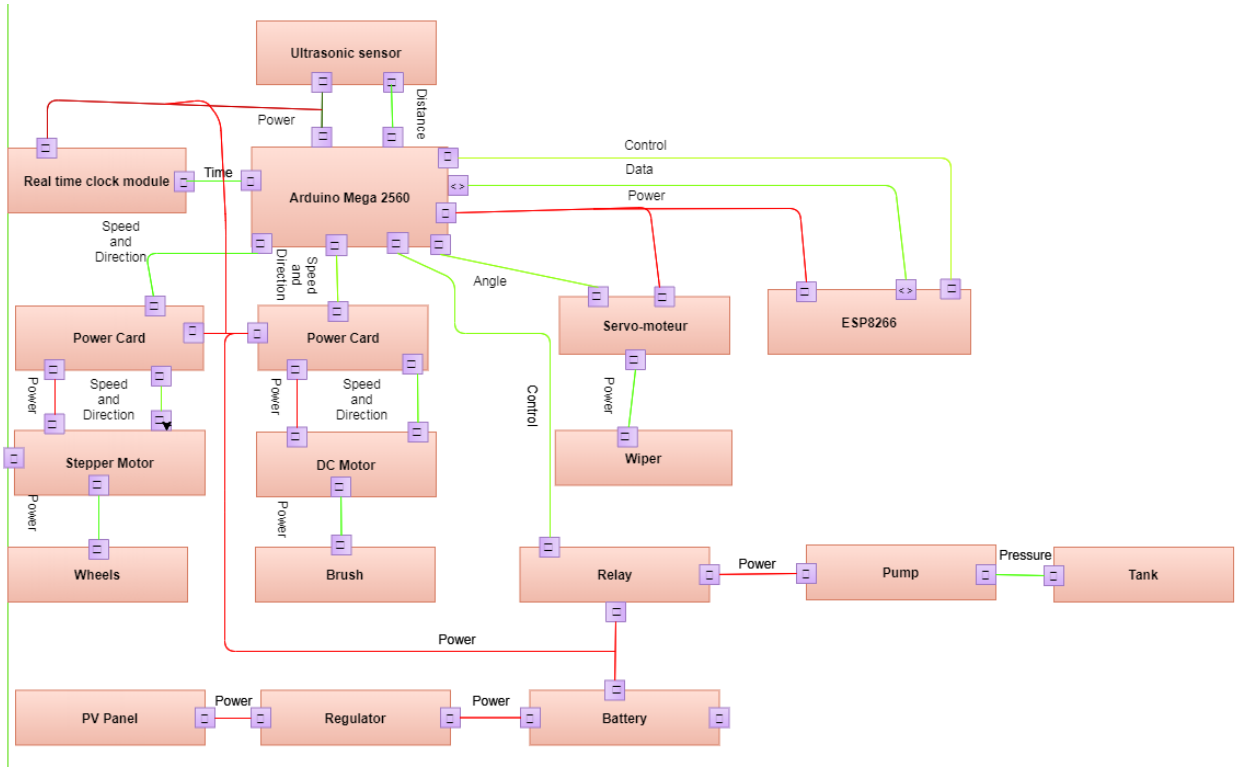

Fig.4.4. The interne block diagram of the proposed robot.

IV.3.4. Robot movement and cleaning strategy

As stated above, three modes can be used to control the robot and start cleaning: manual control; automatic control by communicating with other electronic devices installed in the field; automatic control via web link application allowing users to set a scheduled time for cleaning. Fig.4.5 illustrates the robot movement control algorithm and the cleaning strategy. It is essential to mention that the robot is designed to ensure PVP cleaning in both directions (forward and backward). Therefore, the front and rear sections of the robot are indistinguishable and the cleaning process and the direction of movement are the same. Before starting the cleaning, the robot is located each on the right or on the left of the PV system and mounted on metal support appropriate to its shape and away by 0.5 m from the edges of the PVP. The system is always waiting for control signals each from users or electronic devices. Then, the robot checks its current position to move each in the right or left directions with a distance of 0.5 m, while the appropriate wiper is powered. Following, the water injection is done for 2 seconds and the robot again checks its current positions, but this

time its vertical position, in order to move each up or down while the brush is rotating. When the edges of the PV system column are detected, the vertical movement ends. Then, the robot is horizontally moved with 0.5 m and the cleaning frame goes up or down (when the robot moves up, the rotating brush direction is changed). This process is repeated until the horizontal ends of the edges of the PV system are detected. The robot prototyping is being finalized and validated at the Green Energy Park research facility (GEP), considering several PV technologies and different PV systems geometries. The proposed cleaning robot is low cost and lightweight equipment due to its mechanical design which divides the entire system into two main frames. This aspect allows the robot to be more efficient and stable, in particular it mass is well distributed on the PVP surface. Furthermore, the flexibility of the proposed solution is a main key allowing the robot to be easily adapt to any PV system or technology. The front and rear sides of the robot are the same, allowing the cleaning process in two directions since the robot locates exactly its current position before starting cleaning. In addition, users can easily monitor the robot status and control it using the web application. This functionality is very advantageous if several cleaning robots are installed in the same field, which facilitate monitoring and maintenance and considerably reduces the human intervention. The proposed robot architecture and features seem to be a very promising, robust and low-cost technology.

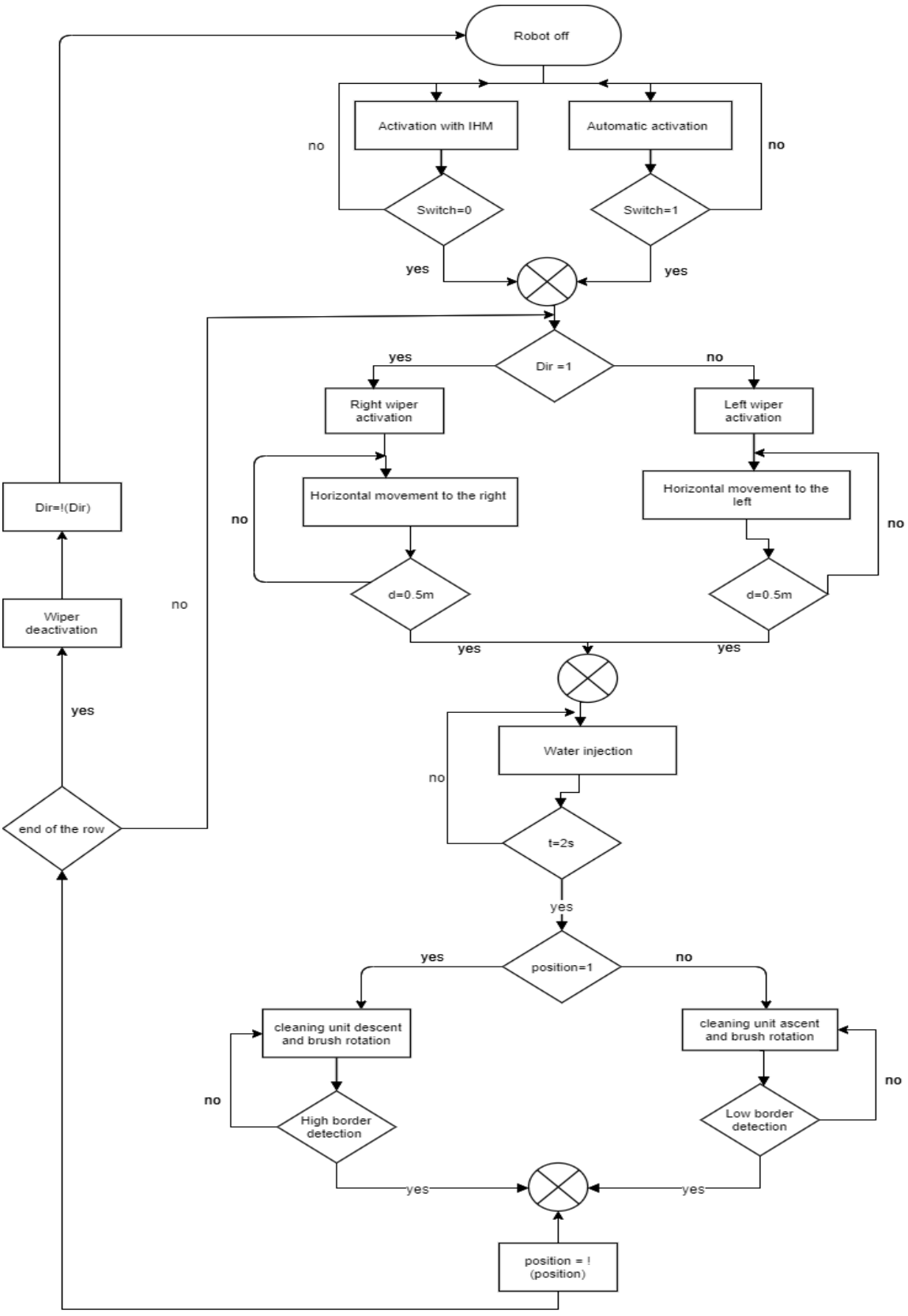

Fig.4.5. Flowchart illustrating the robot movement control algorithm and the cleaning strategy.

IV.4. PV cleaning classification

Table 4.2 show comparison and classifications of PV cleaning methods, respectively. The comparison shows that some of the cleaning methods are manual, automatic or preventive.

Cost of the selected method is important and related to the case study and many parameters need to be investigate before cleaning method final selection. Some of these parameters are PV system size, location, design elements, weather parameters, water availability, dust characteristics, etc.

Table 4.3 illustrate a comparison between the main three methods proposed in Fig.4.1 based on operation cost, CO2 emissions, labor costs, water wastage, air pollution, fuel consumption, human safety, advantages and disadvantages. Table 4.3 provides a general impression of the different aspects of PV cleaning methods, technologies and approaches. However, further investigation is required to find indicators that accurately describe those technologies and to assess them cost-effectively. Hence, it is part of the researcher task to conduct deeper investigation of each aspect mentioned in Table 4.3.

Based on the above discussion, Fig.5.6 demonstrates a suggested methodology that can be followed through research studies to determine an appropriate cleaning method described in the flow chart. The first step to be acquiring the necessary information such as PV and plant connections, current cleaning plan (if any) and costs, schematics of the PV plant infrastructure, etc. This step is followed by performance evaluation of the PV to assess the cleaning quality of the current cleaning strategy (if available). The first stage consists of analyzing the current cleaning strategy by investigating its quality, approach, speed and cost-effectiveness. This will serve as a benchmark to start cleaning method selection study. The second stage is aimed to compare the different methods proposed by researchers, scientists, and other companies to clean PV. The comparison is made through an evaluation criterion, which are made to find the optimum cleaning approach. The comparison is similar to Table 4.2 but is more specific and detailed. The most suitable solution to achieve the desired outcomes of the study will be chosen. The proposed solution will be evaluated economically to fit the cost-criterion of cleaning cost per PV and then compared to the remaining techniques, discussed in stage 2. The second performance evaluation will be done to assess the quality of the proposed approach after its implementation.

Table 4.2. Comparison of cleaning methods.

Cleaning system	Advantages	Disadvantages
Forced air flow of air conditioning systems	Force air used and effective for dry cleaning. No power consumption since it uses rejected air from AC.	It is AC operation dependent. The air is hot which may reduce PV efficiency if stay for more time.
Natural cleaning using rain and wind	No cost or resources.	It is weather related method.
Water cleaning	Effective to remove dust particles and cover all PV panel parts. Cooled or hot water could be used.	Required water, pump, and controller. Sometime static system used, and other time specific vehicle used.
Manual cleaning	Environment friendly, no electricity needed.	Human intervention is required, costly, Need water
Mechanical cleaning (blowing or brushing)	Mechanical remove the dust using cloths.	Scratching happened sometime
Electrical screens (EDS)	Efficient and effective to	Required high voltage,

	remove dust particles with no need to moving parts.	converter, digital signal device and it is costly.
Super hydrophobic aircraft (SHOP)	No moving parts. However, natural rain or dew is useful. No need for water or human intervention.	Reduce the screen efficiency due to coating. Need more investigation in different environment.
Super water jet (SHIP)	No moving parts. More effective to breakdown dirt and dissolve it.	Reduce the screen efficiency due to coating.
Self-cleaning ultrasonic	Use ultrasonic energy through the air to the surface. No water or people is needed.	Less effective with humidity. Need specific power supply.
Heliotex's automatic cleaning	Water will reach all PV panel parts also, it provides PV cooling	Required water, filter and there is some waste.
Cleaning solutions	Different chemical solution could be used. Reduce surface tension. Safe and non-toxic.	Some solutions are costly and sometimes it produces a layer make scatter for solar irradiation.
Vibrating/rotating the PV panel	Useful for dry weather and accelerate the PV surface to remove dust particles. Automatic method.	Need motor, control circuit and power supply.

Table 4.3. Comparison between various cleaning methods

Method	**Manual**	**Automatic**			**Coating method**	
	Washing & brushing	Water Spray Machine	Static Robotic Cleaning	Portable Robotic Cleaning	Superhydrophilic coating	Superhydrophobic coating
Operational Cost	"High"	"Medium"	"Low"	"Low"	"Low"	"Low"
CO2 Emissions	"Medium"	"Medium"	"Low"	Nil	"Low"	"Low "
Labor costs	"High"	"Low"	Nil	Nil	"Low"	"Low "
Water wastage	"High"	"High"	"Medium"	"Low"	"Low"	"Low "
Air pollution	"Medium"	"Medium"	"Medium"	"Medium"	"Low"	"Low "
Fuel consumption	"High"	"High"	"Low"	"Low"	"Low"	"Low "
Human safety	"Low"	"High"	"High"	"High"	"High"	"High "
Major Advantage	Reliable	Sustainable and require almost no human intervention			Easier method to remove dust, especially for titled PV's	
Major Disadvantage	Slow and labor intensive	High costs of maintenance			Reduced electrical efficiency due to reduced solar irradiance absorption	

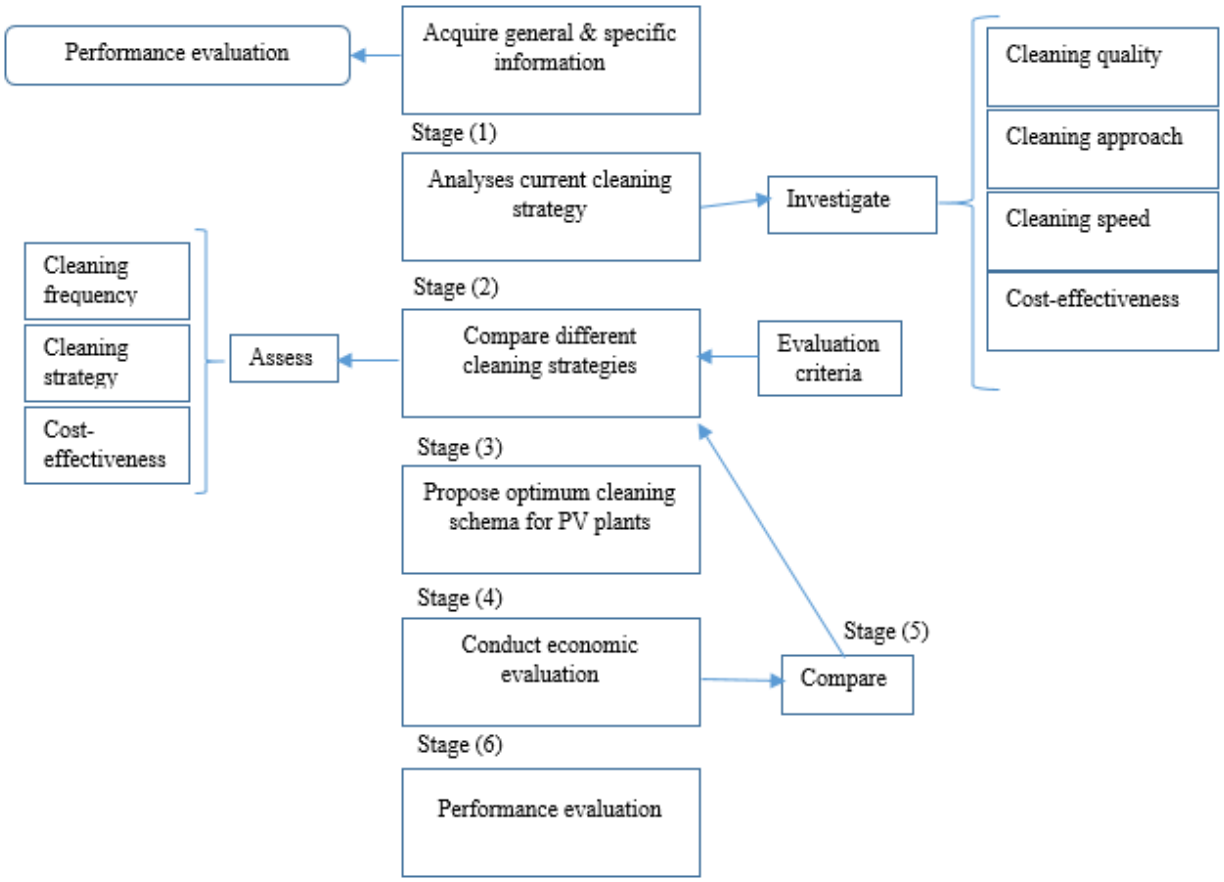

Fig. 5.6. Methodology flowchart.

IV.5. Cleaning cost

The manual cleaning cost in the green energy park is calculated with Eq. 1:

$$C = (Pw \,.\, Q \,.\, Nb \,.\, Nn) + (P) + (L \,.\, Nn) \quad (1)$$

with:

C_m: The cleaning cost per month with manual cleaning (€/month).
Pw: The price of a cubic meter of water (€/m^3).
Q: The amount of water needed to clean one module per day (m^3/day).
Nb: Number of modules in the string.
Nn: Number of cleaning days per month (day/month).
P: The price of cleaning equipment per month (€/month).
L: The labor for cleaning a day (€/day).

For example the cleaning of the string composed with 23 modules (Nb=23), the amount of water used for cleaning a module is (Q=0.002 m^3/day) with a frequency of eight times per month (Nn=8 day/month), using a cleaning equipment of (P= 3€/month). It is assumed that a person can clean the entire string with a salary of (L= 5€/day).

From the previous equation Eq. 1, the cleaning cost of PV strings is calculated as:

$$C_m = (1.23 \times 0.002 \times 23 \times 8) + 3 + (5 \times 8) = 43.45 \text{ €/month}$$

Based on our first assumptions and the Eq. 1 the cleaning cost using the new self-cleaning robot is calculated as:

Where, the assumed price of the self-guided cleaning robot is 500 € per units with total replacement costs of 5% per year and a lifetime of 10 years.

$$C_r = (1.23 \times 0.0005 \times 23 \times 8) + 6.25 = 6{,}36\ €/\text{month}$$

As noticed from the economical results, the amount of water used for the cleaning and the labor coast really increase the cleaning coast and by using our developed robot we clearly notice a decrease with an amount of ≈37 € per months.

General conclusion

The study of the impact of soiling on the performance of photovoltaic (PV) systems in the climatic conditions of Morocco is absolutely crucial to optimize the operation of such systems. In this context, little knowledge is available on the sustainability of PV systems in arid and semi-arid climates of Morocco. This imperatively includes the influence of the actual climatic conditions of operation on the various technologies of the PV modules. This thesis is a contribution to the understanding of the impact of soiling on different modules based on crystalline and thin films technologies, for a semi-arid climate of Morocco, Benguerir. This region has significant solar resources for which, this thesis work has enabled us to propose a cleaning strategy of PV module adapted to the climatic conditions of Morocco.

The first part of this work, relating to chapter 1, was devoted to generalities on PV technologies, the different forms of degradation and the soiling phenomena. These generalities are initially focused on cell manufacturing technologies and their modular topologies. Next, a detailed description of the different form of the PV degradation such as the (corrosion, delamination, cracks, and…) and the main parameters that cause this form of degradation. On the other hand, we detailed the soiling phenomena and its impact on the PV performance regarding the literature, the main parameters causing the soiling phenomena and the dust life cycle.

The second part of this work, relating to chapter 2, was devoted to study the effect and prediction of soiling rate on the performance of the PV panels in the semi-arid climate by using experimental results of an amorphous PV system and the different metrological parameters. The main conclusions of this work are summarized as follows:

- The major components of the local dust are silicate, calcium, aluminum, and iron.
- The morphology of the dust particles changes with increasing exposure time.
- The accumulated soiling losses reached 28% by the end of the test.
- The daily soiling ratio reaches an average of 0.35%/day and 0.017%/day in the dry and rainy periods respectively.
- The total energy loss throughout the test period was 82.5 kWh.
- The energy loss due to soiling effect reached 0.61 kWh/day and 0.03 kWh/day during the dry and rainy periods respectively.
- The MLRWI has a higher R^2 and adj-R^2 and lower RMSE compared to those of a simple regression MLR model.
- The statistical parameters obtained are $R^2 = 0.23$, adj-$R^2 = 0.21$ and RMSE = 0.0567; $R^2 = 0.48$, adj-$R^2 = 0.46$ and RMSE = 0.046; $R^2 = 0.51$, adj-$R^2 = 0.47$ and RMSE = 0.0464; $R^2 = 0.813$ and RMSE = 0.026 for the MLR, MLRWI, RSM, and ANN models respectively.
- The soiling ratio is high for periods with high Tamb (> 30 °C) and high amount of precipitation (> 15 mm).
- The ambient temperature Tamb as individual parameter and in interaction with the other parameters as WS, RH, and precipitation has a significant ($p < 0.05$) effect on model performance.

The third part of this work, relating to chapter 3, was devoted to develop a solution that aims to fully calculate the soiling rate and automate the cleaning operation of photovoltaic panels, which results in less involvement of the human factor and will be economical in terms of resources, precise and effective.
The system developed met the specifications of this project in terms of several criteria, among them:

- Autonomy.
- Data acquisition.
- The ability to adapt the system to a wide range of PV technologies.

In this chapter, we have also presented the different hardware of the system, the programming of the Raspberry pi onboard board using the interpreted python language, thus creation of a Flask interface and the FTP (File Transfer Protocol) used to transfer files between a Raspberry Pi and another computer connected to the same network of the card, and finally the simulation of the system under ISIS PROTEUS software.

The fourth and last part of this work, relating to chapter 4, was devoted to present the technic of the PV cleaning, its different types and principle of operation. We then carried out the design of a developed robot using the SysML language then the sizing of the robot by specifying the tools and the mechanical and electronic equipment necessary for the realization. We then performed an electrical simulation of the robot's operation using ISIS and Arduino IDE software as well as a 3D mechanical simulation with Catia5 and Matlab.

Reference

[1] F. Cassore, G. Orlandi, M. Rau, et J. Persello, « Cellules photovoltaïques à colorant ».

[2] G. EPIA, « Solar generation 6–solar photovoltaic electricity empowering the world », *Bruss. Belg. Eur. Photovolt. Ind. Assoc. EPIA*, 2011.

[3] A. Ndiaye, A. Charki, A. Kobi, C. M. Kébé, P. A. Ndiaye, et V. Sambou, « Degradations of silicon photovoltaic modules: A literature review », *Sol. Energy*, vol. 96, p. 140-151, 2013.

[4] M. Munoz, M. C. Alonso-García, N. Vela, et F. Chenlo, « Early degradation of silicon PV modules and guaranty conditions », *Sol. Energy*, vol. 85, n° 9, p. 2264-2274, 2011.

[5] M. Vázquez et I. Rey-Stolle, « Photovoltaic module reliability model based on field degradation studies », *Prog. Photovolt. Res. Appl.*, vol. 16, n° 5, p. 419-433, 2008.

[6] J. A. Tsanakas, L. Ha, et C. Buerhop, « Faults and infrared thermographic diagnosis in operating c-Si photovoltaic modules: A review of research and future challenges », *Renew. Sustain. Energy Rev.*, vol. 62, p. 695-709, 2016.

[7] C. Buerhop, D. Schlegel, C. Vodermayer, et M. Nieß, « Quality control of PV-modules in the field using infrared-thermography », 2011, p. 3894-3897.

[8] M. Köntges *et al.*, « Performance and reliability of photovoltaic systems, subtask 3.2: review of failures of photovoltaic modules », *Report2014*, 2014.

[9] « Sarah Kurtz " Photovoltaic Module Reliability." NREL PV Module Reliability. 2010. » .

[10] M. Köntges, I. Kunze, S. Kajari-Schröder, X. Breitenmoser, et B. Bjørneklett, « Quantifying the risk of power loss in PV modules due to micro cracks », 2010, p. 3745-3752.

[11] M. Köntges, I. Kunze, S. Kajari-Schröder, X. Breitenmoser, et B. Bjørneklett, « The risk of power loss in crystalline silicon based photovoltaic modules due to micro-cracks », *Sol. Energy Mater. Sol. Cells*, vol. 95, n° 4, p. 1131-1137, 2011.

[12] S. Djordjevic, D. Parlevliet, et P. Jennings, « Detectable faults on recently installed solar modules in Western Australia », *Renew. Energy*, vol. 67, p. 215-221, 2014.

[13] M. D. Kempe, « Control of moisture ingress into photovoltaic modules », 2005, p. 503-506.

[14] J. H. Wohlgemuth et S. Kurtz, « Reliability testing beyond qualification as a key component in photovoltaic's progress toward grid parity », 2011, p. 5E-3.

[15] A. Realini, « Mean time before failure of photovoltaic modules », *Final Rep. MTBF Proj. Fed. Off. Educ. Sci. Tech Rep BBW*, vol. 99, 2003.

[16] D. Carlson *et al.*, « Corrosion effects in thin-film photovoltaic modules », *Prog. Photovolt. Res. Appl.*, vol. 11, n° 6, p. 377-386, 2003.

[17] C. Osterwald, A. Anderberg, S. Rummel, et L. Ottoson, « Degradation analysis of weathered crystalline-silicon PV modules », 2002, p. 1392-1395.

[18] A. Skoczek, T. Sample, E. Dunlop, et H. Ossenbrink, « Electrical performance results from physical stress testing of commercial PV modules to the IEC 61215 test sequence », *Sol. Energy Mater. Sol. Cells*, vol. 92, n° 12, p. 1593-1604, 2008.

[19] P. Sánchez-Friera, M. Piliougine, J. Pelaez, J. Carretero, et M. Sidrach de Cardona, « Analysis of degradation mechanisms of crystalline silicon PV modules after 12 years of operation in Southern Europe », *Prog. Photovolt. Res. Appl.*, vol. 19, n° 6, p. 658-666, 2011.

[20] N. G. Dhere, « Reliability of PV modules and balance-of-system components », 2005, p. 1570-1576.

[21] N. Dhere et M. Pandit, « Study of delamination in acceleration tested PV modules », 2001, p. 572-575.

[22] K. Jansen et A. Delahoy, « A laboratory technique for the evaluation of electrochemical transparent conductive oxide delamination from glass substrates », *Thin Solid Films*, vol. 423, n° 2, p. 153-160, 2003.

[23] T. Silverman, J. Wohlgemuth, D. Miller, M. Kempe, et P. McNutt, « Review of observed degradation modes and mechanisms from fielded modules », *Natl. Renew. Energy Lab. NREL USA*, 2015.
[24] « Kempe MD, Jorgensen GJ, Terwilliger KM, McMahon TJ, Kennedy CE, Borek TT. Acetic acid production and glass transition concerns with ethylene-vinyl acetate used in photovoltaic devices. Solar energy materials and solar cells. 2007 Feb 15;91(4):315-29. »
[25] F. Pern, A. Czanderna, K. Emery, et R. Dhere, « Weathering degradation of EVA encapsulant and the effect of its yellowing on solar cell efficiency », 1991, vol. 1, p. 557-561.
[26] F. Pern et A. Czanderna, « Characterization of ethylene vinyl acetate (EVA) encapsulant: Effects of thermal processing and weathering degradation on its discoloration », *Sol. Energy Mater. Sol. Cells*, vol. 25, n° 1-2, p. 3-23, 1992.
[27] « Pern FJ, Czanderna AW. EVA degradation mechanisms simulating those in PV modules. InAIP Conference Proceedings 1992 Dec 1 (Vol. 268, No. 1, pp. 445-452). American Institute of Physics. »
[28] H. J. Wenger, C. Jennings, et J. J. Iannucci, « Carrisa Plains PV power plant performance », 1990, p. 844-849.
[29] E. Molenbroek, D. Waddington, et K. Emery, « Hot spot susceptibility and testing of PV modules », 1991, vol. 1, p. 547-552.
[30] H. Ziar, S. Mansourpour, E. Afjei, et M. Kazemi, « Bypass diode characteristic effect on the behavior of solar PV array at shadow condition », 2012, p. 229-233.
[31] E. Karatepe, M. Boztepe, et M. Colak, « Development of a suitable model for characterizing photovoltaic arrays with shaded solar cells », *Sol. Energy*, vol. 81, n° 8, p. 977-992, 2007.
[32] H. Tian, F. Mancilla–David, K. Ellis, E. Muljadi, et P. Jenkins, « Determination of the optimal configuration for a photovoltaic array depending on the shading condition », *Sol. Energy*, vol. 95, p. 1-12, 2013.
[33] E. Kaplani, « Degradation in field-aged crystalline silicon photovoltaic modules and diagnosis using electroluminescence imaging », 2016.
[34] « J. Wohlgemuth, D.W. Cunningham, A. Nguyen, G. Kelly, D. Amin, Failure Modes of Crystalline Si Modules, PV Module Reliability Workshop 2010 (NREL, Golden, USA, 2010) ». .
[35] I. PVPS, « Review of Failures of Photovoltaic Modules », *Int. Energy Agency*, 1995.
[36] « Mau S, Krametz T, Jahna W, Fechner H. Quality testing for PV-modules according to standards and performance control for supporting manufacturing. In19th Eur. Photovoltaic Sol. Energy Conf. Exhib., Paris, France 2004 Jun 7. »
[37] « Gostein M, Dunn L. Light soaking effects on photovoltaic modules: Overview and literature review. In2011 37th IEEE Photovoltaic Specialists Conference 2011 Jun 19 (pp. 003126-003131). IEEE. »
[38] M. Muñoz-García, O. Marin, M. Alonso-García, et F. Chenlo, « Characterization of thin film PV modules under standard test conditions: Results of indoor and outdoor measurements and the effects of sunlight exposure », *Sol. Energy*, vol. 86, n° 10, p. 3049-3056, 2012.
[39] « Virtuani A, Müllejans H, Dunlop ED. Comparison of indoor and outdoor performance measurements of recent commercially available solar modules. Progress in photovoltaics: Research and Applications. 2011 Jan;19(1):11-20. »
[40] M. A. Green *et al.*, « Solar cell efficiency tables (version 49) », *Prog. Photovolt. Res. Appl.*, vol. 25, n° 1, p. 3-13, 2017.
[41] A. Phinikarides, N. Kindyni, G. Makrides, et G. E. Georghiou, « Review of photovoltaic degradation rate methodologies », *Renew. Sustain. Energy Rev.*, vol. 40, p. 143-152, 2014.
[42] D. Mutungi, « Degradation of photovoltaics in central Finland: A comparative study of polycrystalline and heterojunction with intrinsic thin layer technologies », 2013.

[43] F. Trieb, C. Schillings, T. Pregger, et M. O'Sullivan, « Solar electricity imports from the Middle East and North Africa to Europe », *Energy Policy*, vol. 42, p. 341-353, 2012.
[44] M. Kahia, M. S. B. Aïssa, et C. Lanouar, « Renewable and non-renewable energy use-economic growth nexus: The case of MENA Net Oil Importing Countries », *Renew. Sustain. Energy Rev.*, vol. 71, p. 127-140, 2017.
[45] A. Azouzoute, A. A. Merrouni, et S. Touili, « Overview of the integration of CSP as an alternative energy source in the MENA region », *Energy Strategy Rev.*, vol. 29, p. 100493, 2020.
[46] A. Azouzoute, A. A. Merrouni, M. Garoum, E. G. Bennouna, A. Ghennioui, et M. E. Ydrissi, « The impact of optical soiling losses on the electrical production of CSP power plant », *AIP Conf. Proc.*, vol. 2123, n° 1, p. 020090, juill. 2019, doi: 10.1063/1.5117017.
[47] A. Azouzoute, M. Chouitar, M. Garoum, E. G. Bennouna, et A. Ghennioui, « A new PV soiling monitoring device for optimized cleaning strategy », 2019, vol. 2190, p. 020068.
[48] A. Azouzoute, A. A. Merrouni, M. Garoum, et E. G. Bennouna, « Comparison of soiling effect of two different solar mirrors in mid-south of Morocco », *AIP Conf. Proc.*, vol. 2126, n° 1, p. 190002, juill. 2019, doi: 10.1063/1.5117699.
[49] M. Abderrezek et M. Fathi, « Experimental study of the dust effect on photovoltaic panels' energy yield », *Sol. Energy*, vol. 142, p. 308-320, 2017.
[50] M. Saidan, A. G. Albaali, E. Alasis, et J. K. Kaldellis, « Experimental study on the effect of dust deposition on solar photovoltaic panels in desert environment », *Renew. Energy*, vol. 92, p. 499-505, 2016.
[51] A. Azouzoute, A. A. Merrouni, et M. Garoum, « Soiling loss of solar glass and mirror samples in the region with arid climate », *Energy Rep.*, vol. 6, p. 693-698, 2020.
[52] T. Sarver, A. Al-Qaraghuli, et L. L. Kazmerski, « A comprehensive review of the impact of dust on the use of solar energy: History, investigations, results, literature, and mitigation approaches », *Renew. Sustain. Energy Rev.*, vol. 22, p. 698-733, juin 2013, doi: 10.1016/j.rser.2012.12.065.
[53] M. H. Bergin, C. Ghoroi, D. Dixit, J. J. Schauer, et D. T. Shindell, « Large reductions in solar energy production due to dust and particulate air pollution », *Environ. Sci. Technol. Lett.*, vol. 4, n° 8, p. 339-344, 2017.
[54] P. Piedra et H. Moosmüller, « Optical losses of photovoltaic cells due to aerosol deposition: Role of particle refractive index and size », *Sol. Energy*, vol. 155, p. 637-646, 2017.
[55] K. K. Ilse *et al.*, « Comprehensive analysis of soiling and cementation processes on PV modules in Qatar », *Sol. Energy Mater. Sol. Cells*, vol. 186, p. 309-323, 2018.
[56] K. K. Ilse, B. W. Figgis, V. Naumann, C. Hagendorf, et J. Bagdahn, « Fundamentals of soiling processes on photovoltaic modules », *Renew. Sustain. Energy Rev.*, vol. 98, p. 239-254, 2018.
[57] P. M. Martin-Sanchez *et al.*, « Monitoring microbial soiling in photovoltaic systems: A qPCR-based approach », *Int. Biodeterior. Biodegrad.*, vol. 129, p. 13-22, 2018.
[58] A. Einhorn *et al.*, « Evaluation of soiling and potential mitigation approaches on photovoltaic glass », *IEEE J. Photovolt.*, vol. 9, n° 1, p. 233-239, 2018.
[59] M. A. Shirakawa *et al.*, « Microbial colonization affects the efficiency of photovoltaic panels in a tropical environment », *J. Environ. Manage.*, vol. 157, p. 160-167, 2015.
[60] R. Conceição, H. G. Silva, J. Mirão, et M. Collares-Pereira, « Organic soiling: the role of pollen in PV module performance degradation », *Energies*, vol. 11, n° 2, p. 294, 2018.
[61] S. C. Costa, A. S. A. Diniz, et L. L. Kazmerski, « Solar energy dust and soiling R&D progress: Literature review update for 2016 », *Renew. Sustain. Energy Rev.*, vol. 82, p. 2504-2536, 2018.
[62] S. C. Costa, A. S. A. Diniz, et L. L. Kazmerski, « Dust and soiling issues and impacts relating to solar energy systems: Literature review update for 2012–2015 », *Renew. Sustain. Energy Rev.*, vol. 63, p. 33-61, 2016.
[63] S. Ghazi, A. Sayigh, et K. Ip, « Dust effect on flat surfaces–A review paper », *Renew. Sustain. Energy Rev.*, vol. 33, p. 742-751, 2014.

[64] M. Al-Addous, Z. Dalala, F. Alawneh, et C. B. Class, « Modeling and quantifying dust accumulation impact on PV module performance », *Sol. Energy*, vol. 194, p. 86-102, 2019.
[65] S. A. Said, G. Hassan, H. M. Walwil, et N. Al-Aqeeli, « The effect of environmental factors and dust accumulation on photovoltaic modules and dust-accumulation mitigation strategies », *Renew. Sustain. Energy Rev.*, vol. 82, p. 743-760, 2018.
[66] B. Figgis *et al.*, « Investigation of factors affecting condensation on soiled PV modules », *Sol. Energy*, vol. 159, p. 488-500, 2018.
[67] G. Mastekbayeva et S. Kumar, « Effect of dust on the transmittance of low density polyethylene glazing in a tropical climate », *Sol. Energy*, vol. 68, n° 2, p. 135-141, 2000.
[68] M. S. El-Shobokshy et F. M. Hussein, « Effect of dust with different physical properties on the performance of photovoltaic cells », *Sol. Energy*, vol. 51, n° 6, p. 505-511, 1993.
[69] M. S. El-Shobokshy et F. M. Hussein, « Degradation of photovoltaic cell performance due to dust deposition on to its surface », *Renew. Energy*, vol. 3, n° 6-7, p. 585-590, 1993.
[70] A. A. Hegazy, « Effect of dust accumulation on solar transmittance through glass covers of plate-type collectors », *Renew. Energy*, vol. 22, n° 4, p. 525-540, 2001.
[71] M. J. Adinoyi et S. A. Said, « Effect of dust accumulation on the power outputs of solar photovoltaic modules », *Renew. Energy*, vol. 60, p. 633-636, 2013.
[72] S. Boppana, *Outdoor soiling loss characterization and statistical risk analysis of photovoltaic power plants*. Arizona State University, 2015.
[73] L. Boyle, H. Flinchpaugh, et M. Hannigan, « Natural soiling of photovoltaic cover plates and the impact on transmission », *Renew. Energy*, vol. 77, p. 166-173, 2015.
[74] A. Ullah, A. Amin, T. Haider, M. Saleem, et N. Z. Butt, « Investigation of soiling effects, dust chemistry and optimum cleaning schedule for PV modules in Lahore, Pakistan », *Renew. Energy*, vol. 150, p. 456-468, 2020.
[75] J. Kaldellis et A. Kokala, « Quantifying the decrease of the photovoltaic panels' energy yield due to phenomena of natural air pollution disposal », *Energy*, vol. 35, n° 12, p. 4862-4869, 2010.
[76] S. A. Said et H. M. Walwil, « Fundamental studies on dust fouling effects on PV module performance », *Sol. Energy*, vol. 107, p. 328-337, 2014.
[77] H. Zitouni *et al.*, « Experimental investigation of the soiling effect on the performance of monocrystalline photovoltaic systems », *Energy Procedia*, vol. 157, p. 1011-1021, 2019.
[78] A. M. El-Nashar, « Effect of dust deposition on the performance of a solar desalination plant operating in an arid desert area », *Sol. Energy*, vol. 75, n° 5, p. 421-431, 2003.
[79] A. M. El-Nashar, « Seasonal effect of dust deposition on a field of evacuated tube collectors on the performance of a solar desalination plant », *Desalination*, vol. 239, n° 1-3, p. 66-81, 2009.
[80] A. Hassan, U. A. Rahoma, H. K. Elminir, et A. Fathy, « Effect of airborne dust concentration on the performance of PV modules », *J Astron Soc Egypt*, vol. 13, n° 1, p. 24-38, 2005.
[81] H. K. Elminir, A. E. Ghitas, R. Hamid, F. El-Hussainy, M. Beheary, et K. M. Abdel-Moneim, « Effect of dust on the transparent cover of solar collectors », *Energy Convers. Manag.*, vol. 47, n° 18-19, p. 3192-3203, 2006.
[82] H. K. Elminir, A. E. Ghitas, R. H. Hamid, F. El-Hussainy, M. M. Beheary, et K. M. Abdel-Moneim, « Effect of dust on the transparent cover of solar collectors », *Energy Convers. Manag.*, vol. 47, n° 18-19, p. 3192-3203, 2006.
[83] A. Gholami, A. Saboonchi, et A. A. Alemrajabi, « Experimental study of factors affecting dust accumulation and their effects on the transmission coefficient of glass for solar applications », *Renew. Energy*, vol. 112, p. 466-473, 2017.
[84] A. Azouzoute, M. Garoum, F. Jeffali, et A. Ghennioui, « Experimental study of dust effect on the transmission of a glass PV panel for a fixed and tracking system », *Mater. Today Proc.*, 2020.

[85] H. Qasem, T. R. Betts, H. Müllejans, H. AlBusairi, et R. Gottschalg, « Dust-induced shading on photovoltaic modules », *Prog. Photovolt. Res. Appl.*, vol. 22, n° 2, p. 218-226, 2014, doi: 10.1002/pip.2230.
[86] G. Picotti, P. Borghesani, M. Cholette, et G. Manzolini, « Soiling of solar collectors–Modelling approaches for airborne dust and its interactions with surfaces », *Renew. Sustain. Energy Rev.*, vol. 81, p. 2343-2357, 2018.
[87] Y. N. Chanchangi, A. Ghosh, S. Sundaram, et T. K. Mallick, « Dust and PV performance in Nigeria: A review », *Renew. Sustain. Energy Rev.*, vol. 121, p. 109704, 2020.
[88] Y. Shao, « A model for mineral dust emission », *J. Geophys. Res. Atmospheres*, vol. 106, n° D17, p. 20239-20254, 2001.
[89] Y. Shao, M. R. Raupach, et J. F. Leys, « A model for predicting aeolian sand drift and dust entrainment on scales from paddock to region », *Soil Res.*, vol. 34, n° 3, p. 309-342, 1996.
[90] J. F. Kok, E. J. Parteli, T. I. Michaels, et D. B. Karam, « The physics of wind-blown sand and dust », *Rep. Prog. Phys.*, vol. 75, n° 10, p. 106901, 2012.
[91] E. Kim, D. Kalman, et T. Larson, « Dry deposition of large, airborne particles onto a surrogate surface », *Atmos. Environ.*, vol. 34, n° 15, p. 2387-2397, 2000.
[92] O. Aluko et K. E. Noll, « Deposition and suspension of large, airborne particles », *Aerosol Sci. Technol.*, vol. 40, n° 7, p. 503-513, 2006.
[93] S. Friedlander, « Smoke, Dust », *Haze-Fundam. Aerosol Behav.*, 1977.
[94] W. C. Hinds, *Aerosol technology: properties, behavior, and measurement of airborne particles*. John Wiley & Sons, 1999.
[95] R. J. Isaifan, D. Johnson, L. Ackermann, B. Figgis, et M. Ayoub, « Evaluation of the adhesion forces between dust particles and photovoltaic module surfaces », *Sol. Energy Mater. Sol. Cells*, vol. 191, p. 413-421, 2019.
[96] B. Figgis, A. Ennaoui, S. Ahzi, et Y. Rémond, « Review of PV soiling particle mechanics in desert environments », *Renew. Sustain. Energy Rev.*, vol. 76, n° Supplement C, p. 872-881, sept. 2017, doi: 10.1016/j.rser.2017.03.100.
[97] M. Gostein, T. Düster, et C. Thuman, « Accurately measuring PV soiling losses with soiling station employing module power measurements », 2015, p. 1-4.
[98] D. Goossens et E. Van Kerschaever, « Aeolian dust deposition on photovoltaic solar cells: the effects of wind velocity and airborne dust concentration on cell performance », *Sol. Energy*, vol. 66, n° 4, p. 277-289, 1999.
[99] B. Guo, W. Javed, B. Figgis, et T. Mirza, « Effect of dust and weather conditions on photovoltaic performance in Doha, Qatar », 2015, p. 1-6.
[100] J. Kaldellis, P. Fragos, et M. Kapsali, « Systematic experimental study of the pollution deposition impact on the energy yield of photovoltaic installations », *Renew. Energy*, vol. 36, n° 10, p. 2717-2724, 2011.
[101] H. A. Kazem et S. Al-Bahri, « Saud Al-Badi, Haifa Al-Mahkladi and Ali HA Al-Waeli," Effect of Dust on Photovoltaic Performance », 2012, p. 1-4.
[102] T. Khatib, H. Kazem, K. Sopian, F. Buttinger, W. Elmenreich, et A. S. Albusaidi, « Effect of dust deposition on the performance of multi-crystalline photovoltaic modules based on experimental measurements », *Int. J. Renew. Energy Res. IJRER*, vol. 3, n° 4, p. 850-853, 2013.
[103] Z. Ahmed, H. A. Kazem, et K. Sopian, « Effect of dust on photovoltaic performance: Review and research status », *Latest Trends Renew. Energy Environ. Inform.*, p. 193-199, 2013.
[104] W. Javed, B. Guo, et B. Figgis, « Modeling of photovoltaic soiling loss as a function of environmental variables », *Sol. Energy*, vol. 157, p. 397-407, 2017.
[105] R. Conceição, H. G. Silva, et M. Collares-Pereira, « CSP mirror soiling characterization and modeling », *Sol. Energy Mater. Sol. Cells*, vol. 185, p. 233-239, 2018.

[106] G. K. Uyanık et N. Güler, « A study on multiple linear regression analysis », *Procedia-Soc. Behav. Sci.*, vol. 106, n° 1, p. 234-240, 2013.
[107] M. Tranmer et M. Elliot, « Multiple linear regression », *Cathie Marsh Cent. Census Surv. Res. CCSR*, vol. 5, p. 30-35, 2008.
[108] D. C. Montgomery, *Design and analysis of experiments*. John wiley & sons, 2017.
[109] S. Yi, Y. Su, B. Qi, Z. Su, et Y. Wan, « Application of response surface methodology and central composite rotatable design in optimizing the preparation conditions of vinyltriethoxysilane modified silicalite/polydimethylsiloxane hybrid pervaporation membranes », *Sep. Purif. Technol.*, vol. 71, n° 2, p. 252-262, 2010.
[110] M. Mani et R. Pillai, « Impact of dust on solar photovoltaic (PV) performance: Research status, challenges and recommendations », *Renew. Sustain. Energy Rev.*, vol. 14, n° 9, p. 3124-3131, 2010.
[111] B. Figgis, A. Ennaoui, B. Guo, W. Javed, et E. Chen, « Outdoor soiling microscope for measuring particle deposition and resuspension », *Sol. Energy*, vol. 137, p. 158-164, 2016.
[112] Y. Kim *et al.*, « Effects of relative humidity and particle and surface properties on particle resuspension rates », *Aerosol Sci. Technol.*, vol. 50, n° 4, p. 339-352, 2016.
[113] A. Ibrahim, P. Dunn, et R. Brach, « Microparticle detachment from surfaces exposed to turbulent air flow: Effects of flow and particle deposition characteristics », *J. Aerosol Sci.*, vol. 35, n° 7, p. 805-821, 2004.
[114] N. S. Beattie, R. S. Moir, C. Chacko, G. Buffoni, S. H. Roberts, et N. M. Pearsall, « Understanding the effects of sand and dust accumulation on photovoltaic modules », *Renew. Energy*, vol. 48, p. 448-452, 2012.
[115] S. Mekhilef, R. Saidur, et M. Kamalisarvestani, « Effect of dust, humidity and air velocity on efficiency of photovoltaic cells », *Renew. Sustain. Energy Rev.*, vol. 16, n° 5, p. 2920-2925, 2012.
[116] J. R. Caron et B. Littmann, « Direct monitoring of energy lost due to soiling on first solar modules in California », *IEEE J. Photovolt.*, vol. 3, n° 1, p. 336-340, 2012.
[117] D. C. Miller et S. R. Kurtz, « Durability of Fresnel lenses: a review specific to the concentrating photovoltaic application », *Sol. Energy Mater. Sol. Cells*, vol. 95, n° 8, p. 2037-2068, 2011.
[118] A. Azouzoute, A. A. Merrouni, M. Garoum, et E. G. Bennouna, « Comparison of soiling effect of two different solar mirrors in mid-south of Morocco », 2019, vol. 2126, n° 1, p. 190002.
[119] L. Micheli et M. Muller, « An investigation of the key parameters for predicting PV soiling losses », *Prog. Photovolt. Res. Appl.*, vol. 25, n° 4, p. 291-307, 2017.
[120] A. Azouzoute, A. A. Merrouni, et M. Garoum, « Soiling loss of solar glass and mirror samples in the region with arid climate », *Energy Rep.*, vol. 6, p. 693-698, 2020.
[121] S. M. S. Cabaneros, J. K. Calautit, et B. R. Hughes, « A review of artificial neural network models for ambient air pollution prediction », *Environ. Model. Softw.*, 2019.
[122] S. R. Mohandes, X. Zhang, et A. Mahdiyar, « A comprehensive review on the application of artificial neural networks in building energy analysis », *Neurocomputing*, vol. 340, p. 55-75, 2019.
[123] N. Shahid, T. Rappon, et W. Berta, « Applications of artificial neural networks in health care organizational decision-making: A scoping review », *PloS One*, vol. 14, n° 2, 2019.
[124] H. H. Alkinani, A. T. T. Al-Hameedi, S. Dunn-Norman, R. E. Flori, M. T. Alsaba, et A. S. Amer, « Applications of Artificial Neural Networks in the Petroleum Industry: A Review », présenté à SPE Middle East Oil and Gas Show and Conference, 2019.
[125] J. F. Bermejo, J. F. G. Fernández, F. O. Polo, et A. C. Márquez, « A Review of the Use of Artificial Neural Networks Models for Energy and Reliability Prediction. A Study for the Solar PV, Hydraulic and Wind Energy Sources », *Appl Sci*, vol. 9, p. 1844, 2019.
[126] A. Géron, *Hands-On Machine Learning with Scikit-Learn, Keras, and TensorFlow: Concepts, Tools, and Techniques to Build Intelligent Systems*. O'Reilly Media, 2019.

[127] M. Torres-Ramírez, D. Elizondo, B. García-Domingo, G. Nofuentes, et D. Talavera, « Modelling the spectral irradiance distribution in sunny inland locations using an ANN-based methodology », *Energy*, vol. 86, p. 323-334, 2015.
[128] F.-V. Gutierrez-Corea, M.-A. Manso-Callejo, M.-P. Moreno-Regidor, et M.-T. Manrique-Sancho, « Forecasting short-term solar irradiance based on artificial neural networks and data from neighboring meteorological stations », *Sol. Energy*, vol. 134, p. 119-131, 2016.
[129] « Panneau solaire Polycristallin VICTRON 60W | 60Wc - 12V * SOLARIS-STORE ». https://www.solaris-store.com/2121-panneau-solaire-polycristallin-victron-60w.html (consulté le juill. 06, 2020).
[130] « Capteur de courant ACS712 - 30A - Letmeknow.fr ». https://letmeknow.fr/shop/fr/autres/1565-capteur-de-courant-acs712-30a-0726146001625.html (consulté le juill. 06, 2020).
[131] « Module Capteur de Tension ». https://www.robotshop.com/be/fr/module-capteur-tension.html (consulté le juill. 06, 2020).
[132] « MCP3208 - Mixed Signal - Successive Approximation Register (SAR) A/D Converters ». https://www.microchip.com/wwwproducts/en/MCP3208 (consulté le juill. 06, 2020).
[133] « Raspberry Pi 3 modèle B ». https://www.generationrobots.com/fr/402366-raspberry-pi-3-modele-b.html (consulté le juill. 06, 2020).
[134] « Erreur 404 - MCHobby - Vente de Raspberry Pi, Arduino, ODROID, Adafruit ». https://shop.mchobby.be/fr/relais-modules/507-module-deux-relais (consulté le juill. 06, 2020).
[135] « Ardwinner ! Pour ne pas avoir la loose en Arduino et en informatique », *Ardwinner !* http://ardwinner.jimdofree.com/ (consulté le juill. 06, 2020).
[136] J. R. Gaier et M. E. Perez-Davis, « Aeolian removal of dust types from photovoltaic surfaces on Mars », 1990.
[137] « China Mini Clean Brush from Jinjiang Manufacturer: Jinjiang Jiaxing Company. https://jiaxingbest.manufacturer.globalsources.com/si/6008845131807/pdtl/Carwash/ 1159952867/Mini-Clean-Brush.htm ».
[138] « 3M Commercial Solutions Division. Technical Data Sheet Scotch-Brite™ High Performance Cloth. Tech Data Sheet 2017:1. https://multimedia.3m.com/mws/ media/1459376O/scotch-brite-high-performance-cloth-2010-technical-data-sheet.pdf ».
[139] M. Kegeleers, « The development of a cleaning robot for PV panels », *Fac. Eng. Technol.*, 2015.
[140] A. Gheitasi, A. Almaliky, et N. Albaqawi, « Development of an automatic cleaning system for photovoltaic plants », 2015, p. 1-4.
[141] « Green Energy Park Research facility », 2014. http://www.greenenergypark.ma/ (consulté le mars 07, 2018).
[142] A. Syafiq, A. Pandey, et N. Rahim, « Photovoltaic glass cleaning methods: an overview », 2016.
[143] C. Calle *et al.*, « Dust particle removal by electrostatic and dielectrophoretic forces with applications to NASA exploration missions », 2008, vol. 2008.
[144] A. B. Gurav *et al.*, « Superhydrophobic coatings prepared from methyl-modified silica particles using simple dip-coating method », *Ceram. Int.*, vol. 41, n° 2, p. 3017-3023, 2015.
[145] S. A. Mahadik *et al.*, « Superhydrophobic silica coating by dip coating method », *Appl. Surf. Sci.*, vol. 277, p. 67-72, 2013.
[146] S. Liu, S. S. Latthe, H. Yang, B. Liu, et R. Xing, « Raspberry-like superhydrophobic silica coatings with self-cleaning properties », *Ceram. Int.*, vol. 41, n° 9, p. 11719-11725, 2015.
[147] T. Choi, J.-S. Kim, et J. H. Kim, « Transparent nitrogen doped TiO2/WO3 composite films for self-cleaning glass applications with improved photodegradation activity », *Adv. Powder Technol.*, vol. 27, n° 2, p. 347-353, 2016.
[148] W. H. Lee, C. W. Lai, et S. B. A. Hamid, « One-step formation of WO3-loaded TiO2 nanotubes composite film for high photocatalytic performance », *Materials*, vol. 8, n° 5, p. 2139-2153, 2015.

[149] F. Jumeri, H. Lim, Z. Zainal, N. Huang, et A. Pandikumar, « Titanium dioxide-reduced graphene oxide thin film for photoelectrochemical water splitting », *Ceram. Int.*, vol. 40, n° 9, p. 15159-15165, 2014.
[150] L. Marques, *Advances in mobile robotics: proceedings of the Eleventh International Conference on Climbing and Walking Robots and the support technologies for mobile machines, Coimbra, Portugal, 8-10 September 2008*. World Scientific, 2008.
[151] S. S. Innovations, « Gekko solar ».
[152] « Koebler J. Here's an Autonomous, Solar Panel-CleaningRobot ». https://www.vice.com/en_us/article/wnj4kx/heres-an-autonomous-solar-panel-cleaning-robot.
[153] A. Fuchs-Barbana et S. Schlittler, « Einsatz von Reinigungs-Robotern in FM-Services », 2016, p. 71.
[154] M. T. Grando, E. R. Maletz, D. Martins, H. Simas, et R. Simoni, « Robots for cleaning photovoltaic panels: State of the art and future prospects », *Rev. Tecnol. Cienc.*, n° 35, p. 137-150, 2019.